Chem Soc Rev

Conductive Diamond: Synthesis, Properties, and Electrochemical Applications

Journal:	*Chemical Society Reviews*
Manuscript ID	CS-SYN-11-2017-000757.R2
Article Type:	Review Article
Date Submitted by the Author:	08-Oct-2018
Complete List of Authors:	Yang, Nianjun; Universitat Siegen, Institute of Materials Engineering Yu, Siyu; Universitat Siegen, Institute of Materials Engineering Macpherson, Julie; University of Warwick, Department of Chemistry Einaga, Yasuaki; Keio University, Chemistry Zhao, Hongying; Tongji University, Department of Chemistry Zhao, Guohua; Tongji University, Department of Chemistry Swain, Greg; Michigan State University, Department of Chemistry Jiang, Xin; Chair of Surface and Materials Technology, Institute of Materials Engineering, University Siegen, Germany,

Conductive Diamond: Synthesis, Properties, and Electrochemical Applications

Nianjun Yang,[†*] Siyu Yu,[†] Julie V. Macpherson,[Δ,*] Yasuaki Einaga,[§] Hongying Zhao,[‡] Guohua Zhao,[‡*] Greg M. Swain,[ǀ] Xin Jiang[†*]

[†] Institute of Materials Engineering, University of Siegen, Siegen 57076, Germany
[Δ] Department of Chemistry, University of Warwick, Coventry, CV4 7AL, United Kingdom
[§] Department of Chemistry, Keio University, Yokohama 223-8522, Japan
[‡] School of Chemical Science and Engineering, Tongji University, Shanghai 200092, China
[ǀ] Department of Chemistry, Michigan State University, Michigan 48824, United States
E-mail addresses: nianjun.yang@uni-siegen.de; j.macpherson@warwick.ac.uk; g.zhao@tongji.edu.cn; xin.jiang@uni-siegen.de;

Abstract: (199 words) Conductive diamond possesses unique features as compared to other solid electrodes, such as a wide electrochemical potential window, a low and stable background current, relatively rapid rates of electron-transfer for soluble redox systems without conventional pretreatment, long-term responses, stability, biocompatibility, and a rich surface chemistry. Conductive diamond microcrystalline and nanocrystalline films, structures and particles have been prepared using a variety of approaches. Given these highly desirable attributes, conductive diamond has therefore found extensive use as an enabling electrode across a variety of fields encompassing chemical and biochemical sensing, environmental degradation, electrosynthesis, electrocatalysis, and energy storage and conversion. This review provides an overview of the fundamental properties and highlights recent progress and achievements in the growth of boron-doped (metal-like) and nitrogen and phosphorous-doped (semi-conducting) diamond and hydrogen-terminated un-doped diamond electrode. Applications in electroanalysis, environmental degradation, electrosynthesis electrocatalysis, and electrochemical energy storage are also discussed. Diamond electrochemical devices utilizing micro-scale, ultramicro-scale, and nano-scale electrodes as well as their counterpart arrays are viewed. The challenges and future research directions of conductive diamond are discussed and outlined. This review will be important and informative for chemists, biochemists, physics, material scientists, and engineers engaged in the use of these novel forms of carbon.

1. Introduction

Carbon is an extraordinary element because of its ability to covalently bond with different orbital hybridizations. This leads to a rich variety of molecular structures that constitute the field of organic chemistry.[1] For millennia, there were only two known substances of pure carbon: graphite and diamond. The carbon atoms in graphite are sp^2 hybridized, with an interplanar C−C bond length of 1.42 Å and interplanar spacing of 3.354 Å. A diamond crystal has a body centred cubic structure. Its carbon atoms are sp^3 hybridized and tetrahedrally arranged with a C−C bond length of 1.54 Å.[2] In the mid-1980s a new carbon allotrope, C60 (or buckminsterfullerene) was discovered by Curl, Kroto, and Smalley who were awarded the 1996 Nobel Prize in Chemistry. C60 possesses a soccer-ball shape.[3] In the early 1990s, carbon nanotubes (CNTs) were discovered.[4] They are direct descendants of fullerenes and contain capped tubular structures composed of 5- and 6-membered rings. The large aspect ratio (length to diameter) and crystalline order along the tubes give CNTs unique properties *e.g.* high conductivity, thermal stability, flexibility, and reactivity, etc.[5] In the early 2000s, graphene, a single sheet of carbon atoms arranged in a hexagonal lattice with a bond distance of 0.142 nm, was reported by Geim and Novoselov[6] who were awarded the 2010 Nobel Prize in Physics. Arising from the semi-metallic band structure, this 2D material features interesting electrical properties and presents many useful applications.[7]

The physical, chemical and electronic properties of these carbon allotropes differ from each other since they are determined by their carbon-carbon covalent bonding and the organization of the carbon atoms in their characteristic micro-structures.[2, 8] For example, the exceptional properties of diamond arise because: (i) carbon atoms are relatively small and light, with short range bonds in the lattice, and (ii) these bonds are covalent, sp^3 hybridized in a tetrahedral arrangement and strong. This results in very high material hardness and thermal conductivity. Diamond also possesses extremely low electrical conductivity unless doped e.g. with boron, to significantly increase conductivity, a key property of the material for any electrochemical application.

The first introduction of diamond into electrochemistry was reported in 1983 by Iwaki et al.[9] who used ion-implanted diamond as an electrode. In 1987 Pleskov et al.[10] explored the photoelectrochemistry of a thin polycrystalline diamond film grown on a tungsten substrate. It was stated[10] that this semi-conductor consisted of more than 99% carbon in the diamond crystalline form containing small amounts of chemical (H, O, N) and phase (non-diamond forms of carbon) impurities. Later Fujishima et al. investigated the photoelectrochemical response of

semi-conducting boron-doped diamond (BDD) films[11] and further applied them as photoelectrodes[12]. The early 1990s saw the emergence of electrically conducting diamond as a new carbon electrode material for different electrochemical applications.[13-19] In 1993 Tenne et al.[13] and Swain et al.[14] employed BDD diamond for electroanalytical applications. The same year Loo et al. showed the advantages of BDD as a stable anode for electrochemical wastewater treatment.[15] Miller et al.[16] and Carey et al.[17] conducted anodic oxidation of organic wastes using dimensionally-stable BDD anodes. In 1996, the wide electrochemical potential windows of high quality BDD were revealed by Angus et al.[20] Work that followed increased in intensity with researchers widely recognizing BDD as an electrode that features extremely interesting electrochemical properties beyond those offered by conventional electrode materials. Over the past four decades, conductive diamond, including BDD, nitrogen-doped diamond (NDD), phosphorus-doped diamond (PDD), hydrogen-terminated undoped diamond, have all been utilized in the various fields of electrochemistry for different applications.[2, 21-30]Among them, BDD has been the most extensively employed due to the fact it can be highly doped. For non-boron-doped diamond films (e.g., NDD, PDD) and un-doped hydrogen-terminated diamond, it is not possible to achieve the high electrical conductivities that can be obtained through boron doping.

This review begins with a general introduction of diamond growth (section 2), focusing on the use of chemical vapour deposition (CVD) techniques to synthesize doped diamond films. The formation of conductive diamond nanostructures *e.g.* by means of top-down, bottom-up, and template-free approaches and the production of conductive diamond particles are briefly overviewed. Starting with the surface properties of conductive diamond (*e.g.*, surface terminations, surface reactivity), section 3 deals mainly with the electrochemical properties of conductive diamond (*e.g.*, background currents, potential window, redox response) as well as the effect of dopants, non-diamond carbon (NDC) presence, crystal structure, and surface terminations, *etc*. on these properties. Section 4 details the applications of conductive diamond in the fields of electroanalysis, environmental degradation, electrosynthesis, electrocatalysis, and electrochemical energy storage. Before closing this review, the fabrication and characterization of diamond electrochemical devices (*e.g.*, small-dimensional diamond electrodes and their arrays, scanning probes, and energy devices) is shown in section 5. To conclude, the technological challenges and future research directions of conductive diamond are discussed and outlined in two areas: the growth of conductive diamond and potential electrochemical applications.

2. Synthesis

2.1 CVD synthesis of diamond films

Artificial diamond synthesis by the high-pressure high-temperature (HPHT) method was first reported in 1955 at General Electric[31] where graphite was converted to diamond. Eversole et al. documented the first report on diamond growth at low pressure.[32] In the early 1970s, a major breakthrough was achieved on the CVD diamond growth process when atomic hydrogen was used during growth. The process also permits the nucleation of new diamond crystallites on non-diamond substrates. This work was extended by e.g. Angus et al. at Case Western University[33-36] and by Deryagin and co-workers at the Physical Chemistry Institute in Moscow.[37-39]

Research into CVD diamond growth started in earnest in the early 1980s, pioneered independently by J. Angus in the USA and by V. Varnin in the USSR. Pioneering work by a Japanese group at the National Institute for Research in Materials at Tsukuba, under the leadership of Setaka described the use of different CVD techniques such as hot-filament CVD (HFCVD),[40, 41] microwave plasma CVD (MWCVD),[42] and radio-frequency plasma CVD (RFCVD),[43, 44] for diamond growth.[32] Such developments initiated the growth of numerous global diamond research programmes ranging from: technique development *e.g.* diamond coating processes, diamond coating on various substrates, *etc.*; a mechanistic understanding of CVD diamond nucleation and growth; doping of CVD diamond; characterization and property investigation of CVD diamond *e.g.*, optical, electronic, thermal, mechanical, *etc.* and applications in the physical, engineering, chemical, biomedical, and related fields.[32, 45]

The growth of diamond from the vapour phase on a non-diamond substrate, at a practical rate, requires a hydrocarbon gas (usually methane) mixed in low concentration with hydrogen. Hydrogen is critical for several aspects of growth, in particular, the abstraction of H from both gas phase methane to produce a growth precursor (radical), CH_3•, and from H-terminated surface sites to produce active radical sites for carbon radical addition. Hydrogen also etches NDC much faster than it does diamond, allowing NDC co-deposits to be removed and a much higher growth rate of diamond to be realized. The gases need to be activated and this is typically done by thermal- or plasma-assisted CVD processes. Although CVD techniques are different in the process details, they do own many common features: (i) diamond growth in the presence of atomic hydrogen, (ii) dissociation of carbon-containing source gases, and (iii) diamond growth at moderate substrate temperatures *e.g.* typically between 500 and 1200 ◦C.[46-48] The majority of

carbon radicals, necessary for growth of the diamond, originate from the dissociation of the carbon-containing gas precursor by means of hot-filament, RF-plasma or microwave plasma, *etc*. The growth substrate can be either bulk diamond (either natural or synthetic) or a non-diamond substrate, leading to homoepitaxial (single crystalline) or heteroepitaxial (polycrystalline) growth of diamond films, respectively. Polycrystalline diamond films consist of crystallites with different orientations and associated grain boundaries, in contrast single crystal diamond has no grain boundaries. Since diamond does not grow spontaneously on non-diamond materials, an extra "seeding" step is usually required for deposition on a foreign substrate. For example, the non-diamond substrate can be decorated with diamond nanoparticles (NPs) that serve as initial nucleation sites for growth. Such diamond seed coated substrates then grow three-dimensionally until the grains coalesce, forming a continuous polycrystalline diamond film. The average grain size of polycrystalline diamond films deposited from hydrogen-rich gas mixtures increases as a function of film thickness, which in turn is controlled by growth time.[49]

Polycrystalline diamond can also be deposited from argon-rich gas mixtures as demonstrated in the pioneering work by Gruen and co-workers at Argonne National Laboratory.[50-57] These films contain varied ratios of diamond (sp^3-carbon) to non-diamond carbon (NDC: sp^2-carbon). This is in contrast with hydrogen rich gas mixtures, where the average grain size of polycrystalline diamond films deposited from hydrogen-rich gas mixtures increases as a function of film thickness or the growth time.[49] The high rate of re-nucleation achieved during argon-rich growth prevents the crystallites from getting larger with growth time. Such films are referred to ultrananocrystalline diamond (UNCD).[51, 58-60] Polycrystalline films are generally classified based on their crystallite or grain size as either microcrystalline diamond (MCD) or nanocrystalline diamond (NCD) and are typically grown under hydrogen-rich atmospheres.[55-57] UNCD films thus have a much higher surface to volume ratio than their microcrystalline counterparts and more extensive π-bonding and sp^2 hybridization given the higher NDC content of this material, typically residing in grain boundaries. These films also possess intrinsic electrical conductivity due to the π-states in the bandgap[47, 48] and is a reason for why un-doped UNCD films find use in some electrochemical applications. Polycrystalline diamond films deposited from Ar-rich source gas mixtures are not faceted but rather possess a nodular morphology with negligible crystal faceting. Theoretical results suggest that the nanocrystalline morphology results, at least in part, because of a high rate of re-nucleation due to the C_2 dimer produced during CVD processes using Ar-rich source gas mixtures.[50-57] These UNCD films are very different morphologically and microstructurally from NCD films as the UNCD films possess a smaller

grain size, more grain boundaries.

2.2 Doping of CVD diamond films

Diamond with metal-like conductivity is generally required for most electrochemical applications. Controlled doping is accomplished by the addition of appropriate elements (*e.g.*, boron, nitrogen, or phosphorous) during CVD growth. The substitutional insertion of these non-carbon elements imparts an electrical conductivity to the diamond, the characteristics of which depend on the dopant and level of doping. At low doping levels, $\leq 10^{19}$ atoms cm^{-3}, the diamond behaves electrically and electrochemically as a *p*- or *n*-type semiconductor, depending on the dopant type. It is the substitutionally inserted impurity atoms that contribute to the electrical properties. Dopant atoms can also be segregated in the grain boundaries but these are generally not electrically active. For this reason, actual doping levels measured are higher that determined carrier concentrations. At high doping levels, $\geq 10^{20}$ atoms cm^{-3}, the material behaves as a semi-metal and possesses high electrical conductivity.

Phosphorous,[61] sulphur and arsenic,[62] boron and nitrogen[63] have all been reported as dopants for diamond. Among them, boron and then nitrogen are the most widely accepted, and used to produce *p*- and *n*-type conductive material, respectively, although it is only boron that can added in high enough concentrations to achieve metal-like conductivity due to the small atomic radius of boron. Boron-doped MCD, NCD, and UNCD have all been used in electrochemistry.[64] Electrochemical properties of boron-doped UNCD are similar to those of boron-doped MCD and NCD films.[55-57] The source of boron is generally gas-phase diborane or trimethyl borane, diluted in hydrogen. Since boron is electron-deficient relative to carbon, the doping level of such a *p*-dopant can be in the range of 10^{18} - 10^{21} atoms cm^{-3}, which corresponds to a boron-to-carbon ratio of about 10^{-5} to 10^{-3}. When the doping level reaches values higher than 10^{20} cm^{-3}, the conduction mechanism of these heavily doped films changes and the activation energy approaches zero.[65] Therefore, these films are the most suitable as electrodes for electrochemical applications, and feature predominantly in this review.[66]

When diamond films, containing very large concentrations of boron to carbon (>0.25%) are cooled to below -200 ºC, they are shown to offer no resistance to the flow of electricity *i.e.* they are superconducting.[67] Such superconductivity was for the first time discovered on metal-like polycrystalline BDD synthesized at pressure (8-9 GPa) and temperature (2500-2800 K) by Ekimov et al.[68, 69] with a superconducting transition temperature (T_c) of 4 K. Kawarada et al.

recorded the highest T_c (= 7.4 K) using single crystal (111) BDD; T_c = 3.2 K for (100) BDD.[70-75] Currently, the superconductivity of BDD is mostly of academic interest as the temperature at which it becomes superconducting is very low. However, there are some detectors such as astronomical detectors and devices like the Superconductive Quantum Interference Device (SQUID) for the detection of very small magnetic fields that makes use of this property of BDD could have real world applications in the future.[76]

Other doped diamond films have been synthesized. For example, NDD films were grown using a HFCVD process and their conductivity was recorded to be several mS cm^{-1}, tens to hundreds of times higher than that for metal-like BDD.[77] Nitrogen-doped UNCD films have been grown on silicon[78, 79] or titanium substrates using plasma-assisted CVD.[80] Nitrogen diluted with the mixture of methane, argon[78] or hydrogen,[79, 80] or with triethylamine dissolved in the methanol[81] are generally used as nitrogen sources. Recently, hot-cathode-direct-current plasma CVD (HCDCPCVD) has been used to grow NDD films, achieving a maximum electrical conductivity of 5 S cm^{-1}.[82] The PDD films have been grown on IIa type single crystalline diamond[83] and *p*-type Si substrates.[84] The measured phosphorus concentrations were 7.4×10^{18} and 1.8×10^{18} cm^{-3}, respectively. In both cases, plasma-assisted CVD was used. The source of the phosphorus dopant, carbon, and carrier gas were phosphine, methane, and hydrogen, respectively. Note that, doping levels of nitrogen, phosphorous, and sulphur into diamond films are not high (generally $<10^{19}$ atoms cm^{-3}). Thus, the electronic properties of such diamond films are semiconducting at best. However, the measured electrical conductivities (and resulting electrochemical behaviour) suggest higher doping, which is not possible, and indicates other factors such as NDC and hydrogen content (sections 3 and 4), playing a role.

Finally, it is important to note un-doped diamond substrates emerge from the CVD growth chamber hydrogen terminated due to the hydrogen rich growth atmospheres terminating the dangling bonds on the diamond surface with hydrogen atoms.[47, 48] The as-grown hydrogen-terminated un-doped CVD diamond shows *p*-type surface-induced conductivity once it is immersed into electrolyte solutions (section 3.1).[85, 86]

2.3 Conductive-diamond nanostructures

Various conductive-diamond nanostructures (*e.g.*, nano-pillars, nanowires, pores, foams, *etc.*) have been fabricated using top-down, bottom-up, and template-free approaches.[23, 87, 88] In the top-down approach, BDD is selectively etched away with reactive ions through a hard mask. Applied etching gas (*e.g.*, O_2), etching masks (*e.g.*, size, shape, *etc.*), and the etching conditions (*e.g.*,

temperature, gas atmosphere, pressure, power, time, *etc.*) determine the sizes, lengths, and densities of the as-fabricated nanostructures. Various mask materials (*e.g.*, Al, Au, Ni, Mo, polymers, oxides, nitrides, and diamond nanoparticles, *etc.*) have been used. In the bottom-up approach, diamond nanostructures are produced by the CVD overgrowth of the patterned templates with MCD, NCD or UNCD films. In this way, various diamond nanostructures (*e.g.*, vertically aligned wires, diamond foams, porous membranes, *etc.*) have been formed. Silicon nanowires, CNTs, silicon oxide spheres and highly porous polypyrrole scaffold have been employed as templates.[23, 87, 88] A variety of template-free techniques have also been used. For example, selective and wet-chemical removal of cubic SiC from a diamond-SiC composite film to produce diamond networks.[89] Porous BDD has been formed by (i) thermal etching of diamond *via* a two-step process: graphitization of the BDD film surface by heating in an argon atmosphere at 1000°C followed by removal of the graphitic layer by oxidation in air at 425 °C[90] and (ii) oxidative etching of BDD electrodes within steams or CO_2.[91-93] **Figure 1A** shows typical examples of BDD nanostructures including diamond networks,[89] diamond paper,[94] diamond honeycomb,[95] porous diamond,[96] and diamond nanowires.[97]

Several conductive NDD nanostructures have also been synthesized. For example, NDD nanowires were grown on planar Si substrates using a MWCVD method in which methane (6%) and nitrogen (94%) were the sources of carbon and nitrogen dopant, respectively.[98] NDD microwires and vertically-aligned NDD arrays were produced by overgrowing on titanium alloy microneedles[99] and Si wires[100]. NDD nanorods were fabricated *via* direct reactive ion etching of nanocrystalline NDD films, grown using the MWCVD technique **(Figure 1B)**.[101]

2.4 Conductive diamond particles

Detonation processes using explosive molecules and graphite precursors have been widely applied to produce NPs or powers of diamond. The resulting diamond is called detonation nanodiamond (DND) and has a core-shell structure **(Figure 1C)**.[102] The sp^3 diamond core features a size of 4-5 nm, while the outer shell consists of a mixture of sp^2 and sp^3 carbon as well as oxygen-containing functional groups (*e.g.*, carboxylic acids, esters, lactones, quinones). BDD particles can be produced *via* a core shell approach, which is overgrowth of a substrate powder *e.g.* glassy carbon (GC) or insulating diamond powders with an overlayer of BDD.[103-107] For example, the resulting surface area of the conducting powders can be varied from a few to 100's $m^2\ g^{-1}$ by simply reducing the diameter of the substrate powders. To date, diamond abrasive powder (nm to μm diameters)[103-106] and GC powder[107] have been over-coated with boron-doped

UNCD. A range of carbon nanostructures can, in fact, be produced through adjustments in the source gas ratio (*e.g.*, methane to argon or hydrogen) at constant power (*e.g.* 800 W) and system pressure (*e.g.*, 120-140 torr). For example, various nanostructured carbons have been produced ranging from boron-doped UNCD-coated (using a 1% ratio methane) and graphene nanopetal-coated (when using higher methane levels, 3-5%) GC powders. **Figure 1C** shows SEM micrographs of boron-doped UNCD- and nanopetal-coated GC powders. The GC substrate powder is 5 μm in diameter. The boron-doped UNCD phase readily nucleates and grows directly on carbon substrates that are microstructurally disordered at the surface with a high fraction of exposed graphitic edge plane, such as GC[107] The edge plane sites serve as the initial nucleation sites for diamond growth.[107] UNCD (cauliflower-shaped features) can be observed over-coating the powder surface. The 50-100 nm nodular features present are aggregates of diamond grains that are in the 5-10 nm range. The specific surface area of this coated material is 2-5 m^2 g^{-1} and the electrical conductivity is 2-5 S cm^{-1}. The graphene nanopetal phase can be seen on the surface of the GC powders. The nanopetals are graphitic carbon and they decorate the surface with lengths of several hundred nanometers and heights of several tens of nanometers.[107]

BDD powders can also be produced by milling of BDD films. BDD films were synthesized under HPHT using B-doped graphite intercalation compositions as carbon sources.[23, 108] Recently, small-sized BDD particles (10-60 nm) were produced by multistep milling of nanocrystalline BDD films, followed by purification and surface oxidation.[109]

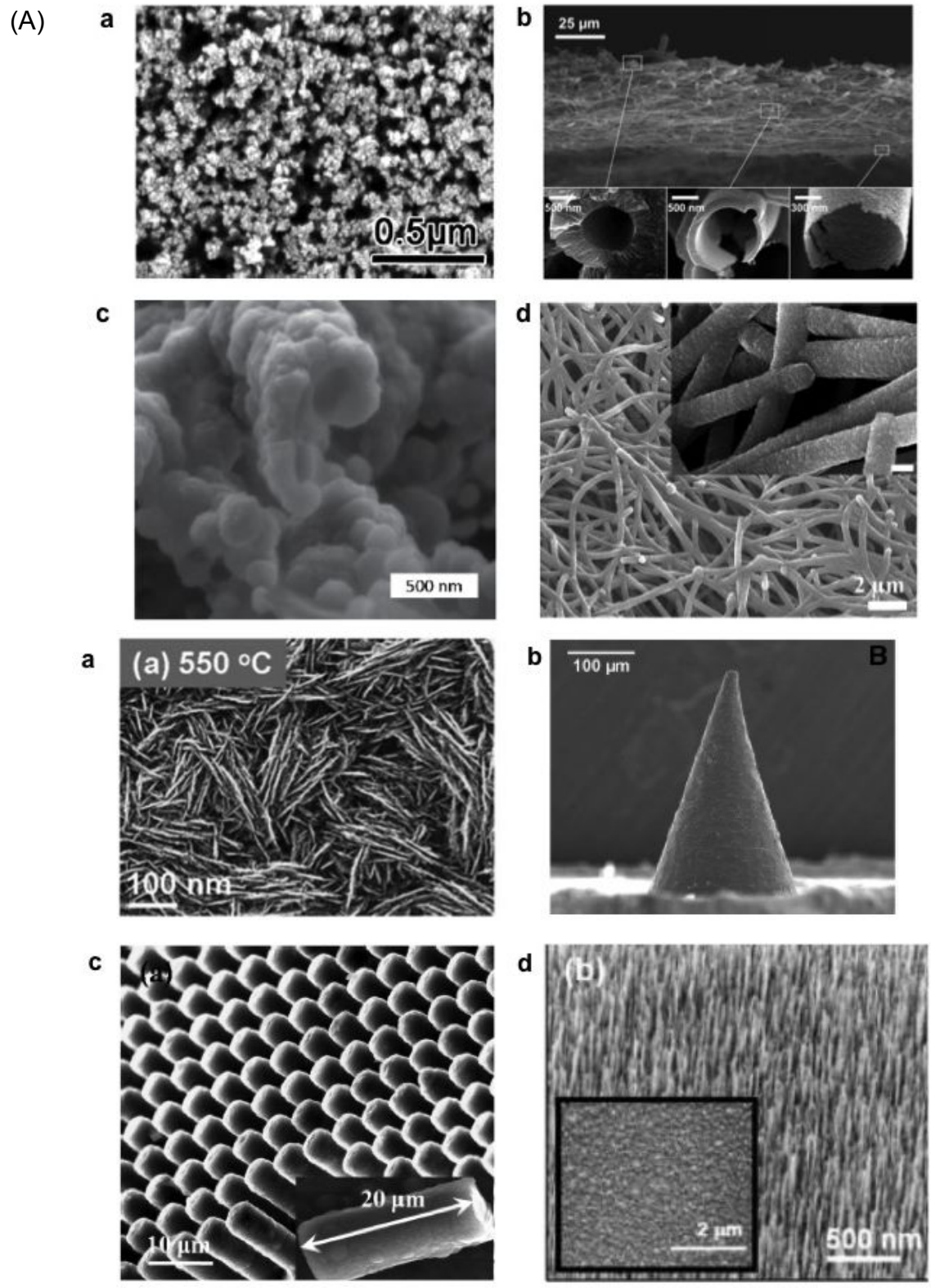
(A)
a
0.5μm
b
25 μm
500 nm
500 nm
300 nm
c
500 nm
d
2 μm
a
(a) 550 °C
100 nm
b
100 μm
B
c
(a)
20 μm
10 μm
d
(b)
2 μm
500 nm

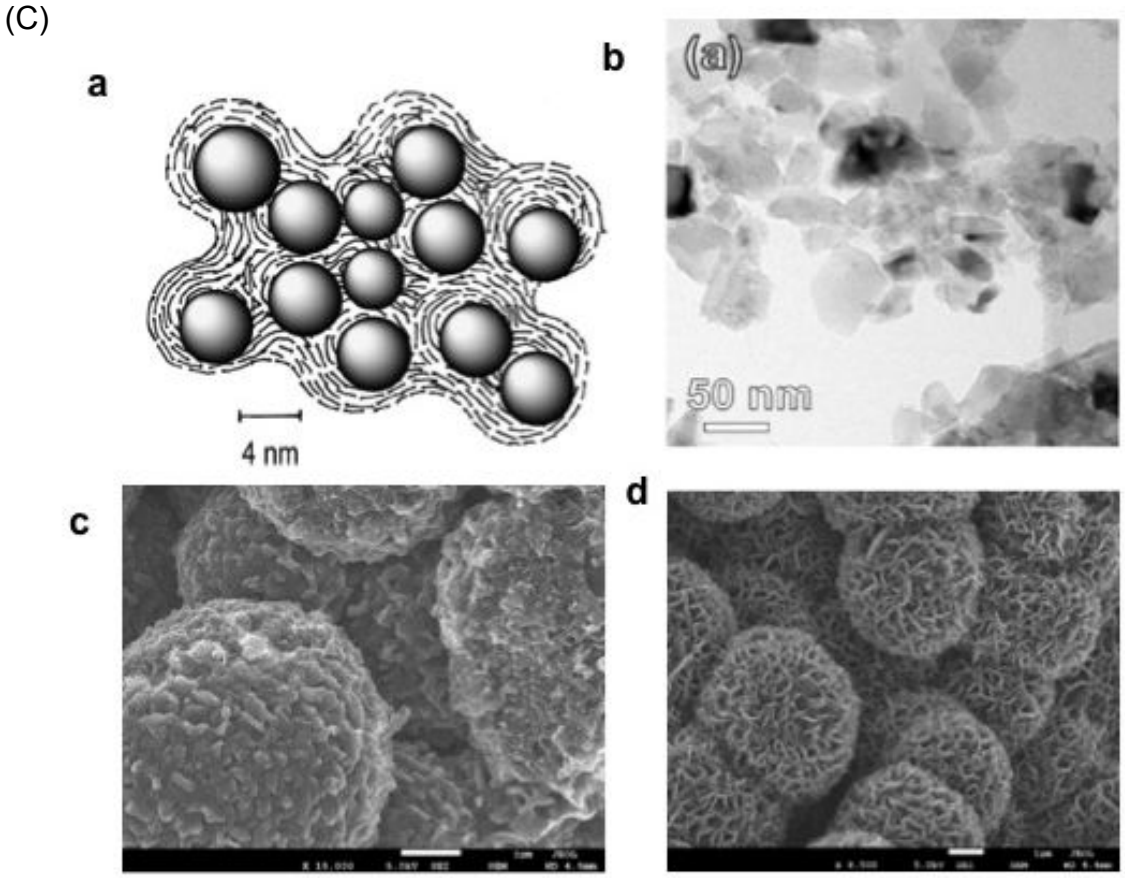

Figure 1. (A) SEM or TEM images of diamond networks (a),[89] diamond paper (b),[94] porous diamond (c),[96] and diamond nanowires (d).[97] Reprinted with permission from ref. [89]. Copyright 2017, American Chemical Society; from [94]. Copyright 2016, American Chemical Society; from ref. [96] Copyright 2017, Elsevier; from ref. [97]. Copyright 2016, American Chemical Society. (B) SEM or TEM images of NDD nanowires (a),[98] vertically aligned NDD microwire arrays (b,c),[99,100] and nanorods (d).[101] Reprinted with permission from ref. [98] Copyright 2013, Royal Society Publisher; from ref. [99]. Copyright 2015, Elsevier; from ref. [100] Copyright 2014, Elsevier; from ref. [101] Copyright 2017, Elsevier. (C) schematic plot of the structure of NDD (a).[102] Reprinted from ref. [102]. Copyright 2005. Elsevier. TEM or SEM image of BDD nanoparticles (b). Reprinted with permission from ref [109]. Copyright 2014. American Chemical Society. SEM micrographs of (c, left) boron-doped UNCD deposited on GC powder 5 μm in diameter. (15,000×). Reprinted with permission from ref [107]. Copyright 2009. American Chemical Society. (d, right) graphene nanopetals formed on GC powder (9500×). The boron-doped UNCD phase was formed using 1% methane and the nanopetal phase was formed using 3% methane in the source gas mixture. The white scale bars in both images are 1 μm in dimension. Reprinted with permission from ref [107]. Copyright 2009. American Chemical Society.

3. Properties

In comparison to other widely employed carbon electrode materials, conductive diamond features multiple unique physical and chemical properties.[2, 110, 111] For example, it is chemically inert, does not swell in electrolyte solutions, and is biocompatible. Weak or no surface bio-fouling has been reported on conductive diamond surfaces. Moreover, it exhibits high chemical stability in harsh environments, at high current densities and potentials. It is ultrahard and thus can be textured with dimensions of typically a few nanometers[112-114] to nanowires with lengths of a few micrometers.[115] In section 3.1, further details regarding surface termination, surface reactivity, and electrochemical properties of conductive diamond are provided. The experimental effects of dopants (in particular boron), NDC content, crystal structure, and post-treatment are also reviewed. The vast majority of the discussion will be focused on BDD, given its wide spread use as an electrode material.

3.1 Surface termination

The diamond surface can be terminated in various ways originating from its rich carbon chemistry. Once the surface atoms of diamond are fully bonded with hydrogen, the surface is hydrogen-terminated (or hydrogenated). It features hydrophobic properties where water contact angles are as high as ~90°. Such a hydrogen-terminated surface ($–C^{\delta-}–H^{\delta+}$) raises both the energy levels of the valence band (E_{VB}) and conduction band (E_{CB}) of diamond at the surface. Since E_{CB} sits above the vacuum level, a negative electron affinity develops. Once the hydrogen-terminated diamond is immersed in aqueous solutions, electron transfer between H_3O^+ and E_{VB} becomes possible (even without doping). A positively charged accumulation layer is formed near the surface leading to a measurable surface conductivity on insulating diamond, as explained by the surface-transfer doping model.[86] A hydrogen-terminated diamond surface can be achieved by different approaches such as hydrogen plasma treatment and cathodic electrochemical treatment (*e.g.*, application of -35 V for 5 min in 2 M hydrochloric acid solution).[116] Although a hydrogen-terminated BDD surface is generally stable in air or in solutions for several months, it does slowly oxidize over time in air or *via* exposure to solution.[117, 118]

When a hydrogen-terminated diamond surface is partially or fully oxidized, the surface becomes hydroxylated or oxygen-terminated (or oxygenated), respectively. The oxygen functional groups are a mixture of –OH, -C-O-C, -C=O, and =C=O.[116] An oxygen-terminated surface ($C^{\delta+}–O^{\delta-}$) has an opposite bond polarity compared to the hydrogen-terminated one ($–C^{\delta-}–H^{\delta+}$) that typically lowers the energy levels relative to the vacuum level. This results in a positive electron affinity.

Oxygen-terminated diamond surfaces are hydrophilic with water contact angles from 0.6° to 65°, depending on the oxidation method, surface roughness, and dopant level, etc.[119] A variety of methods have been used to oxygen terminate diamond surfaces, such as wet-chemical treatment (e.g., boiling in acids or acid mixtures),[120] dry-chemical oxidation (*e.g.*, photochemical or ozonation oxidation,[121] treatment in O_2 at high temperatures[122]), mechanical treatment (*e.g.*, alumina polishing),[123] plasma treatment (*e.g.*, O_2),[57, 124] and electrochemical oxidation.[116, 124-127] On single crystalline diamond, specific crystal faces support specific oxygen functionalities. For an oxygen-terminated single crystal diamond, C–OH groups are the most abundant on the (111) face. The C–O–C and -C=O (and more highly oxidized) groups dominate on the (100) face.[128]

The diamond surface can be also terminated with halogens (*e.g.*, -F, -Cl, *etc.*)[129-132] These halogenated diamond surfaces are hydrophobic: a controversial phenomenon known as polar hydrophobicity. Halogenation with fluorine and chlorine is possible by activating a halogen gas to form free radicals (*via* high temperature or ultra-high vacuum conditions). A milder approach is to employ ultraviolet (UV) photochemical activation in the presence of the halogen gas.[133] The Cl-terminated surface is not very stable in air and readily converts to an oxygen-terminated surface. Furthermore, nitrogen (*e.g.*, -N, -NH, $-NH_2$) terminated diamond surfaces (in most cases so-called aminated surface) have been realized directly using a plasma in the presence of ammonia.[134-136]

X-ray photoelectron spectroscopy (XPS) and contact angle measurements are frequently employed to characterize the diamond surface chemistry.[57] From the related binding energies for different carbon bonds (*e.g.*, C-O-C, C=O, C-F, C-Cl, C-N, *etc.*), XPS is especially useful for semi-quantitative characterization of hydroxylated, oxygenated, halogenated, and aminated diamond surfaces.[57, 127] However, XPS cannot deliver quantitative information on hydrogen-terminated diamond surfaces.[116, 137, 138] Electrochemical techniques (*e.g.*, voltammetry, impedance)[116] and selective grafting of diazonium salts[137, 138] have also been employed as indirect ways to characterize the hydrogen-terminated diamond surface.

3.2 Surface reactivity

A variety of functionalization strategies have been used to chemically modify conductive MCD, NCD and UNCD surfaces. In general, the functionalization routes are of four types: chemical, photochemical, thermal, or electrochemical.[139-143] These functionalized surfaces can be used directly in electrochemical measurements or be further functionalized with target moieties

depending on the desired application.

Photochemically, UV irradiation of hydrogen-terminated diamond covered with a liquid film of the appropriate alkene (one end vinyl terminated, the other end terminated appropriately for the application of interest, *e.g.* amine,[144] carboxylate,[145]) has been employed for grafting organic layers to the diamond surface *via* a C-C bond.[146] Direct amination of the hydrogen-terminated surface is also possible using UV treatment in the presence of a long chain end group protected amine (UV only).[147] Chemically, amino-silane groups can be produced by reacting oxygen terminated diamond with 3-aminopropyltriethoxysilane (APTES). Thermally activated formation of alkene-derived self-assembled monolayers has been also realized on oxygen-terminated diamond surfaces: hydrogen-terminated diamond sites remained unaffected during such a process. This approach is thus complementary to the UV-initiated reaction of alkenes with diamond, which only goes *via* the hydrogen-terminated surface.[143] Electrochemically, reduction of diazonium salts on BDD electrodes is also useful.[112, 113, 148, 149] For example, primary amines and aromatic hydrocarbons (aryl diazonium salts) have been grafted to the diamond surface using this procedure. The diazonium modification can produce monolayer or multi-layer coverage, if continued radical addition is allowed to occur. The grafting efficiency has also been linked to the boron dopant density of the electrode.[150] Diazonium modification is versatile and can be used to introduce a wide variety of functional groups (*e.g.*, –COOH, X, NO_2, *etc.*) onto the electrode surface.[137, 151]

3.3 Electrochemical Properties

BDD exhibits unique electrochemical properties and thus presents many advantages for use over classical metal electrodes and other sp^2 carbon electrodes. These include low and stable background currents, wide electrochemical potential window, weak molecular adsorption, microstructural stability, and relatively rapid electron transfer (ET) kinetics for multiple soluble redox systems often without electrode pretreatment.

3.3.1 Background current

The background current (capacitive and surface reactivity) of BDD is low in both aqueous and non-aqueous electrolyte solutions.[152] For a boron-doped NCD film with a boron-doping level of 5×10^{20} cm^{-3}, the capacitance is about 4 - 7, 14 - 20, and 11 - 15 μF cm^{-2} in aqueous, organic, and ionic liquids, respectively.[153] The lower capacitance values compared with sp^2 carbon electrodes such as GC, arise from the lower density of potential-dependent electronic states[154] and the

absence of pseudocapacitance from electroactive surface carbon-oxygen functional groups.[155] The background current of BDD is also stable in both aqueous and non-aqueous solutions.[82,153] Low and stable background currents are attractive properties that lead to improved signal-to-background and signal-to-noise ratios in electroanalytical measurements (section 4), which in turn lead to improved detection sensitivity, limits of detection and response reproducibility.

3.3.2 Potential window

BDD electrodes exhibit a wide electrochemical potential window. The potential window is arbitrarily determined based on the selected anodic and cathodic current density used. There is no standard convention, but the values used should be stated. When a current density of 1.0 mA cm^{-2} is selected to define the potential window, a potential window of 3.2 V in aqueous solutions (*e.g.*, 0.5 M H_2SO_4),[156] 4.6 V in organic solutions, and 4.9 V at room temperature ionic liquid[157] have been obtained for single crystal BDD (boron concentration of 2×10^{20} cm^{-3}). The wide potential window of BDD arises from the high overpotentials for solvent *e.g.* water decomposition. Focusing predominantly on water, as a highly used solvent system in electrochemistry, the hydrogen evolution reaction (HER) and oxygen reduction reaction (ORR) are inner-sphere "surface sensitive" reactions.[128] Here the kinetics of ET are very sensitive to adsorption of reactants, products or their intermediates (*e.g.*, $^{\bullet}H$) at the electrode surface. As BDD is a poor adsorbent, its catalytic effect toward these reactions is rather weak. In short, within the potential window when the solvent is stable, BDD is suitable for the investigation of different electroactive substances dissolved in the solvent.[158]

NDD and BDD electrodes grown by HFCVD showed similar electrochemical potential windows.[77, 82] As the NDD was semi-conducting, it was thought that NDC impurities present in the electrode were responsible for the solvent window similarity. *In situ* Raman spectroelectrochemical measurements showed that subsequent progressive cycling between -2.5 and 2.5 V (*vs.* Ag/AgCl) electrochemically removed these electrocatalytic impurities, leading to an increase of the potential window.[84] This study also highlighted the need to understand the material surface composition when interpreting the electrochemical response of the electrode.

3.3.3 Redox activity

BDD electrodes are frequently characterized using different redox probes, including aqueous (*e.g.*, $Fe(CN)_6^{3-/4-}$, $Ru(NH_3)_6^{2+/3+}$, $IrCl_6^{2-/3-}$, $Fe^{2+/3+}$, $Ce^{3+/4+}$, $Eu^{2+/3+}$, 4-tert-butylcatechol, methyl viologen, *etc*.) and non-aqueous (*e.g.*, ferrocene) redox systems.[159] Different electrochemical

behavior has been observed for different BDD diamond films and redox probes. In the early days of BDD electrode research, this variability was largely due to differences in material quality produced in different laboratories. Nowadays, boron-doped MCD and NCD films are commercially available from multiple vendors and the general electrochemical behavior of these electrodes is fairly reproducible.[60] Key factors that affect the diamond electrode response for redox analytes are (i) the dopant type, concentration and distribution, (ii) the surface termination and (iii) adventitious NDC phases, as discussed in greater detail in section 3.3.4. All must be taken into account when interpreting the electrochemical response, along with consideration of the choice of redox probe(s) *e.g.*, is it surface insensitive, surface sensitive to surface termination and NDC phases, *etc*.[128]

The surface roughness differences of microcrystalline and nanocrystalline film does not generally affect diffusion-limited currents for redox analytes at conventional scan rates as the diffusion layer thickness is greater than the roughness dimensions.[128] For example, the voltammetric behavior of $Fe(CN)_6^{3-/4-}$ and $Ru(NH_3)_6^{2+/3+}$ recorded on polycrystalline BDD appears similar to that on a GC or platinum electrode,[160] exhibiting close to reversible characteristics (diffusion-limited). This is true for $Fe(CN)_6^{3-/4-}$ if the diamond electrode surface is clean, and presents a specific oxygen functionality.[60, 161] Heterogeneous electron-transfer (ET) rate constants for a variety of aqueous redox probes are in the 10^{-3} to 10^{-1} cm s^{-1} range.[60, 161] These rate constants were determined from cyclic voltammetric ΔE_p – scan rate trends and digital simulation where ΔE_p is the potential difference of obtained anode oxidation wave from cathodic one.

When using techniques such as scanning electrochemical microscopy (SECM)[154] or fourier transformed alternating current voltammetry,[162] which can more accurately determine high ET rate constants, it has been found that the outer-sphere redox probe, $Ru(NH_3)_6^{2+/3+}$, with a standard redox potential close to the valence band position of BDD, has a heterogeneous ET rate constant about an order of magnitude smaller on BDD than GC.[154, 162] This has also been observed for tetrathiafulvalene oxidation and tetracyanoquinodimethane reduction in acetonitrile solution, where the kinetics of ET were found to be ~ an order of magnitude smaller compared to Pt, Au and GC electrodes.[163] Although BDD is a *p*-type semi-conductor degenerately doped to behave metal-like, the number of available charge carriers at each energy state is less than that of a typical metal and will decrease as the standard redox potential for the redox couple becomes more negative. $Ru(NH_3)_6^{2+/3+}$ is also a very useful redox probe for also distinguishing between

conducting and semi-conducting BDD, as the kinetics of ET are strongly retarded for a semi-conducting electrode.[154, 162]

For inner-sphere redox probes that typically undergo ET through some surface interaction, more sluggish ET kinetics are observed on BDD as compared to sp^2 carbon and metal electrodes (*e.g.*, Au, Pt).[60, 161] This behavior reflects the decreased electrocatalytic activity of a BDD surface. Researchers have also studied un-doped hydrogen-terminated diamond electrodes in which the conductivity arises from subsurface hydrogen charge carriers *via* surface-transfer doping. More sluggish ET voltammetric kinetics are observed, as compared to BDD,[164] due to a very limited number of electronic states in the un-doped material available to support the charge transfer.

Minimal electrochemical work has been undertaken on alternatively doped diamond electrodes, with adventitious NDC often being unaccounted for. On semi-conducting NDD films with a microstructure resembling ridges (only few nanometers in width), $Fe(CN)_6^{3-/4-}$ showed quasi-reversible behavior with well-defined redox peaks and a ΔE_p of as low as 80 mV.[79, 165] On an anodically pretreated semi-conducting PDD film with a phosphorus-concentration of $\sim 7.4\times10^{18}$ cm^{-3}, *n*-type diode behavior was found in $Ru(NH_3)_6^{2+/3+}$ solutions, due to the electrical characteristics of this material.[84]

3.3.4. Impact of material properties

Many material properties affect the electrochemical behaviour of a conductive diamond electrode, the key ones include dopants, NDC presence, crystallographic structure and electrode surface termination, discussed below (*e.g.*, capacitive current, potential window, redox response). For example, the electrochemical potential window of the electrode will depend on the solvent and electrolyte employed, the dopant-concentration, the surface termination, and the presence of NDCs. Before interpreting the electrochemical properties it is important the material properties of the diamond electrode are understood, along with their corresponding impact on the electrochemical response. These include (i) dopant type, concentration and distribution, (ii) the surface termination, (iii) adventitious NDC phases and (iv) crystallographic structure. Importantly, the appropriate redox probe(s) (*e.g.*, surface insensitive, surface sensitive to surface termination and NDC phases) or outer sphere species needs to be judiciously selected when assessed the conducting diamond electrode activity and properties. In the following sections, some of the variable issues that affect the electrochemical properties of conductive diamond are reviewed.

3.3.4.1 Dopants

An increase of the boron dopant concentration typically has been found to increase the measured capacitance of BDD electrodes, most likely due to an increasing density of states (DOSs).[123] A concomitant decrease in the apparent potential window has also been observed most likely due to a reduction in the ohmic resistance of the electrode. Contrary to most trends in the literature, researchers reported that an increase in the nitrogen leads to a wider window for nitrogen doped UNCD electrodes.[165]

For boron, doping levels above the metallic threshold of ~10^{20} cm^{-3}, render the conductive diamond semi-metallic (metal-like). Such electrodes are usually the best performing in electrochemical measurements. As the doping level drops below that for metallic doping (~ 10^{20} B atoms cm^{-3}), more irreversible behavior is observed for redox probes *i.e.* sluggish ET kinetics;[66] with the response being very much redox couple dependent in this semi-conducting regime. This is due to a decrease in the density of electronic states available to support the charge transfer reaction. Hence it is important to know whether the material is metal-like or semi-conducting when interpreting the redox behavior. Interestingly, an opposite trend was observed on semi-conducting nitrogen doped UNCD electrodes. An increase in the nitrogen content led to more sluggish ET kinetics for $Fe(CN)_6^{3-/4-}$.[165]

3.3.4.2 Non-diamond carbon impurity

In the early days of diamond electrode work, BDD films were of comparatively low quality, containing significant NDC impurities and containing boron doping levels below the metallic threshold. NDC presence often resulted in the material appearing more electrically conductive than it actually was. This impurity contributed to the electrical conductivity of the materials. Present day BDD diamond electrodes are largely devoid of NDC impurity phases, unless grown in UNCD form, although it is still challenging to grow NDC-free BDD, when the boron levels are so high. There has been work to determine the role of NDC on ET kinetics, capacitance and molecular adsorption. Surface insensitive redox probes, such as $Ru(NH_3)_6^{3+/2+}$, are largely unaffected by NDC impurity phases at the electrode surface, whillst others such as oxygen and dopamine are strongly affected.[166, 167] While these impurity phases can be influential, early work with BDD revealed that the electrochemical activity of these films was not due exclusively to NDC presence.[166, 167]

The presence of NDC thus changes the way the electrode behaves towards different redox systems, especially those that are surface sensitive. In general, the more NDC present, the higher the electrochemical (catalytic) activity of the electrode,[123, 166] An increase of the NDC content in conductive diamond resulted in more facile ET kinetics for certain inner sphere redox couples, suggesting that NDC forms active or electrocatalytic sites at the BDD surface.[128, 165, 166, 168] Although it has been shown BDD diamond electrodes with higher levels of NDCs are favourable for electrochemical pollutant degradation,[169] they exhibit reduced detection limits for target compounds in electroanalysis as well as potentially a greater susceptibility to fouling.[170] Qualitatively, the relative ratio of the peak intensity of the sp^3 carbon (s bonds) to that of the sp^2 (NDC) carbon (G bonds) is often estimated by means of Raman spectroscopy to assess NDC content and hence BDD quality. However, as this method is not truly surface sensitive, electrochemical means are now being adopted *via* analysis of the quinone electrochemical response associated with NDC.[166, 167, 171, 172] Capacitance-wise, the capacitance of NDD and PDD films are generally larger than that for BDD films, even though the dopant levels are much lower in the former. The reason for this is their higher NDC content. In general, the more NDC present, the higher the electrochemical (catalytic) activity of the electrode.[123, 166]

The NDC content in conductive diamond can be enhanced with an increase of doping levels as well as thickness of diamond film, unless the growth process is very carefully controlled, leading to enlarged capacitance currents, reduced potential windows, and facile ET processes of surface sensitive redox probes. NDC impurity phases have been removed from conductive diamond by post-treatment (*e.g.*, mechanical polishing, wet-chemical boiling in the heated mixture of concentrated acids, electrochemical burning at high voltages in acidic solutions).[84, 128, 173] For example, a very convenient pretreatment for significantly reducing removing the NDC is impurity is a 30 min immersion in 30% H_2O_2 at ~50 ^oC followed by a short (30 min) MW or RF treatment in H_2 to re-hydrogenate the surface.

3.3.4.3 Crystal structure

Single crystal BDD electrodes are still in their infancy compared to polycrystalline BDD, as such measurements are often made on lower doped, semiconducting BDD electrodes, leading to low reported ET rate constants for different redox analytes. Furthermore, comparisons are often made between different crystal faces, and not always is account made for the difference in boron dopant densities. For example, it is well known that different diamond crystal planes take up

boron differently, hence growing a (111) face under the same reactor conditions as a (100) face will lead to ~ an order of magnitude difference in the boron dopant density.[174, 175] This difference in doping density (acceptor concentration) has led to faster reported ET kinetic rates for $Fe(CN)_6^{3-}$ reduction on (111) as compared to (100).[175] Whereas for (111) and (100) BDD crystals grown with similar dopant densities, the ET kinetic rates for $Fe(CN)_6^{3-/4-}$ were found to be similar.[174, 175]

For MCD, NCD, and UNCD films all feature different grain sizes, surface roughness, and NDC contents. Larger grain sizes are seen on thicker films. On rougher surfaces, higher absolute capacitive currents were obtained due to the increased enlarged surface areas. More facile ET processes were also obtained.[176]

3.3.4.4 Surface termination

As discussed above, pretreatment of conductive diamond can be used to alter the electrode surface termination, which in turn can affect the electrochemical response. For example, hydrogen-terminated BDD has a lower voltammetric background current and capacitance as compared to the oxygen-terminated counterpart,[83, 84] which can impact the ET kinetics of surface sensitive (inner sphere) redox couples.[128, 177]

Surface termination changes also affect the wetting properties of the electrode, which in turn effects electrolyte organization at the electrode-electrolyte interface. The polarity of the surface bond results in electrostatic interactions that can raise or lower E_{VB} and E_{CB}.[128] For redox systems such as $Ru(NH_3)_6^{2+/3+}$, methyl viologen, chlorpromazine, and ferrocene characterized by outer-sphere ET pathways, ET kinetics are relatively insensitive to the physicochemical properties of BDD, provided the material is doped above the metallic threshold. In contrast, for the redox couple of $Fe(CN)_6^{3-/4-}$ that proceeds *via* a surface-sensitive route, its ET kinetics are more sensitive to the surface termination of BDD.[159]

In addition, simply changing the method of oxygen termination can influence the ET kinetics. This is because different oxidation approaches generate different types and densities of oxygen functional groups on the BDD surface, as confirmed by XPS in the majority of most cases. For example, alumina polishing of microcrystalline BDD promoted near reversible ET rates for $Fe(CN)_6^{4-/3-}$,[123] whilst anodic polarization resulted in a significant reduction in ET kinetics.[126]

In the past, $Fe(CN)_6^{4-/3-}$ has been employed as a redox couple to assess the viability of a BDD material for electrochemical measurements.[66] However, given its sensitivity to surface termination, a redox system such as $Ru(NH_3)_6^{2+/3+}$ is more reliable. This is because it is outer sphere, and thus surface insensitive and can further provide insight as to whether the material is suitably doped with minimal ohmic resistance, the first key step for the electrochemist wanting to use a BDD electrode.[128]

4. Electrochemical applications

BDD presents many advantages for use over classical metal electrodes and other sp^2 carbon electrodes due to carbon atom arrangement, electronic properties, and nanoscale structures. For example, CNT materials used for electrochemistry are generally complex "ropes" consisting of bundles of nanotubes of various sizes.[178, 179] Graphene itself is challenging to prepare for electrochemical applications, and graphene layers which stack together are more common, leading to the loss of some of the unique properties of graphene itself.[180, 181] Therefor, BDD has been extensively utilized in different electrochemical applications.

4.1 Electroanalysis

BDD has found widespread use as an electrode in electroanalytical applications because of its highly favourable properties.[160] Generally, BDD electrodes provide significant improvements in the linear dynamic range, response reproducibility and stability and limit of detection when used stand-alone or in electrochemical detection schemes coupled with flow injection analysis (FIA) and liquid chromatography (LC).[177] The original example of using BDD for electroanalysis was the detection of azide by both voltammetric methods and FIA with amperometric detection.[182] Another class of analytes that can be detected using conductive diamond but not so with other graphitic carbon electrodes is aliphatic polyamines.[183-185]

BDD electrodes often excel in the detection of analytes that require positive potentials for detection (*e.g.*, azide, tyrosine, tryptophan and estrogenic compounds). This is because of the microstructural stability of diamond and its resistance to oxidative damage. In other words, the diamond surface is less prone to significant chemical and microstructural changes under potential control, as compared to sp^2 carbon and metal electrodes that can easily oxidise leading to large and progressively increasing background current and noise. BDD is most often used without conventional pre-treatment. However, researchers have demonstrated that cathodic[116, 118, 186] and anodic pre-treatment,[123, 187] can produce partial hydrogenated or oxygenated surfaces,[124]

respectively. In some cases, such pre-treatment has been shown to improve the electrode response for a particular redox analyte.[188, 189]

The inertness of the BDD surface leads to weak adsorption of polar molecules. This is a beneficial property when trying to avoid electrode fouling (either from the products of electrolysis or from the sample environment itself *e.g.* biofilm formation[190]) in complex measurement environments. Fouling attenuates the electrochemical signal and is one of the major problems to overcome when developing electrochemical sensors. In the event a BDD electrode were to experience some fouling, electrochemical cleaning procedures involving cathodic or anodic[191] potentiostatic and potentiodynamic treatments (with anodic the production of hydroxyl radicals may also play a role),[192, 193] can be successfully employed.

4.1.1 Direct sensing

In electroanalysis, using conventional cyclic voltammetry or current-time approaches in quiescent solutions is often not sufficient to achieve the required detection limits due to the current signals not being high enough. Often potential pulse techniques are employed, in stationary solutions to discriminate against the background currents or convective flow systems implemented, such as microflow or FIA,[194] to increase the currents measured. Such systems are often found implemented in BDD electroanalysis. For example, there are a variety of recent descriptions of the integration of BDD microband electrodes into fluidic flow cells, operating under laminar flow conditions. The BDD can either be encapsulated so that it lies co-planar with an insulating diamond surround,[195, 196] or patterned directly on top of an insulating substrate such as alumina[197] or silicon oxide.[198] The BDD can play the role of counter, reference and working electrodes.[197] For example, isatin detection was recently conducted using a BDD 3-in-1 sensing platform.[199]

4.1.1.1 Direct chemical sensing

There are many examples of redox analyte sensing using an unfunctionalized BDD electrode, ranging from metal inorganic ions,[200] to a vast variety of organic species,[201, 202] with pharmaceutical drug molecules and neurotransmitters, proving particularly popular.[203] For example, in the pharma area molecules such as the sulfanomides,[204] methotrexate,[205] and acetaminophen[206] have been electroanalyzed, whilst for the neurotransmitters, detection of dopamine, serotonin, adrenaline, *etc* is common.[207-209] On an unfunctionalized BDD electrode with hydroxylated terminations, direct electrochemistry of cytochrome c has been also

realized.[210, 211] Studies are also often undertaken not just using model systems but in real systems e.g. urine, blood, using the dissolved pharmaceutical tablet, or *in-vitro* and *in-vivo* for the case of neurotransmitter detection. To mitigate against possible interference effects from redox active species also present in the sample matrix, different approaches have been taken, depending on the chemical properties of the system. For example, it has been shown by changing the BDD surface chemistry it is possible to modify the ET kinetics of one species with respect to another so their signals no longer overlap. This was the case for an electrochemically oxidized BDD electrode, which was found to retard oxidation of oxytocin (hormone and neurotransmitter) compared to vasopressin (secreted at the same time in the body), resulting in voltammetric wave separation.[212]

In some cases, the as-prepared BDD is not sufficiently electrocatalytically active towards the analyte of interest. The challenge is to increase electrode responsiveness towards the target analyte but not at the expense of compromising the beneficial properties of BDD. Two approaches have been taken in this regard: one is to add NDC to the electrode, which is more electrocatalytically active than BDD. The second is to add highly electrocatalytic metallic NPs to the electrode surface. NDC incorporation can be achieved during BDD growth[172, 213] or by deliberate incorporation of NDC into the surface in spatially controlled locations using laser ablation[214] and ion implantation[215] techniques. The impact of NDC content in BDD has also been considered in the electrochemical incineration field (section 3.3.4.2). In electroanalysis, it has been shown that NDC presence in BDD is essential for the cathodic detection of hyperchlorite (free chlorine under alkaline conditions) at high concentrations.[216] Oxidised NDC regions of the BDD electrode have also been shown to display a Nernstian sensitivity to pH,[214] resulting in a BDD pH sensing electrode. In an interesting twist on the fabrication process, CNTs have been used as a support for BDD growth, resulting in CNT-BDD hybrid materials with significant porosity. Such electrodes have reported increased ET rates (for simple redox systems such as $Fe(CN)_6^{3-}$),[217] compared to their planar analogues and have been applied in FIA for the detection of acetaminophen and epinephrine.[218]

Production of metal NPs on the BDD surface is typically achieved using either electrodeposition strategies or evaporation, sputtering techniques. NPs offer reduced background currents and increased mass transfer, compared to the planar metallic electrode.[219-223] However, there is a question regarding the long-term stability of metal NP-BDD electrodes due to the fact the metal can oxidise or dissolve dependant on operating conditions. Nonetheless, there are many

interesting examples where metal NP-BDD electrodes have made a powerful combination in the electroanalysis field. For example, for detecting pharmaceutical impurities in drug formulations, in particular, detection of the inner sphere redox species hydrazine in the presence of acetaminophen, separation of the two voltammetric signals was possible by switching from Au NPs to Pt NPs on BDD.[224] Detection of H_2O_2, an important by-product in many enzymatic reactions, has also been achieved using metal NP-BDD electrodes. Such signals were also used as a means to indirectly detect important analytes such as cholesterol.[225]

There are examples, where additional BDD electrodes have been added to the conventional electrochemical arrangement in order to bring further capabilities to the electrochemical measurement. For example, in fluid flow arrangements, upstream BDD electrodes, with respect to the BDD working electrode, have been added to either function as an interference species elimination electrode[197, 226] or a pH generating electrode.[227-229] Using dual BDD electrodes, pH control has been used as a means to electrochemically detect hydrogen sulphide in neutral pH solutions. Here the upstream electrode was employed to generate a local alkaline environment in the vicinity of the working electrode, by directly reducing water, in order to convert hydrogen sulphide into the electrochemically detectably SH^- form.[227] Similar concepts have been used to shift pH dependant equilibrium towards favourable electrochemical detection (acidic pH conditions) in heavy metal analysis. These concepts are most useful for situations where the sensor will monitor directly at the source e.g. river, sea, lake, and the solution pH is far from favourable.[228, 229] BDD elimination electrodes have also found use in heavy metal detection.[226]

4.1.1.2 Bio-interfaces

Diamond has long been recognised as a surface that is biocompatible, demonstrating very low toxicity when injected into live animals in the NP form.[230] It is also described as bioinert due to its inability to promote inflammation or promote coagulation.[231, 232] For these reasons, in addition to its high detection sensitivity,[233, 234] reduced fouling capabilities, BDD electrodes have been used in two major ways in medical applications.

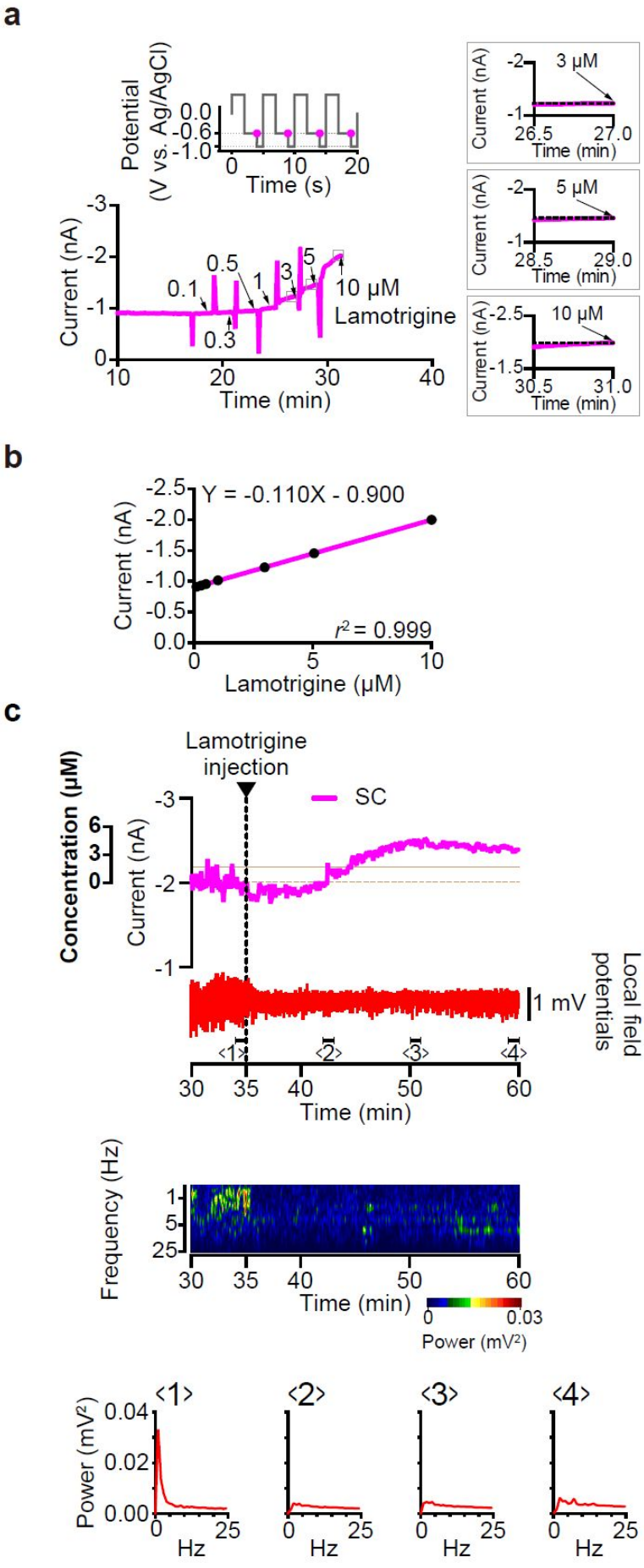
a
Potential (V vs. Ag/AgCl)
0.0
-0.6
-1.0
0
10
20
Time (s)
Current (nA)
-3
-2
-1
0
0.1
0.3
0.5
1
3
5
10 μM
Lamotrigine
10
20
30
40
Time (min)
Current (nA)
-2
-1
3 μM
26.5
27.0
Time (min)
Current (nA)
-2
-1
5 μM
28.5
29.0
Time (min)
Current (nA)
-2.5
-1.5
10 μM
30.5
31.0
Time (min)
b
Current (nA)
-2.5
-2.0
-1.5
-1.0
-0.5
0.0
Y = -0.110X - 0.900
r² = 0.999
0
5
10
Lamotrigine (μM)
c
Concentration (μM)
6
3
0
Lamotrigine injection
SC
Current (nA)
-3
-2
-1
1 mV
Local field potentials
<1>
<2>
<3>
<4>
30
35
40
50
60
Time (min)
Frequency (Hz)
1
5
25
30
35
40
50
60
Time (min)
0
0.03
Power (mV²)
Power (mV²)
0.04
0.02
0.00
<1>
<2>
<3>
<4>
0
25
Hz

Figure 2. Simultaneous recording of bumetanide and neuronal activity in the rat brain. **a**, The experimental setup. A BDD microsensor for the detection of bumetanide, a double-barrelled glass microcapillary encasing a reference electrode (RE) (Ag/AgCl) and counter electrode (CE) (platinum) and a glass microelectrode for the measurement of LFPs were inserted into the surface area of the parietal region through a small hole made in the skull. **b**, Cyclic-voltammogram measurement using a BDD microsensor in the brain of a rat. The potential protocol is shown in the inset (see Fig. 2b). **c**, Simultaneous recording of the BDD-sensor current and brain LFPs. The same rat as the one examined in **b** was used. The top panel shows raw data of the recording. The 'subtraction current' was allowed to reach a stable level and then, 35 min after the onset of recording, bumetanide (50 mg kg–1 in phosphate buffer solution) was injected into the lateral tail vein of the rat (arrowhead). The upper trace (green) displays the BDD-microsensor subtraction current. The bumetanide concentration (far left axis) was predicted from the in vitro calibration curve of this BDD microsensor. The brown dashed and solid lines show the in vitro and in vivo limits of detection for the microsensor in this experiment, respectively. The lower trace (red) indicates LFPs recorded at the same time by a glass microelectrode. The LFP data were analysed by FFT and are shown as a dynamic spectrum in the middle panel. The power (mV2) is indicated by a pseudocolor log scale. In the bottom panels, instantaneous power spectra during periods marked by bars (1–6) in the upper panel are shown. Black dashed lines indicate the peak power amplitude recorded over the 1 min immediately before the bumetanide injection (1). Reproduced with permission from ref. [235]. Copyrightt 2017, Nature Publishing Group.

The first is the *in-vitro*[236] and *in-vivo* detection of neuronal neurotransmitters, whilst the second encompasses diamond implants capable of both electrically stimulating and recording neuronal cell activity (as a voltage fluctuation). In neurotransmitter detection, more recent work has focused on *in vivo* analysis,[235] where the electrode is inserted directly into the live animal **(Figure 2)**. Due to the reported low-protein biofouling, BDD electrodes exhibited no change in electrochemical properties, after six weeks implanted into a rat. This represented a significant improvement over other carbon electrode materials.[237] To make the implants more flexible and thus mitigate unnecessary strain during insertion, BDD transferral from the growth substrate to a more flexible material (Parylene-C) is also being explored.[238]

For neural stimulation, high-capacitance electrodes are required in order to inject large charges into the neuron, whilst neuronal activity recording electrodes have need of low capacitance or

impedance electrodes to enable detection of small voltage changes. High capacitance is not a property traditionally associated with BDD, unless the surface area is increased significantly. However, very heavily doped BDD material, B concentration 5.5×10^{21} cm^{-3}, has been shown to exhibit high capacitance,[239] likely due to the large amount of boron leading to the creation of significant NDC. Alternatively, growing NCD under high nitrogen content also leads to large amounts of NDC in the film, resulting in a conductive material with extremely high capacitance.

4.1.2 Chemically functionalised electrodes

For analytes of interest that are not redox active within the aqueous solvent window, indirect electrochemical detection strategies can still be employed. One way to achieve this is to functionalise the surface of the electrode such that it contains both analyte-specific capture molecules and molecules to reduce non-specific binding events, important when working in complex media, such as blood, urine, dialysates *etc*. The capture event is then monitored using electrochemical techniques such as electrochemical impedance spectroscopy (EIS), which measures factors such as changes in the double layer capacitance and charge transfer resistance at the interface between electrode and electrolyte, as a result of analyte detection. BDD is preferred as the electrode material over others due to improved sensitivity, stability and fast response times.[147, 240]

4.1.2.1 Doped diamond

Using functionalization routes, such as those discussed in section 3.2, a variety of different biosensors have been proposed in conjunction with EIS based detection strategies. For example, a BDD electrode was functionalised with polyclonal anti-M1 antibodies, the universal biomarker for the influenza virus, M1 protein.[241] A limit of detection of 1 fg ml^{-1} in saliva buffer for this biomarker was achieved, corresponding to 5–10 viruses per sample in 5 min. Complementary EIS studies[242] also demonstrated the detection of several dozen plaque-forming units of the influenza virus on a BDD electrode terminated with a sialic acid-mimic peptide **(Figure 3A).** Comparison studies using a GC electrode proved less effective, thought to be due to the fact BDD is less likely to encourage adsorption of the albumin protein molecules present, which could interfere with the sensing capabilities of the electrode.

Researchers have also employed ligand to metal chemical functionalization routes as a means of tethering the receptor molecule to a metal NP-BDD electrode surface for e.g. cancer biomarker detection.[243] BDD electrodes have also been used to monitor DNA binding, with single stranded

DNA bound to the surface (**Figure 3B**),[244] hybridising with complementary strands in solution.[147, 244-246] EIS measurements of charge transfer resistance were employed to monitor such hybridization events, with a reported detection limit of 1 nM. Improved performance was found using BDD nanowire electrodes (**Figure 3C**) due to the well-designed spacing for efficient DNA hybridization using only tip-functionalized nanowires to immobilize single strand DNA.[247, 248] Denaturation events could also be followed[147] along with discrimination between DNA hybridization with a perfect DNA complement and a one base pair mismatch.[249]

(A)

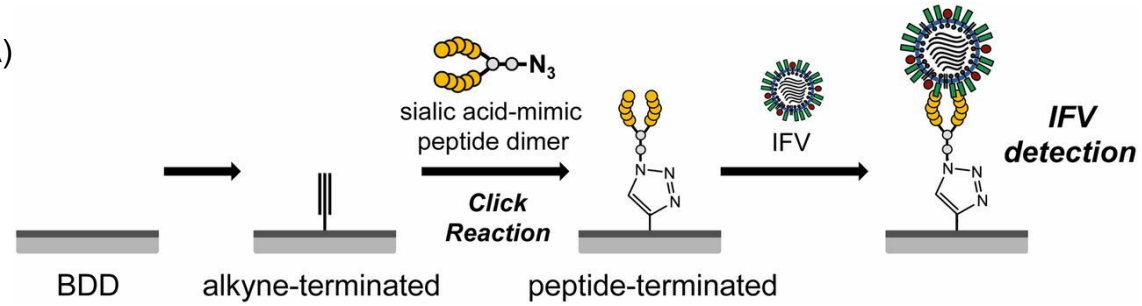

(B)

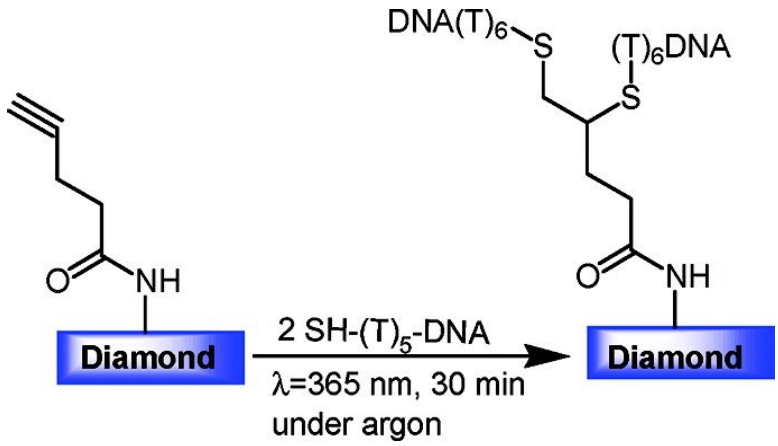

(C)

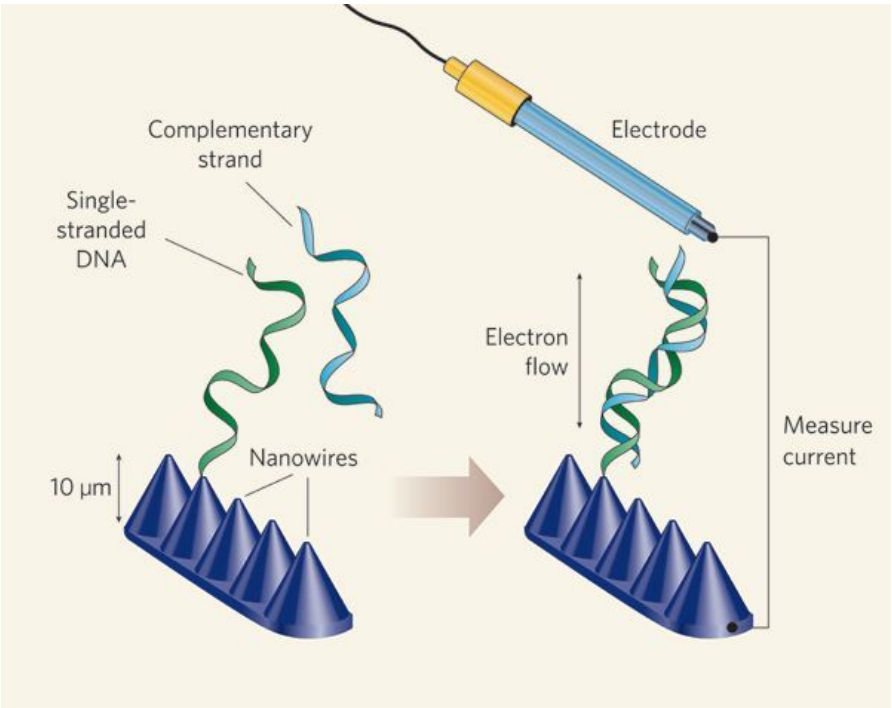

Figure 3. (A) Schematic illustration of the preparation of a peptide-terminated BDD electrode and influenza virus (IFV) detection. The sialic acid-mimic peptide dimer was immobilized on the alkyne-terminated BDD electrode via a click reaction. IFV capture was detected electrochemically. Reproduced with permission from ref. [242]. Copyright 2016, National Academy of Science. (B) Thiol-yne reaction on BDD electrodes: application for the electrochemical detection of DNA–DNA hybridization events. Reproduced with permission from ref. [244]. Copyright 2012, American Chemistry Society. (C) Yang *et al*.[250] have prepared DNA sensors by attaching single strands of DNA to diamond nanowires that have been constructed on a diamond surface. Both DNA and diamond conduct electricity, so electrons from the diamond substrate can flow along the DNA. The conductivity of the system changes when complementary strands of DNA bind to the tethered DNA. This effect can be quantified by immersing the diamond sensor in a solution of DNA, placing an electrode close to the diamond surface and measuring the current that flows between them. Reproduced with permission from ref. [250]. Copyright 2008, Nature Publishing Group.

4.1.2.2 Un-doped diamond

Triggered by the surface-induced conductivities of hydrogen-terminated undoped diamond, such films have been employed to construct field effect transistors (FETs) for biosensing and bioelectronics applications.[47, 85, 251] These transducing devices are sensitive to pH[252-255] and have been used to monitor local pH changes induced during hybridization or enzymatic reactions.

Moreover, the diamond FETs display facile integration, high gate sensitivity (resulting from their enhanced transconductances)[251, 256, 257] and low-frequency noise levels.[251, 258] Furthermore, diamond FETs can be grafted with a variety of surface functional groups, paving the way for immobilization of various biomolecules on their surfaces.[48, 251] For example, ion-selective FET (ISFETs), solution-gate FETs (SGFETs),[251, 257, 259-261] and enzyme-modified FETs (ENFETs)[262] have been constructed for detecting DNA hybridization events,[257, 259, 263] sensing protein binding to DNA or RNA aptamers[260] as well as studying the electrical activity of cells[251, 261] and enzymes.[262]

Diamond SGFETs have been utilised for both DNA and protein detection,[260] where hybridization of DNA, RNA, or protein binding to DNA or RNA aptamers, was efficiently detected by monitoring the change in surface charge.[260, 264] SGFETs have also been employed to rapidly detect 3-mer mismatched DNA; the possibility of monitoring single-base mismatched DNA was also demonstrated. [257, 259, 262] The electrical activity of different electrogenic cells (*e.g.*, cardiac muscle (cardiomyocyte) cells) cultured on diamond SGFET arrays has also been studied (**Figure 4A**).[261] The simultaneously recorded concurrent and repeated spikes on all individual working transistors corresponded to the action potentials of the cells (**Figure 4B**).[261] It was suggested that such diamond biohybrid devices are promising for the detection of cell signals in important medical applications (*e.g.*, neuroprostheses) and for fundamental research on communication processes in networks.[251, 261] Finally, an ENFET device was shown to be capable of detecting biologically relevant analytes such as penicillinase and the neurotransmitter acetylcholinesterase immobilized using different organic linker molecules and cross-linking chemistries.[262]

(A)

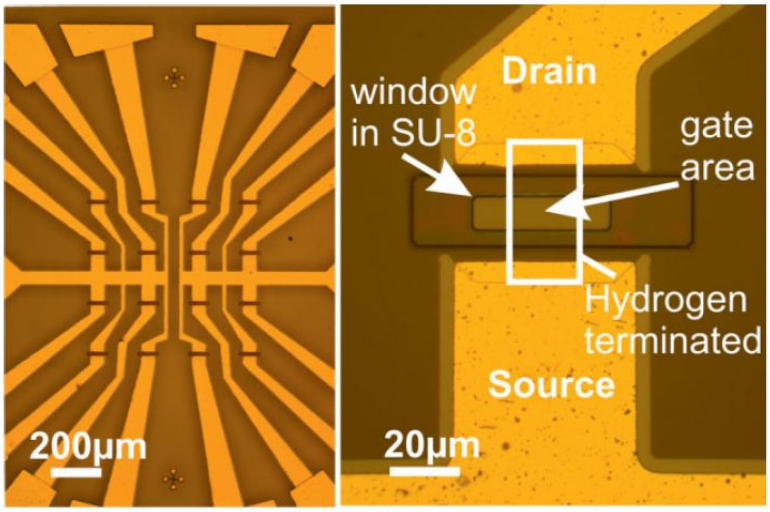

(B)

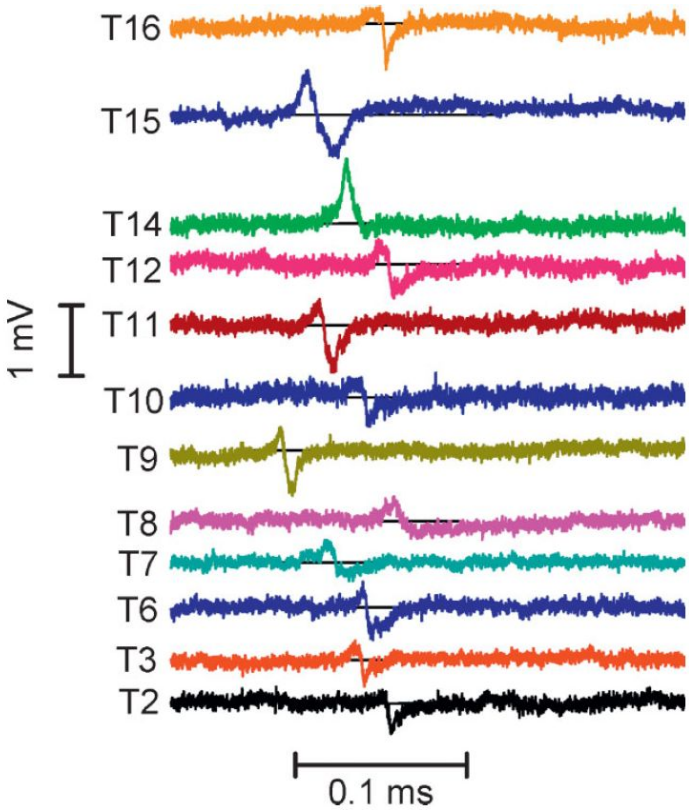

Figure 4. (A) Left: Image of a 4×4 FET array with leads to the bond pads before sealing with PDMS. Right: Image of a single transistor with the Ti/Au drain and source contacts above and below the gate area. The intersection between the opening in the SU-8 passivation layer and the hydrogen terminated area of the diamond (not visible, but indicated), represents the gate area. The channel conductivity depends on the applied potential with respect to the RE. (B) Transistor recordings with an enlarged time axis. The gate voltage of all 12 transistors was recorded simultaneously. The measured action potential signals show different time delays for different transistors on this time scale. Most transistors record a signal shape similar to the one most clearly visible for transistor 15 with a positive peak followed by a negative peak typical of a capacitive response. Reprinted with permission from ref. [261]. Copyright 2009, WILEY-VCH Verlag GmbH & Co. KGaA.

4.1.3 Sensing using small-dimensional diamond electrodes

4.1.3.1 Small-sized electrodes

When planar and macroscopic polycrystalline BDD electrodes are employed for sensing applications, only average electrochemical signals, over the entire electrode area, are detected. However, these planar and macroscopic BDD electrodes can suffer from non-uniform boron doping[265], boundary effects, and varied ratios of NDC to sp^3-diamond for different diamond films.[2, 21-26, 152, 266-269] To overcome these shortcomings and obtain more sensitive

electrochemical signals for BDD electrodes, various conductive diamond nanostructures (section 2.3) and particles (section 2.4) have been produced. These have been employed for electrochemical and bioelectrochemical sensing of different targets in solutions before and after further surface modification.[23, 87, 88]

Among various diamond nanostructures, small dimensional BDD electrodes, especially those at the micro- and submicron- dimensions have been fabricated (Section 5 in this review).[270-273] Depending on their dimensions (*e.g.*, electrode diameters), these BDD electrodes are classified as either BDD microelectrode (ME) when the diameters are in the range of 25 to 100 μm, BDD ultramicroelectrode (UME) when the diameters are in the range of 0.1 to 25 μm, or BDD nanoelectrode (NE) when the diameters are smaller than 100 nm.[271] These small-dimensional BDD electrodes have shown many advantages in comparison to planar and macroscopic BDD electrodes.[270-273] For example, they feature reduced ohmic resistances, enhanced mass transport rates, decreased charging currents, decreased deleterious effects of solution resistance, and suitability for fast voltammetric measurements.[274-284] Therefore, such electrodes have been widely explored for electrochemical sensing applications in both non-aqueous[274] and aqueous solutions,[275-283] to detect *e.g.* dopamine in the mouse brain,[276] monitor norepinephrine release in a mesenteric artery,[281, 285] investigate the role of adenosine in the modulation of breathing within animal tissue,[282] inspect serotonin as a neuromodulator,[236, 283] determine ozone,[286, 287] catecholamines,[288] oxytocin,[212, 288-290] zinc ions,[288] dissolved oxygen,[288] and peroxynitrite.[288] In comparison to planar and macroscopic conductive diamond electrodes as well as to carbon fibers and metal wires, these diamond MEs and UMEs have shown superior analytical figures of merit in terms of signal-to-noise ratios, linear dynamic ranges, limits of detection, and response precisions towards different analytes in solutions.[207, 291-296]

Small-dimensional diamond electrodes have been also integrated with other techniques such as capillary electrophoresis (CE)[280, 297] and in flowing systems (*e.g.*, microfluidic devices).[123, 298] Some novel sensing applications have been investigated using all-diamond MEs.[299, 300] For example, diamond MEs were used as solid state probes for localized electrochemical sensing, for example to investigate corrosion.[300]

In terms of biosensing measurements, *in vivo* neural recordings using a BDD ME have been reported[301] on the buccal mass of the Aplysia sea slug, which showed improved signal-to-noise and reduced fouling compared to a stainless steel electrode. The BDD electrode was functional

for nine continuous days, highlighting the capability of BDD for long-term *in vivo* neural recording.[235] Human measurements have also been documented where implanted BDD MEs have been used to measure in real time the neurochemical release (here an adenosine like signal) in response to a patient undergoing deep brain stimulation.[232]

4.1.3.2 Small-sized electrode arrays

Single small-sized electrodes (*e.g.*, MEs, UMEs, or NEs) generate only small currents. In some cases, these small currents are relatively difficult to detect with conventional electrochemical instrumentation. To improve the situation, individual small-sized BDD electrodes are assembled and operated in parallel. When these electrodes are regularly arranged, the term array is often used, or else it is termed as an ensemble. Provided that these arrays and ensembles are well designed (*e.g.*, suitable diameter, optimized distance between electrodes, etc.), the signals of individual BDD MEs, UMEs, or NEs can be amplified whilst at the same time retaining the beneficial characteristics of the individual small dimensional BDD electrode. For example, various diamond ME arrays (MEAs) and UME arrays (UMEAs) have been applied for many different sensing applications, e.g., for the detection of environmental analytes (*e.g.*, nitrate, 4-nitrophenol,[302-304] Cr(VI) ions, Ag(I) ions, sulphate, peroxodisulfate,[305] hydrogen peroxide),[306] for bio-detection (*e.g.*, detection of dopamine,[307-312] neuronal measurements,[313-316] quantal catecholamine secretion from chromaffine cells[317]), and for SECM generation and detection of peroxidisulfate.[291] On BDD UMEAs, the lowest detection limit (1.0 nM) was achieved for dopamine detection in the presence of ascorbic acid. This detection limit is 50 - 100 times lower than that reported using macroscopic and planar BDD electrodes.[318] On oxygen-terminated BDD NE arrays (NEAs), the reported sensitivity for the detection of dopamine in the presence of ascorbic acid was 57.9 nA μM^{-1} cm^{-2}.[319] BDD NEAs have also proved to be an ideal electrode to investigate surface-sensitive adsorption behaviour. Here the adsorption behaviour of electroactive species (*e.g.*, neutral methyl viologen) was shown to vary with the surface termination of the NEA as well as with the type and concentration of the buffer solutions.[320]

MEAs have also been used for neural recording over larger areas, for example in the auditory cortex of a guinea pig.[305] Retinal stimulation diamond implants,[321] incorporating up to 256 independently controlled electrodes have also been developed.[322] Recent work also focused on the fabrication of more flexible, polyimide-based three-dimensional retinal implants.[323] BDD MEAs and UMEAs featuring various geometries have also been used to monitor electrical activity and neurotransmitter release in a variety of excitable and neuronal tissues.[315] Multiplex

diamond MEAs (3 × 3 format, 200 µm in diameter) have been employed for the reproducible and sensitive detection of a model *Escherichia coli K12* bacterium using EIS.[324]

Electrochemical and physical properties of various BDD MEAs and UMEAs as well as their applications for recording released neurotransmitter molecules and all-or-none action potentials from living cells have been recently reviewed (**Figure 5**).[315, 316] Examples include how high-density BDD MEAs and UMEAs are able to resolve localized exocytotic events from subcellular compartments and applications of low-density MEAs to monitor oxidizable neurotransmitter release from populations of cells in culture and tissue slices. It has been stated[256] that interfacing diamond UMEs and MEAs with excitable cells is currently leading to the promising opportunity of recording electrical signals as well as creating neuronal interfaces through the same device.

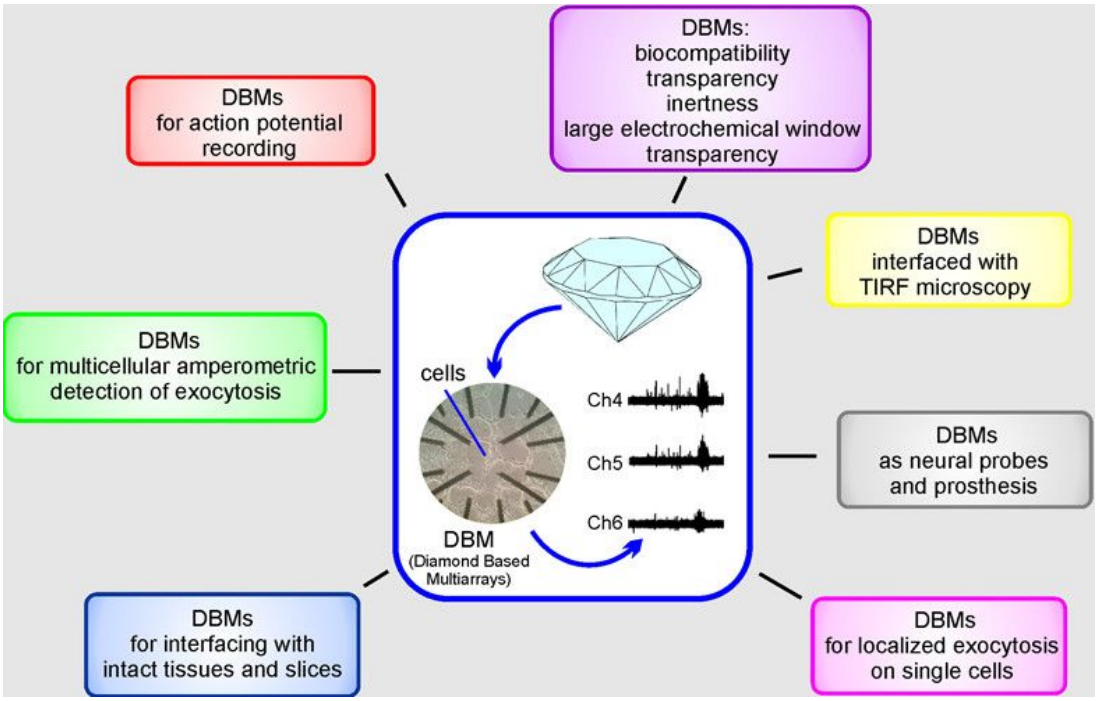

Figure 5. Planar diamond-based multiarrays (DBMs) to monitor neurotransmitter release and action potential firing. Reproduced with permission from ref.[242, 315]. Copyright 2017, American Chemistry Society.

4.2 Electrochemical degradation

Ecological degradation or environmental depletion occurs in two ways by human processing and natural forms. Advanced oxidation process (AOP) is one of the most promising, efficient, and environmentally friendly methods of human processing, which has been developed to remove organic pollutants and synthetic dyes from wastewaters.

For AOPs, BDD electrodes function as promising anodes to electrochemically degrade environmental pollutants, so-called electrochemical environmental degradation. This is because on BDD electrodes hydroxyl radicals (•OH) are generated efficiently during AOP processes in both acid and neutral media.[192, 325-329] This radical is a very strong oxidizing species due to its high standard potential (E^o = 2.80 V vs. NHE), and is extremely reactive and can be produced in sufficiently high concentrations. Moreover, it reacts non-selectively with most organic pollutants and synthetic dyes *via* abstraction of a hydrogen atom (dehydrogenation) or addition to a nonsaturated bond (hydroxylation) until total mineralization or conversion into CO_2, water, and inorganic ions.[192, 330, 331] Conversely, in both acidic and alkaline solutions, only partial mineralization of most aromatics is realized on conventional AOP anodes (*e.g.*, Pt, PbO_2, doped PbO_2,[332] doped SnO_2, and IrO_2).

On BDD anodes, further reactions can occur, i.e., the formation of persulfate,[333, 334] perphosphate and percarbonate,[335] and hypochlorite,[336-338] which can also be used for waste water treatment. The synthesis of ferrates, ozone water,[287, 339, 340] and aromatic hydroxylation formation mediated by •OH radicals produced electrochemically, has been reported.[341] In addition, BDD possesses several technology essential characteristics such as an inert surface with low adsorption properties, remarkable corrosion stability (even in strongly acidic media) and an extensive potential window in aqueous and non-aqueous electrolytes. Therefore, electrochemical AOP (EAOP) using BDD anodes[342-366] has been widely investigated to degrade organic components, especially those in wastewaters.

4.2.1 Generation of hydroxyl radicals

Hydroxyl radicals (HO•) can be *chemically* produced by disproportion of peroxynitrous acid or decomposition of hydrogen peroxide by metal ions, which are known as Fenton[367, 368] or Fenton-like[369] reactions. *Electrochemically*, hydroxyl radicals are formed by direct electrochemical oxidation of water, which adsorb on the electrode surface and act as mediators of oxygen evolution ((1) and (2)).

$$H_2O \rightarrow HO\bullet + H^+ + e^- \qquad (1)$$

$$2\ HO\bullet \rightarrow O_2 + 2H^+ + 2e^- \qquad (2)$$

The reactivity of the hydroxyl radicals on the electrode surface depends on the electrode material.[192] An “active electrode” shows a strong interaction between the hydroxyl radical and

the electrode surface, while a "non-active electrode" shows a weak interaction. On "active electrodes", the adsorbed hydroxyl radicals may interact with the electrode, with the surface changing to a higher oxide (3). Then, the competitive reactions, i.e., the oxidation of organic compounds (4) and chemical decomposition of the higher oxide to form oxygen (5) occur.

$$M(\bullet OH) \rightarrow MO + H^+ + e^- \quad (3)$$
$$MO + R \rightarrow M + RO \quad (4)$$
$$MO \rightarrow M + \tfrac{1}{2}O_2 \quad (5)$$

On a "non-active electrode", the interaction between the hydroxyl radicals and the electrode surface is weak. Therefore, hydroxyl radicals are physically adsorbed at the electrode surface. Then the oxidation of organic compounds is mediated only by the hydroxyl radicals (6). In fact, the hydroxyl radicals can discharge to oxygen without any participation of the electrodes (7).

$$M(\bullet OH) + R \rightarrow M + mCO_2 + nH_2O + e^- \quad (6)$$
$$M(\bullet OH) \rightarrow M + \tfrac{1}{2}O_2 + H^+ + e^- \quad (7)$$

The BDD electrode is considered to be an ideal non-active electrode, since it has an inert surface of sp^3 carbon and its surface has very weak adsorption properties. Consequently, the water oxidation reaction at a BDD electrode in aqueous solution induces the formation of hydroxyl radicals[192, 325-329] instead of oxygen evolution. Evidence for generation of hydroxyl radicals in aqueous solution at the BDD electrode has been confirmed using different *ex-* and *in- situ* techniques.[192, 327]

4.2.2 Degradation of individual pollutants

Using BDD anodes, AOP degradation of different kinds of organic pollutants has been conducted. The degradation performance was judged from the parameters of chemical oxygen demand (COD), biochemical oxygen demand (BOD), total organic carbon (TOC), dissolved organic carbon (DOC), final products (e.g. CO_2, H_2O), and removal efficiencies under different degradation conditions (*e.g.*, current, voltage, or temperature). For example, efficient degradation or complete mineralization of phenolic pollutants,[370] maleic acid,[344] tetrahydrofuran (THF), [371-373] m-dinitrobenzene,[374] p-nitrophenol,[375] herbicide tebuthiuron,[376] reactive orange 16,[377] pseudomonas aeruginosa,[378] 4-hydroxyphenyl acetic acid,[379] brilliant green,[380] sulfonylurea

herbicide,[381] Rhodamine B-19,[382] and reactive black 5 azo dye[383] have all been realized. Compared with other anodes (*e.g.*, Ti/SnO_2-Sb/PbO_2, and Ti/SnO_2-Sb), BDD anodes had a much stronger mineralization performance towards the degradation of pesticides and organic pollutants. This is due to the efficient and effective reaction of organic compounds with free hydroxyl radicals.[375]

To improve on the degradation and complete mineralization of organic pollutants, various combined degradation methods have been developed. As summarized in **Table 1**, these techniques mainly include the combination of EAOP with Fenton, UV irradiation, ultrasound, microwave, and ozonation.[384-389] Here the Fenton method refers to the activation of hydrogen peroxide in acidic effluents.[367, 368] These combined techniques further enhanced the degradation performance of BDD anodes.[390-393] For example, combining ultrasonic oxidation with AOPs led to much enhanced degradation performance of some non-biodegradable organic pollutants (*e.g.*, alkylphenol ethoxylate surfactants, trichloroethylene, poly(n-alkyl acrylates), and phthalic acid esters).[370, 391, 394, 395] Ultrasound assisted AOP influenced remarkably the degradation performance of phenol and phthalic acid, including degradation efficiency, electroxidation energy consumption, mass transport, and electrochemical reaction. A reduction of the average electroxidation energy consumption by a factor of 74% and 69% was reported for phenol and phthalic acid, respectively. The mass transport process was also greatly accelerated using ultrasound, as confirmed by a 32% increase of the oxidation peak current for phenol (**Figure 6A**).[348]

The combination of microwave with EAOP also enhanced the degradation of 2,4-dichlorophenoxyacetic acid and triclosan.[360] Increased temperature or mass transport conditions, induced by focused microwaves at a BDD was thought to be responsible for enhancing the electrochemical oxidation of phenol in aqueous NaOH and NaCl solutions.[360, 396, 397] Ozonation improved EAOP mineralization of p-nitrophenl,[392, 393] nitrobenzene and m-nitrotoluene[391, 398]. In aqueous solutions, the TOC removal was up to 91% when a time of 60 min for the electrolysis-ozone process was applied. With the same reaction time, only 20% and 44% of TOC was removed by individual electroxidation and ozonation treatment.

(A)

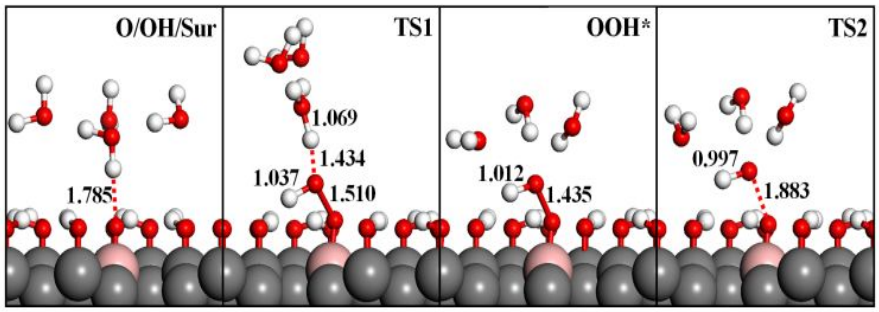
O/OH/Sur
TS1
OOH*
TS2
1.785
1.069
1.434
1.037
1.510
1.012
1.435
0.997
1.883

(B)

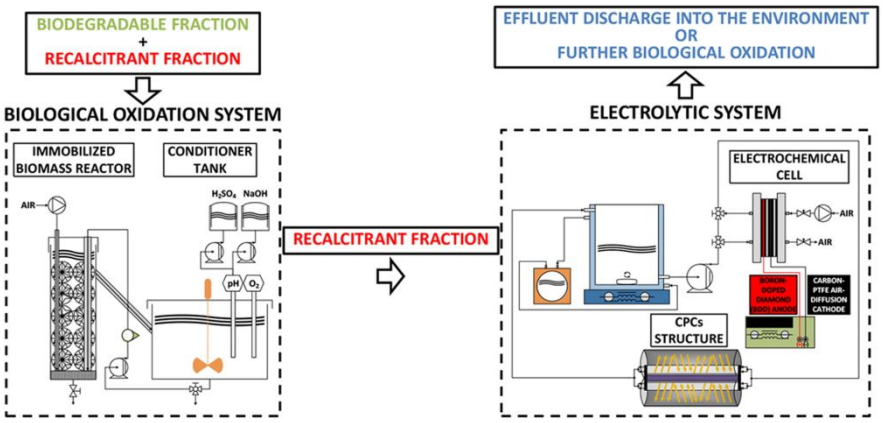
BIODEGRADABLE FRACTION
+
RECALCITRANT FRACTION
BIOLOGICAL OXIDATION SYSTEM
IMMOBILIZED BIOMASS REACTOR
CONDITIONER TANK
AIR
RECALCITRANT FRACTION
EFFLUENT DISCHARGE INTO THE ENVIRONMENT
OR
FURTHER BIOLOGICAL OXIDATION
ELECTROLYTIC SYSTEM
ELECTROCHEMICAL CELL
CPCs STRUCTURE

(C)

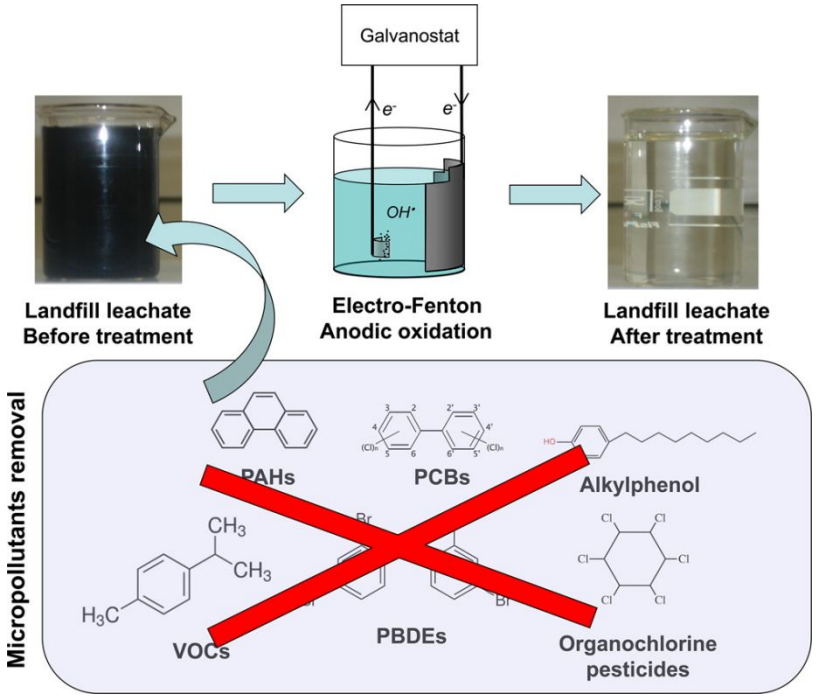
Galvanostat
e⁻
e⁻
OH•
Landfill leachate
Before treatment
Electro-Fenton
Anodic oxidation
Landfill leachate
After treatment
Micropollutants removal
PAHs
PCBs
Alkylphenol
VOCs
PBDEs
Organochlorine
pesticides

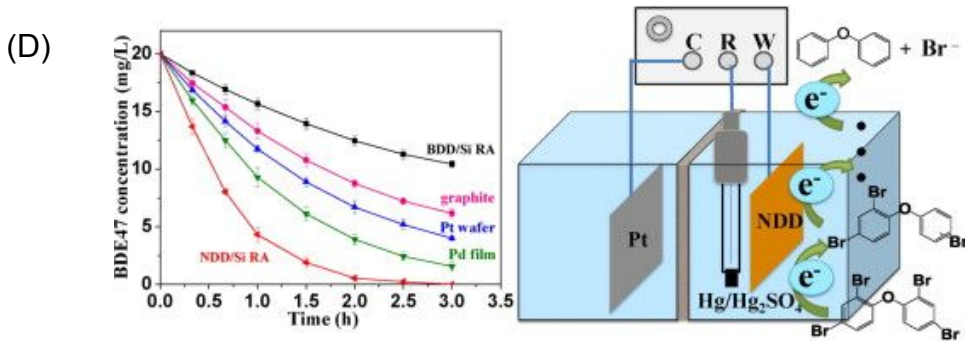

Figure 6. (A) Reaction pathway and mechanism of ultrasonic electrochemical reaction on BDD electrodes. Reproduced with permission from ref. [348] Copyright 2015, John Wiley and Sons. (B) Remediation of a winery wastewater combining aerobic biological oxidation, EAOP, and BDD anodes. Reproduced with permission from.[399]. Copyright 2015, Elsevier. (C) Occurrence and removal of organic micropollutants in landfill leachates treated by EAOP and BDD anodes. Reproduced with permission from ref.[400]. Copyright 2015, American Chemical Society. (D) Nitrogen-doped nanodiamond rod array electrode with superior performance for electroreductive debromination of polybrominated diphenyl ethers. Reproduced with permission from ref. [100]. Copyright 2014, Elsevier.

Table 1. EAOPs degradation performance using BDD anodes

Method	Pollutant(s)	Degradation conditions		Degradation performance			Ref.
		Current / mA cm^{-2}	T / °C	Parameters	Final Products	Removal efficiency	
Electrochemical oxidation	2,4,5-trichlorophenoxyacetic acid	2, 8, 15, 30	35	TOC	$CO_2 + H_2O$	100%	346
	Sodium dodecyl benzene sulfonate	25 – 75	80 - 450	COD	$CO_2 + H_2O$	100%	347
	Malic acid and ethylenediaminetetraacetic acid	4	41	COD	$CO_2 + H_2O$	85 to 100%	344
	Glucose and potassium hydrogen phthalate		24	COD, TOC	$CO_2 + H_2O$	90%	401
	Atrazine		25	TOC	$CO_2 + H_2O$	94%	402
	Enrofloxacin	400	35	TOC	$CO_2 + H_2O$	51%	403
	2-naphthol	15-60		COD	$H_2O + CO_2$	100%	331
	4,6-dinitro-o-cresol	33-150		TOC	$H_2O + CO_2$	85%	330
Fenton Oxida	2,4-dichlorophenoxyacetic acid	100	35	TOC	Formic acid	79%	404

tion	DMPO	23, 160	15	TOC	$CO_2 + H_2O$	100%	[192]
Ultrasound Oxidation	Phenol, phthalic acid	20	10	COD	$CO_2 + H_2O$	79 and 32%	[384]
Microwave Oxidation	2,4-dichlorophenoxyacetic acid	10		COD	$CO_2 + H_2O$	46.8 - 98%	[361]
	Azo dye (methyl orange)	25		TOC	$CO_2 + H_2O$	78%	[360]
Ozonation	Platinum anode p-nitrophenol	8	30	TOC	$CO_2 + H_2O$	91%	[393]
	Industrial effluents	10, 20, 30		COD	$CO_2 + H_2O$	99.9%	[405]

Using these combined degradation techniques and BDD anodes, EAOP degradation of various organic pollutants (*e.g.*, synthetic dyes) has been reported. [406-428] For example, degradation of metribuzin,[413, 414] o-nitrophenol,[415] acid violet 7 dye,[416] reactive Orange 16,[417] a mixture of three pesticides (*e.g.*, chlortoluron, carbofuran, and bentazon),[347, 388, 415, 418-420] nitrate,[390, 421] pharmaceuticals (*e.g.*, ciprofloxacin, sulfamethoxazole, and salbutamol),[422] bisphenol A,[422-424] fluorinated antidepressant fluoxetine,[421] aspirin[330, 343, 344] caffeine,[425] ethidium bromide,[426] and Ponceau 4R (**Figure 6B**)[399, 428] have all been reported. Safranin T and bromophenol blue have also been degraded. Safranin T was completely removed at a constant current through its reaction with electro-generated hydroxyl radicals.[408-410] Fluorinated antidepressant fluoxetine[421] was degraded into four aromatic products. Among Pt, RuO_2, and BDD anodes, the BDD anode showed the highest mineralization rate due to the fastest production of hydroxyl radicals. For degradation of aspirin using BDD anodes, the degradation mechanism involves both direct and indirect electrochemical oxidation, while there is only indirect oxidation of aspirin on a PbO_2 electrode.[330]

4.2.3 Degradation of multiple pollutants in real wastewaters

Degradation of different real wastewaters, e.g., ground water, pond water, river water, house hold wastewater, municipal wastewater, *etc*. has been carried out using BDD anodes.[365, 411, 427, 429-448] For example, EAOP degradation of (i) commonly used parabens,[434] (ii) coking wastewater,[375] (iii) paper mill wastewater,[427] (iv) municipal solid waste landfill leachates containing recalcitrant organic matter (*e.g.*, micro pollutants, humic substances, *etc.*),[435] (v) real water matrix containing the food azo dye (*e.g.*, Ponceau 4R),[399, 428] (vi) rubber industries wastewaters,[436] (vii) olive oil mill wastewater containing vanillic acid and sinapinic acid,[437-439]

(viii) effluents containing low-levelled nitrogen pollutants (*e.g.*, ammonia ions and ammonium, and in some instances in the nitrite form),[440] (ix) soil washing effluents containing atrazine,[441] industrial wastewater containing chromium compound[442, 443] (x) natural ground water containing perfluoroalkyl acids[365, 444] (xi) synthetic tannery wastewater,[445] (xii) Sago industries pollutants,[446] (xiii) textile dyehouse effluents,[447] and (xiv) winery wastewater,[448] have all been successfully conducted.

Complete depletion of four hexaclorocyclohexanes isomers was confirmed with a mineralization degree of 90% after an electrolysis time of 4 h at a current intensity of 400 mA. Hexaclorocyclohexanes and chlorobenzenes were transformed respectively into chlorinated and hydroxylated intermediates that were rapidly oxidized to non-toxic carboxylic acids.[432, 433] As confirmed by phototoxicity tests, BDD anodes are useful for reducing the toxicity of hazardous wastewater.[411] Compared to the Ti-Ru-Sn ternary oxide anodes, the BDD anode exhibited faster and more efficient maximum COD removal but with less energy consumption for degradation of paper mill wastewater.[427] A BDD anode enabled complete COD, colour and ammonium removal after 8 h of electrolysis. Evaluated using COD and DOC, a higher degradation efficiency of bioorganic contaminant wastewater was achieved on BDD anodes in comparison to Ti/Pt-IrO_2 and Ti/SnO_2-Sb anodes.[429-431] Once again, a BDD anode exhibited much better degradation performance in terms of evolution of aromatic compounds, COD, ammonium, colour removal, current efficiency, and energy consumption (**Figure 6C**).[400, 435, 440, 449-452] The suspension of persistent chromium complexes in wastewater was degraded and almost complete Cr abatement (over 99%) was obtained.[453] Efficient degradation of EDTA in the waste solution and the removal of Pb, Zn, and Cd from Sugarcane industries pollutants were also investigated with the metals removed via an electrochemical electroplating process. Removal ratios of up to 98.1, 96.1, and 99.1% were obtained for Pb, Zn, and Cd, respectively. The degradation of chelant was up to 99.1%.[454] The degradation of THF from industrial wastewaters with an efficiency of up to 95% has also been reported, leading to the statement, BDD anodes have great potential for the practical treatment of industrial wastewaters containing high concentrations of THF.[371-373] **Table 2** lists some examples of EAOP degradation of multiple organic pollutants in real wastewaters.

Table 2. Electrochemical degradation performance of pollutants in real wastewaters using BDD anodes

Pollutants	Current Density	Parameters	Final	Removal	Ref.

	/ mA cm^{-2}		Products	Efficiency	
Hexaclorocyclohexanes	3.7	TOC	$CO_2 + H_2O$	90%	390
2,6-dichlorobenzamide	50	TOC	$CO_2 + H_2O$	80%	433
Parabens	38.97	TOC	$CO_2 + H_2O$	100%	434
Surplus ammonia–nitrogen	20-60	COD	$CO_2 + H_2O$	60%	375
Municipal wastewater, human urine, river water, slaughterhouse wastewater	35.7	COD	$CO_2 + H_2O$	84-91%	440
Micro pollutants, humic substances	21	TOC	$CO_2 + H_2O$	93%	400
Pharmaceuticals, pesticides	9.8- 19.6	COD	$CO_2 + H_2O$	100%	435
Carbamazepine	1.8 - 17.7	TOC	$CO_2 + H_2O$	52 - 73%	455
Municipal solid waste	20 - 80	COD	$CO_2 + H_2O$	35 – 65 %	411

4.2.4 Effects of conductive diamond on degradation performance

Besides the properties and concentrations of organic pollutants, their degradation performance is much dependent on the material properties of the employed diamond anodes (*e.g.*, NDC impurities, dopants, surface structures, *etc*.). It has been found that the NDC content of BDD anodes affects electrochemical degradation performance of the electrode towards organic pollutants. This is based on the differences observed in the production of $S_2O_8^{2-}$ ions[456] and hydroxyl radicals for different levels of NDC impurities on the BDD surface,[457] as well as electrochemical degradation performance towards reactive Orange 16[417] and 2,4-dichlorophenoxyacetic acid in synthetic wastewater containing chlorides[458] and Rhodamine B[169]. Higher quality BDD films (smaller NDC levels) were found to be better suited for EAOP degradation of organic pollutants into carbon dioxide. Conversely, high NDC content favours the electrochemical conversion of organic dyes (*e.g.*, Rhodamine B[169] and enrofloxacin[403]) due to the efficient adsorption of such reactants on the NDC and formation of many intermediates.

The dopant level and type of diamond anode also influences electrochemical degradation performance towards the organic pollutants. For example, EAOP degradation of rubin F-2B,[459] enrofloxacin,[403] and reactive orange 16[460] was more efficient using higher doped than lower doped BDD electrodes. As for the effect of the type of the dopant, **Figure 6D** shows one example using a NDD rod array electrode for electroreductive debromination of polybrominated diphenyl ethers.[100] Since such an electrode exhibited a low hydrogen evolution potential (−1.95 V *vs.* Hg/Hg_2SO_4 electrode), it showed superior activity for electroreductive debromination of the persistent 2,2′,4,4′-tetrabromodiphenyl ether (BDE-47). Over 97% BDE-47 (20 mg L^{-1}) was electrochemically reduced in 2 h at −1.85 V (*vs.* Hg/Hg_2SO_4 electrode) with a

first-order kinetic constant of 1.93 h^{-1}, which was ×8.7, ×4.7, ×3.5 and ×2.3 greater than that at BDD, graphite, Pt wafer, and Pd film electrodes, respectively, under the experimental conditions applied. Note although NDD films[80, 82, 100] have been employed as the cathodes for the degradation of organic pollutants, the comparison of anodic degradation performance of organic pollutants using BDD anodes with that using NDD anodes is missing in the literature.

Finally, surface nanostructuring of BDD anodes (*e.g.*, porous diamond,[461-463] diamond nanowires,[464] *etc.*) enhanced the degradation performance of organic pollutants. For example, a porous BDD anode was found to be more effective, leading to completely mineralization and rapid degradation of methylene blue.[412] In general, porous BDD anodes were more effective at oxidising organic pollutants, leading to complete mineralization in comparison to planar BDD and PbO_2 anodes.[461-463] The greater surface area and enhanced mass transfer of the porous BDD anode led to enhanced EAOP degradation of glyphosate and phenol in terms of reaction rate, current efficiency, and energy consumption.[409, 412]

4.3 Electrosynthesis

Electrochemical organic synthesis is considered as a "green" technology for organic synthesis, because only electrons are used as reagents and almost no reagent waste is produced.[465] For example, for normal molecular transformations including cleavage of carbon-hydrogen bonds, oxidation or reduction with metal catalysts are necessary. On the other hand, oxidant or reductant free and catalyst free molecular transformations are possible in electrochemical synthesis by precise adjustment of electrochemical parameters such as redox potential, current density, *etc*. Furthermore, novel reaction chemistry occurring *via* electrochemically generated intermediates is also possible.

Electrochemical synthesis using BDD electrodes shows some advantages in comparison with those using conventional electrodes. These are due to the unique electrochemical properties of BDD electrodes, including the wide potential window and generation of active species such as hydroxyl radicals. Therefore, applications of BDD electrodes in electrochemical synthesis are very promising for novel chemical transformation.[22] In this section, electrochemical synthesis applications through anodic oxidation and cathodic reduction reactions are reviewed and discussed.

4.3.1. Transformation by anodic oxidation

Hydroxyl radical generation using a BDD electrode has been widely applied as a direct approach in the waste water treatment area (section 4.2). Interestingly this property of the electrode can also be used in electrochemical synthesis where reactions are driven via radical "active species".

4.3.1.1 Electrochemical synthesis via methoxy radicals

In 2004, Comninellis et al. reported the first example of an electrochemical reaction *via* methoxy radicals generated by the anodic reaction of methanol using BDD electrodes. Anodic oxidation of 1,2-diphenyl-ethanes in CH_3OH-H_2SO_4-H_2O solution produced *p*-tert-butylbenzaldehyde dimethyl acetal *via* carbon-carbon bond cleavage due to the formation of methoxyl radicals.[466] Furthermore, trimethylorthoformate production by anodic oxidation of formaldehyde dimethylacetal in solutions containing methanol using BDD electrodes, was also reported.[467] Electron spin resonance (ESR) was used to confirm generation of the methoxy radicals (**Figure 7**).[468] Anodic oxidation of methanol containing 0.1 M $LiClO_4$ and 1 mM DMPO (radical trapping agent: 5,5-dimethyl-1-pyrroline-N-oxide) was performed at a constant potential of +1.6 V (*vs.* Ag/AgCl) using a BDD electrode. The ESR signal of the product mixture showed the magnetic field value anticipated for nitroxyl radicals, which were generated by the reaction of methoxyl radicals with 5,5′-dimethyl-1-pyrroline *N*-oxide.[468] The same experiments using both GC and Pt electrodes showed lower intensities of the ESR signals for the radicals, indicating that methoxyl radical generation was more effective at the BDD electrodes.

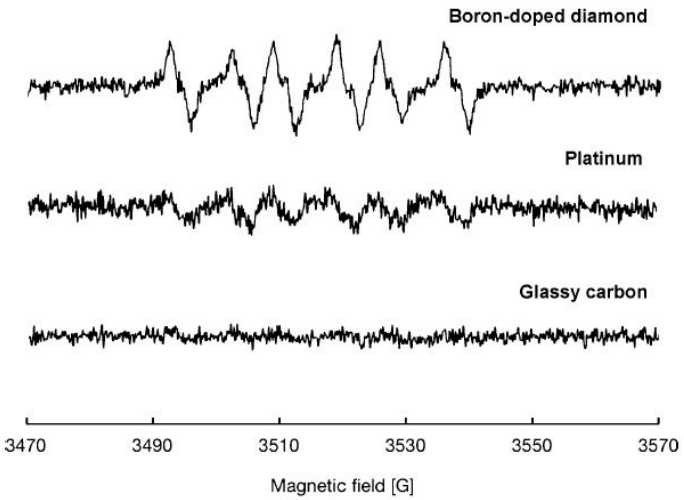

Figure 7. ESR spectra obtained for the methoxy radical on several electrode materials. Standard condition: 10 mM solutions of 5, 5'-dimethyl-1-pyrroline N-oxide in 0.1 M $LiClO_4$ dissolved in MeOH, Pt-wire cathode (Applied potential: 1.06 V *vs.* SCE), A_N (hyperfine coupling constant of N) value: 13.37 G (cf. 13.58 G), A_H (hyperfine coupling constant of H) value: 7.98 G (cf.

7.61G). (Reproduced with permission from ref. [468]. Copyright 2012, WILEY-VCH Verlag GmbH & Co. KGaA.

Furthermore, electrochemical oxidation of isoeugenol (**1**) using BDD electrodes produced benzofuran-type neo-lignan (**3**: lycarin A), molecule **5**, as a result of coupling of the intermediate (**2**) with produced methoxy radicals, and molecule **4** as a result of self-coupling of **2** (**Scheme 1**). [468] Recently, anodic methoxylation of 2-oxozolidinone using BDD electrodes has also been reported.[469]

Scheme 1: Electrochemical synthesis of licarin A (3). Reprinted with permission from ref. [468]. Copyright 2012, WILEY-VCH Verlag GmbH & Co. KGaA, Weinheim.

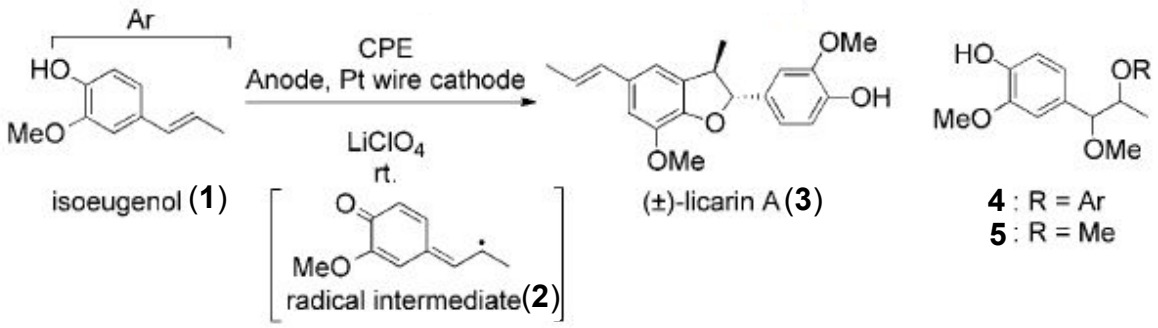

4.3.1.2 Anodic coupling reactions

Formation of the biaryl skeleton is one of the most important subjects in organic synthesis. Waldvogel et al. reported several examples showing C-H activation reaction and C-C coupling reaction of phenols, arenes, and heterocyclic compounds using BDD electrodes.[470] [471, 472] In 2006, they demonstrated chemoselective anodic ortho-coupling reaction of 2,4-dimethylphenol. Anodic oxidation using BDD electrodes, under solvent-free conditions, produced very highly selective formation of 2, 2'-biphenol, with other possible bi-products formed only at trace level.[470] Further developments saw improvements in the yield and selectivity of several homo-coupling of phenols in the presence of highly fluorinated alcohols, i.e., 1,1,1,3,3,3-hexafluoroisopropyl alcohol (HFIP).[471] In 2010, anodic and selective phenol-arene cross-coupling reactions in HFIP using BDD electrodes (**Scheme 2**) was developed.[472]

Scheme 2: The anodic cross-coupling reactions between phenols and arenes using BDD electrodes. Reprinted with permission from ref. [472]. Copyright 2010, WILEY-VCH Verlag

GmbH & Co. KGaA, Weinheim.

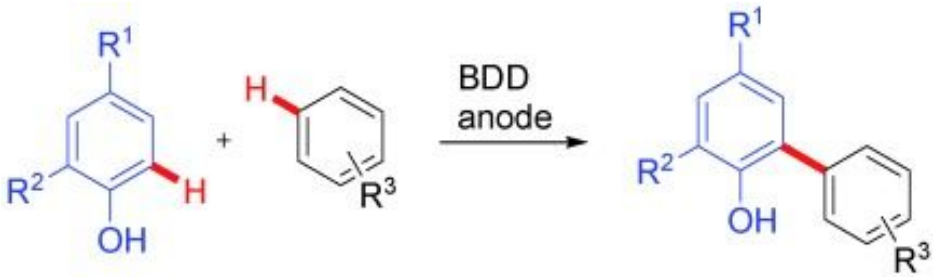

Furthermore, employing water or methanol as the mediator in the solution was found to improve the selectivity and synthetic yields, due to the shift of the oxidation potential.[473-475] In addition, partially protected nonsymmetric 2,2'-biphenols were selectively formed with high yields. The anodic reaction of O-silyl-protected phenols produced the desired nonsymmetric 2,2'-biphenols since the use of bulky silyl groups for blocking one hydroxyl moiety, prevents the oxidation of the final products (**Scheme 3**).[476] Recently, C-C cross coupling of phenols with thiophenes, that are heterocyclic compounds, has also been reported.[477]

Scheme 3: General reaction pathway for the anodic synthesis of partially protected nonsymmetric biphenols. PG: protecting group. Reprinted with permission from ref. [476]. Copyright 2016, WILEY-VCH Verlag GmbH & Co. KGaA, Weinheim.

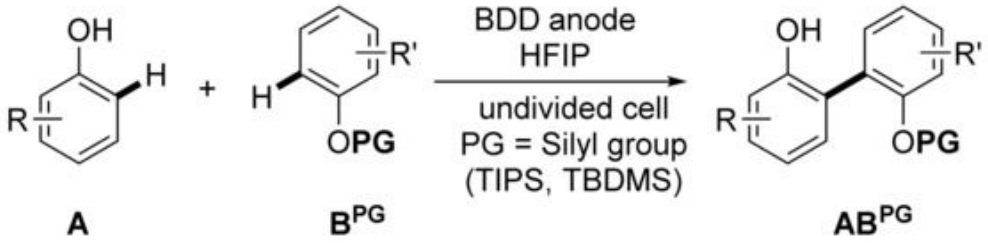

Electrochemical oxidation of isoeugenol in HFIP solution using BDD electrodes has also been studied. A stereoselective and electrocatalytic coupling reaction of isoeugenol was observed. The particular C-C bond formation and diastereoselectivity was driven by an interaction between the generated radical species and isoeugenol molecules. It was suggested that the reactant confined in the HFIP solvate cage induced the specific molecular orientation. The reason for the stereoselective conversion was considered to be the solvate interaction between HFIP and the substrate (**Scheme 4**).[478]

Scheme 4: Postulated electrocatalytic cycle of the anodic conversion of isoeugenol. Reproduced with permission from ref. [478]. Copyright 2018, Royal Society of Chemistry.

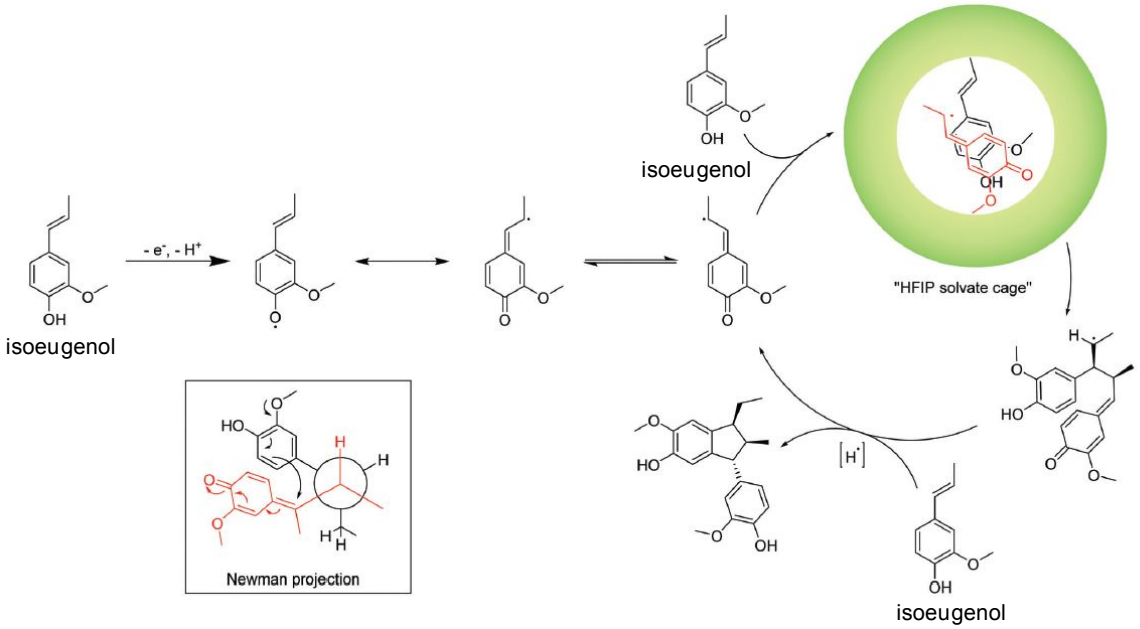

4.3.2. Transformation by cathodic reduction

Electrochemical reductive coupling reaction using BDD electrodes as an indirect approach has also been reported.[479] The radical intermediate derived from the one-electron reduction of phenylacrylate is different to that obtained by anodic oxidation of 4-hydroxyphenyl-1-propene (**Scheme 5**). Novel neolignan-type dimeric compounds were found by the reductive dimerization of cinnamic acid derivatives.

Scheme 5: Expected coupling products from one-electron oxidation (left) and one-electron reduction (right) of C_6–C_3 compounds. Reproduced with permission from ref. [479]. Copyright 2015, Beilstein-Institut, Germany.

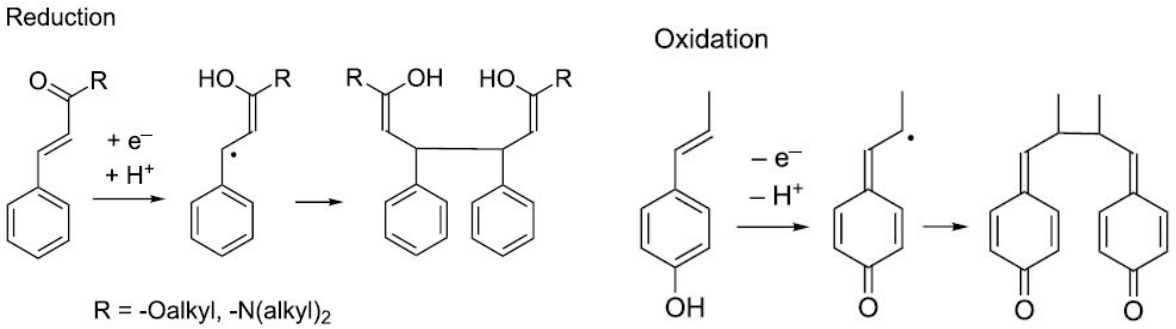

Electrochemical reduction of ester methyl cinnamate (**6**) at a constant current in acetonitrile produced (**7**), (**9**), and the hydrodimer, dimethyl 3,4-diphenylhexanedioate (**8**) (**Scheme 6**) [479]

Although GC electrodes gave similar products to that of the BDD electrode, Pt and Mg electrodes showed mainly hydrogen evolution. The hydrodimer (**8**) was then successfully converted by chemical reactions to neoligan-type compounds.[480]

Scheme 6: Electrochemical reduction of ester methyl cinnamate (**6**) using a BDD electrode. Reproduced with permission from ref. [479]. Copyright 2015, Beilstein-Institut, Germany.

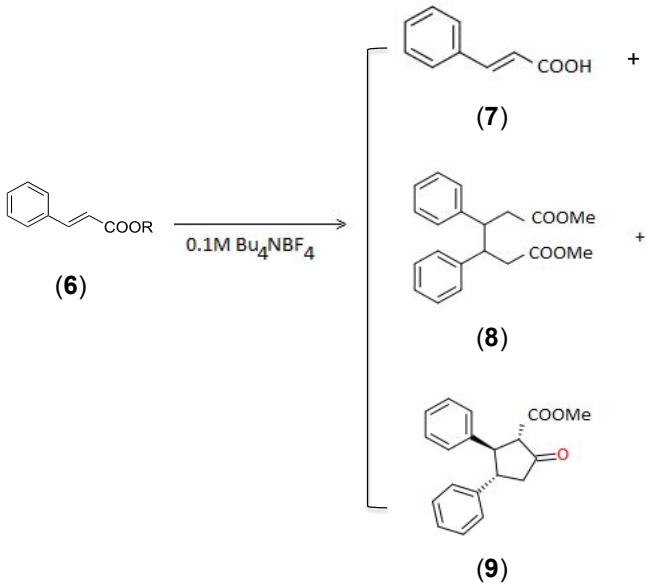

The following facts have been thus established for electrosynthesis using BDD electrodes:[22] (i) BDD electrodes are required with low NDC content and high conductivity (BDD with high boron levels); (ii) no effect of BDD surface termination on electrosynthetic applications has yet been found; (iii) initiation of electrochemical reactions occurs only after the formation of oxyl radicals; (iv) there are no advantages of BDD electrodes over other electrodes unless radical compounds are formed; v) the wide potential window of BDD electrodes plays a key role and determines the selectivity of the products; (vi) the applied current or potential is crucial for product selectivity.[22]

4.4 Electrocatalysis

BDD and NDD films have been employed as the electrode or catalyst support for electrocatalytic applications. For example, electrochemical and photoelectrochemical reduction of carbon dioxide, one hot topic in the field of electrocatalysis,[481-487] has been conducted using conductive diamond as a metal-free electrocatalyst (also named carbocatalyst).[384] Conversely, loading of metal catalysts onto the surface of the conductive diamond has expanded the usage of diamond films into fuel cells.

4.4.1. CO_2 reduction

The conversion of carbon dioxide (CO_2) into useful chemicals has attracted much attention in recent years.[481] Many kinds of electrodes, generally metals, have been studied for electrochemical reduction of CO_2.[482-487] Hori et al. found that the products of electrochemical CO_2 reduction depend on the surface properties of the electrode materials (*e.g.*, the adsorption of CO_2 onto the electrode surface).[483] "Active electrodes" which adsorb CO_2 generate CO in aqueous solutions and $HCOO^-$ in non-aqueous solutions. Conversely, "non-active electrodes" which do not adsorb CO_2, produce $HCOO^{\bullet-}$ and $CO_2^{\bullet-}$ in non-aqueous and aqueous solutions, respectively. Note that the CO_2 reduction generally occurs at around the same potential as hydrogen evolution, which is thus the competitive reaction.[483-487]

Several reports have been published concerning the utilization of conductive diamond for CO_2 reduction. For example, on un-doped diamond with hydrogen termination, reduction of aqueous CO_2 to CO was achieved with a product selectivity of greater than 90% (**Figure 8A**). The radicals of $CO_2^{\bullet-}$ were produced by solvated electrons through illumination of inexpensive diamond substrates with UV light.[488] Later, hydrogen-terminated diamond NPs with an average diameter of 125 nm were employed to initiate selective photochemical reduction of CO_2 to CO.[489]

Other conductive (doped) diamond has also been employed for electrochemical CO_2 reduction. On BDD electrodes, electrochemical reduction of CO_2 in methanol containing tetrabuthylammonium perchlorate (TBAP) was found at a potential of -1.5 V (*vs.* Ag/AgCl), with hydrogen evolution commencing at a potential of around -1.8 V (*vs.* Ag/AgCl). Under a potential of -1.5 V (*vs.* Ag/AgCl), the main products were formaldehyde and formic acid. In comparison to other electrodes (*e.g.*, GC, Cu, Sn, Ag, W), their yield efficiencies using BDD were the highest (**Figure 8B**). It was explained that BDD with its sp^3 carbon bonds functions as an ideal "non-active electrode" known to have lower adsorption properties. The radical $CO_2^{\bullet-}$ was possibly formed, followed by the formation of formaldehyde or formic acid.[482] Such mechanisms were further elaborated by Koper et al. who discussed the importance of disproportion and chemical reaction including base-catalysed Cannizzaro reactions.[490]

To improve the performance of CO_2 reduction on BDD electrodes, the optimization of solution compositions (*e.g.*, alkali-metal cations,[491] ammonia solution as the absorber[492, 493]) and the

effect of boron-concentration[494, 495] was further conducted. When a flow cell system was applied (**Figure 8C**), a faradaic efficiency for the production of formic acid as high as 94.7 % was obtained with a rate of production up to 473 μmol m^{-2} s^{-1}.[491] BDD was also decorated with a catalytically active cobalt complex for electrochemical CO_2 reduction. Such surfaces exhibited good stability and electrocatalytic activity toward electrochemical reduction of CO_2 to CO in acetonitrile solution.[496] Silver NP coated oxygen-terminated BDD films showed excellent selectivity for photoelectrochemical CO_2 reduction into CO (*e.g.*, estimated CO:H_2 mass ratio of 318:1) and recycle ability (*e.g.*, stable for five cycles of 3 h each) under 222 nm irradiation.[480] Furthermore, copper-modified BDD electrodes were able to produce C_2 and C_3 species (*e.g.*, ethanol, acetaldehyde, and acetone) at a relatively low potential (-1.0 V *vs.* Ag/AgCl).[493]

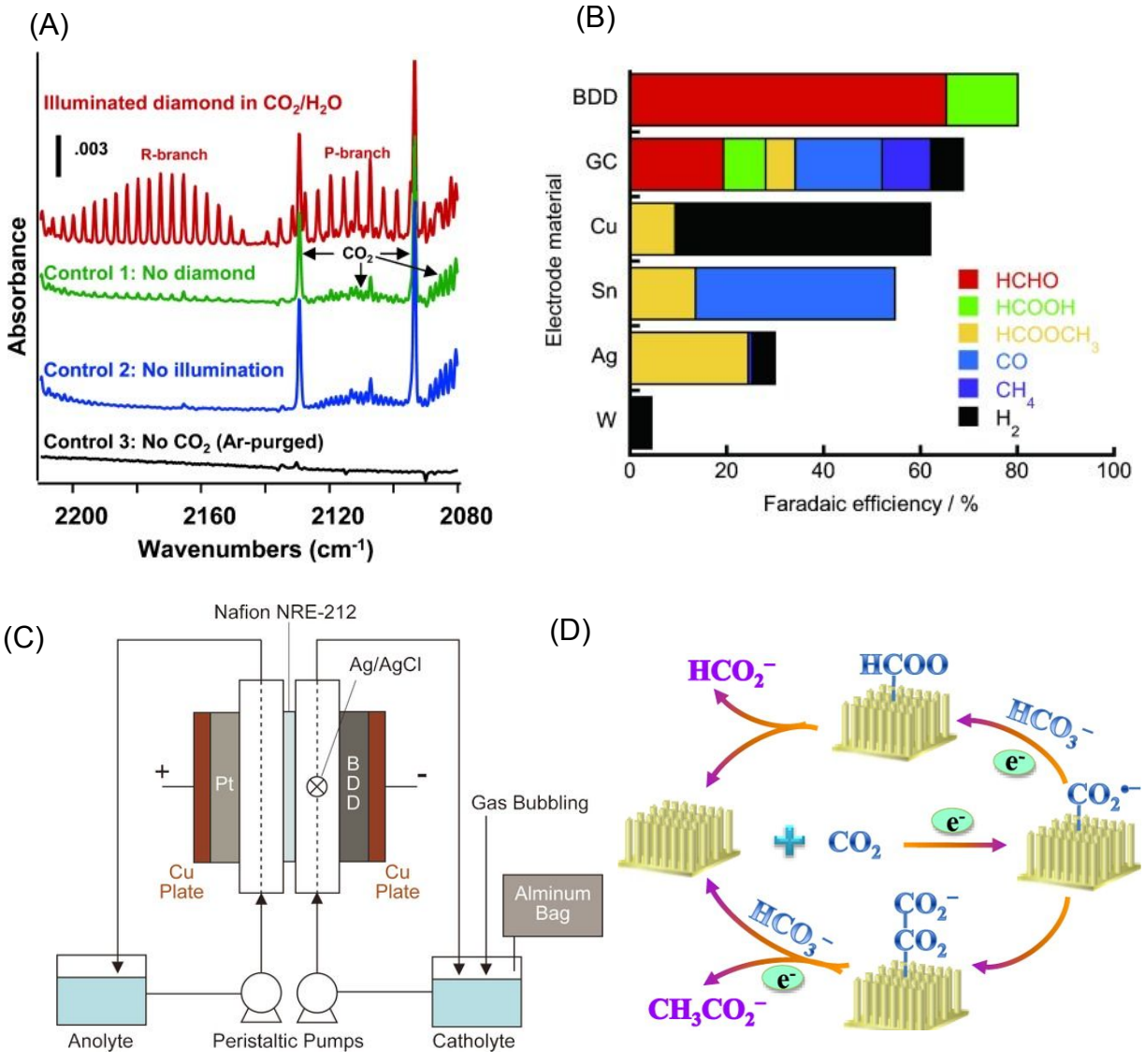

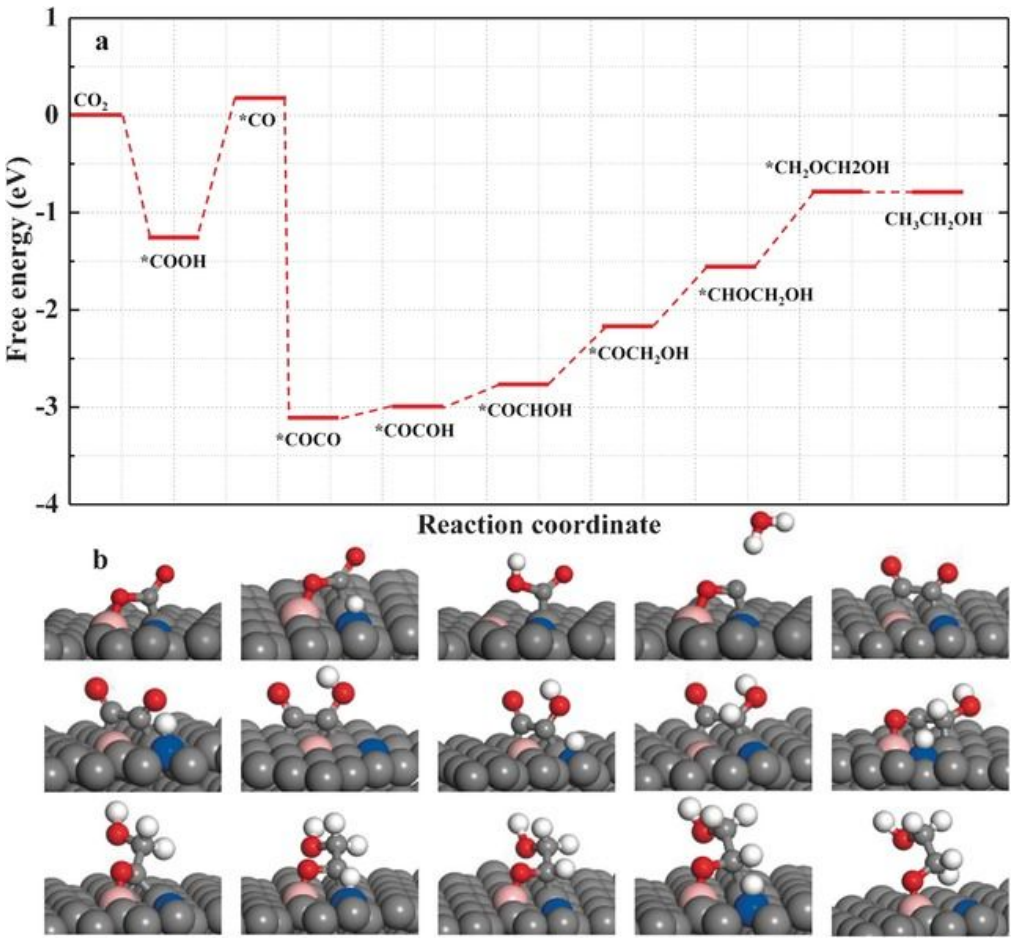

Figure 8. (A) FTIR spectra of gaseous head space demonstrating reduction of CO_2 to CO by illuminated diamond, along with control samples. Reprinted with permission from ref. [489]. Copyright 2014, WILEY-VCH Verlag GmbH & Co. KGaA, Weinheim. (B) Faradaic efficiency of the products generated by the electrochemical reduction of CO_2 using various electrodes in a MeOH electrolyte. The electrochemical reduction was performed at −1.5 V (*vs.* Ag/Ag^+) using a platinum counter electrode in a two-compartment cell (100 mL) separated by Nafion for 1 h at room temperature and atmospheric pressure. Reprinted with permission from ref. [482]. Copyright 2014, WILEY-VCH Verlag GmbH & Co. KGaA, Weinheim. (C) Diagram of the two-compartment flow cell. Reprinted with permission from ref. [491]. Copyright 2018, WILEY-VCH Verlag GmbH & Co. KGaA, Weinheim. (D) Schematic pathway for electrocatalytic CO_2 reduction on N-doped nanodiamond coated Si rod array electrode. Reprinted with permission from ref. [497]. Copyright 2015, American Chemical Society. (E) a) Free energy diagrams for CO_2 reduction on (111) facet of boron- and nitrogen- co-doped diamond (BND), b) Energetically favorable structures for elementary steps of CO_2 reduction on (111) facet of BND (gray = C, pink = B, blue = N, red = O, white = H). Reprinted with permission from ref. [63]. Copyright 2017, WILEY-VCH Verlag GmbH & Co. KGaA.

On a nitrogen-doped nanodiamond coated Si rod array, CO_2 was preferentially and rapidly converted to acetate over formate with an onset potential of -0.36 V (*vs.* RHE). A faradic efficiency of 91.2 - 91.8% was achieved for CO_2 reduction at -0.8 to -1.0 V. Such superior performance for CO_2 reduction was attributed to its high overpotential for hydrogen evolution and nitrogen doping, where N-sp^3 carbon species were highly active for CO_2 reduction. Electrokinetic data and *in situ* infrared spectrum revealed the main pathway for CO_2 reduction as $CO_2 \rightarrow CO_2^{\bullet-} \rightarrow (COO)_2^{\bullet} \rightarrow CH_3COO^-$ (**Figure 8D**).[497] While on the boron and nitrogen co-doped nanodiamond (BND) electrode, efficient, stable, and selective reduction of CO_2 to ethanol was achieved with a high Faradaic efficiency of 93.2 % at -1.0 V (*vs.* RHE). The synergistic effect of boron and nitrogen co-doping, high nitrogen content and overpotential for hydrogen evolution were proposed to explain such a superior performance. The possible pathway for CO_2 reduction revealed by DFT computation (**Figure 8E**) was suggested as $CO_2 \rightarrow {}^*COOH \rightarrow {}^*CO \rightarrow {}^*COCO \rightarrow {}^*COCH_2OH \rightarrow {}^*CH_2OCH_2OH \rightarrow CH_3CH_2OH$.[63]

4.4.2 Fuel cells

The application of conductive diamond (mainly BDD) for the construction of fuel cells has been explored. In these studies, diamond is frequently used as electrode support to load various electrocatalysts (*e.g.*, PtNi,[498] PtRu,[499] Pt/TiO_2,[500] Pt/TiN,[501] Pt/RuO_x,[502] *etc.*). The catalytic activity of these electrocatalyst deposited diamond electrodes has been investigated toward methanol oxidation or oxygen reduction. For example, the electrolytic activity of a PtNi coated BDD electrode was tested using cyclic voltammetry, chronoamperometry and linear sweep voltammetry.[498] This electrode exhibited higher catalytic activities for both methanol oxidation and oxygen reduction reactions than Pt coated BDD, as well as greater stability compared to PtNi coated XC-72 carbon.[498] With the primary objective of pursuing a corrosion-resistant carbonaceous electrocatalyst support for proton exchange membrane fuel cells, diamond powders were employed.[105, 107]

In conclusion, various conductive diamond films and structures are useful for electrochemical energy conversion. Their surface chemistry as well as dimensions determines the catalytic performance for these energy storage applications.

4.5 Electrochemical energy storage

Due to the unique advantages of BDD (*e.g.*, wide electrochemical potential window, varied surface termination, high mechanical hardness, high thermal conductivity, chemical inertness, and excellent stability in various harsh environments and under extremely tough conditions, *etc.*),[503] BDD has been utilized recently as electrode material to construct various electrochemical energy storage devices (*e.g.*, supercapacitors, batteries, solar cells, *etc*.).

4.5.1 Supercapacitors

Supercapacitors (SCs), also named electrochemical capacitors, fill the gap between conventional capacitors and rechargeable batteries from the energy and power density point of view. In comparison to batteries, SCs feature higher power density (> 1000 - 1500 W kg^{-1}), shorter charging-discharging times (within 0.1 s), improved cycling stability (up to 1 000 000 charging-discharging cycles), wider ranges of operating temperatures (from -40 to 70 °C), and better safety.[504] In other words, SCs own higher energy densities than conventional capacitors and much larger power densities compared to batteries. According to the charge storage mechanisms, SCs can be classified into two types: electrical double layer capacitors (EDLCs) based on ion adsorption/accumulation at interfaces of the electrode and electrolyte and pseudocapacitors (PCs), which rely on reversible faradaic reactions of redox species immobilized on the electrodes or dissolved in the solution. The performance of a SC is generally evaluated by four physical parameters: capacitance (*C*), power (*P*) and energy densities (*E*), as well as the cycling stability (or capacitance retention). The development of high performance SCs, namely those with high and stable *C* as well as high *E* and *P*, is the core of SC researches for both science and industry. Nowadays, the applications of SCs have been expanded to a variety of areas, ranging from low-emission hybrid electric vehicles, pulse power sources, to backup sources for high power delivery or uptake. Moreover, flexible, printable, and wearable SCs have been integrated as well into smart clothes, sensors, wearable electronics, and drug delivery systems.[505-508]

To improve the capacitance of conductive diamond SCs, producing diamond electrodes with large surface areas is a promising and efficient approach. Moreover, conductive diamond has a rich surface carbon chemistry and varied surface terminations. Therefore, besides acting as a capacitor, BDD can be integrated with other sp^2 carbon materials to form hybrid films. Such diamond-based films are expected to deliver much higher capacitances than BDD itself. Additionally, through the combination of diamond-based nanostructures with redox species loaded onto the electrode or dissolved in the solution, PCs with enhanced performance have been

fabricated. The performance of SCs based on various conductive diamond nanostructures and different electrolytes are shown in **Figure 9**.

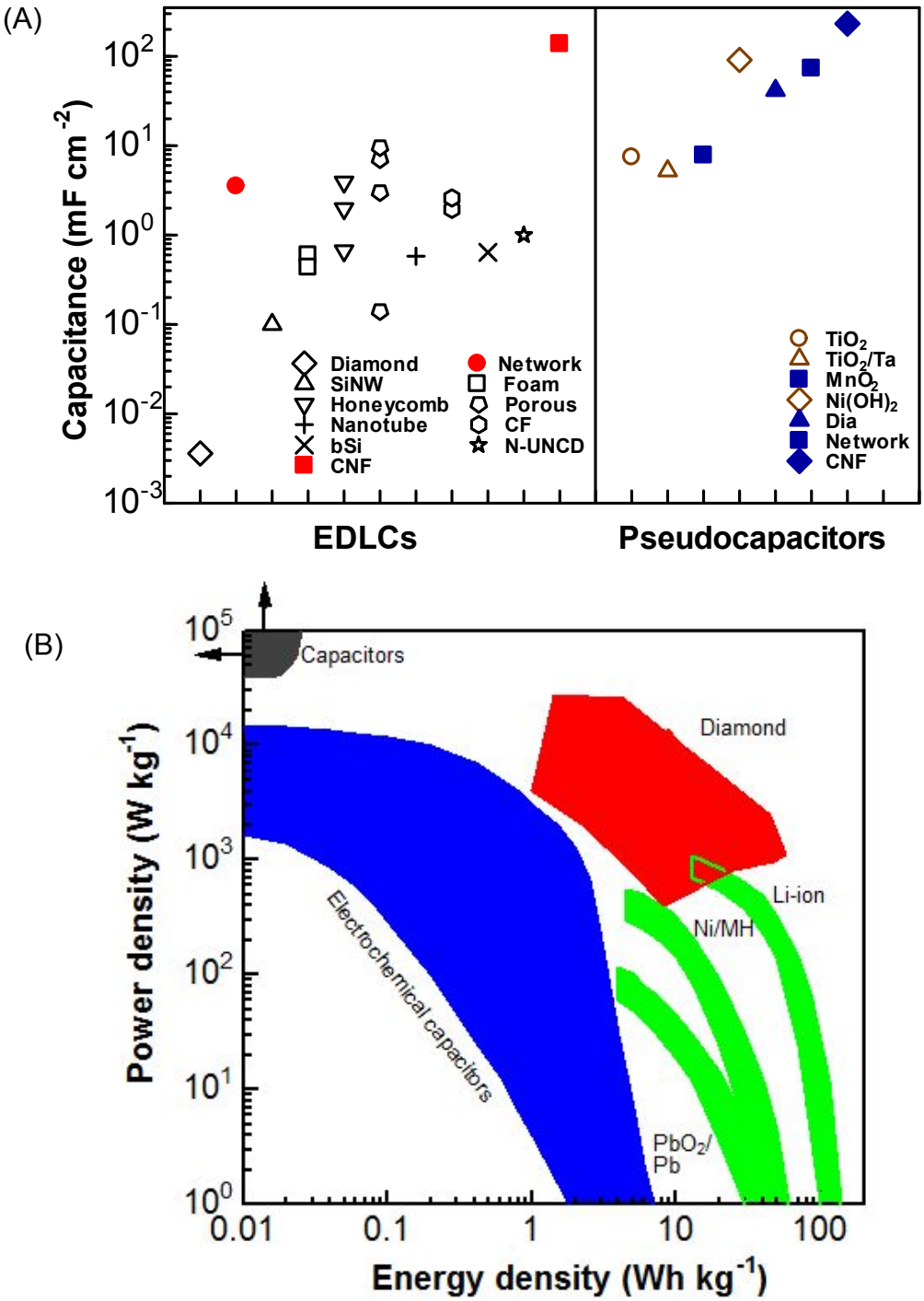

Figure 9. (A) Comparison of capacitances of conductive diamond SCs. (B) Comparison of power and energy densities of battery-like conductive diamond SCs with capacitors, electrochemical capacitors and batteries. Reprinted with permission from ref. [509]. Copyright 2018, University of Siegen, Siegen, Germany.

4.5.1.1 Conductive Diamond EDLCs

Various porous nanostructures (*e.g.*, diamond paper,[94] honeycomb diamond,[95] porous diamond,[96] and diamond nanowires,[97] *etc*.) (section 2.3) have been applied as the capacitor electrodes for the construction of EDLCs. In most cases, a three-electrode system was employed to estimate the capacitances of these capacitor electrodes. The comparison of their capacitances are shown in **Figure 9(A)**.[509] For example, a honeycomb structured BDD based EDLC showed a specific capacitance of 3910 μF cm^{-2} and 666 μF cm^{-2} in aqueous and organic solution, respectively.[510] A roughened BDD surface layer with excavated holes was produced by catalytic dissolving of the carbon structures with nickel, cobalt, and platinum NPs in hydrogen atmosphere under a high temperature. This procedure resulted in a larger surface area and thus the capacitance of this BDD electrode was ×15 enhanced in comparison to a planar diamond electrode.[511]

Diamond foam based EDLCs, produced *via* overgrowth of SiO_2 spheres with thin BDD films, attained specific capacitances of 598 and 436 μF cm^{-2} in aqueous and organic solutions, respectively, as well as a high power density of 807 W cm^{-3}. These diamond foam based EDLCs are close to producing the best power performance of electrolytic capacitors.[512] The capacitance of a BDD (with a thickness of 240 nm) coated silicon nanowire structure was 105 μF cm^{-2} in the ionic liquid 1-methyl-1-propylpyrrolidinium bis(trifluoro methylsulfonylimid). An energy density of 84 μJ cm^{-2}, a power density of 0.94 mW cm^{-2}, and good stability (retention stability of 93.3% after 10,000 cycles at the scan rate of 5 V s^{-1}) were demonstrated.[513] An alternative porous BDD structure produced using a highly porous polypyrrole scaffold as the template exhibited a capacitance up to 3 mF cm^{-2} in aqueous $LiClO_4$ and a low electrochemical impedance. At low frequency, between 0.1 Hz and 10 Hz, the impedance of the electrode with an area of 0.12 cm^{-2} was measured to be ×600 lower than that of a planar diamond electrode.[514]

Porous BDD films overgrown on CNTs showed about ×450 enhancement in electro-active area and double-layer capacitance in comparison to that for a planar BDD electrode.[515] BDD films grown on carbon fibers obtained from poly-acrylonitrile precursors through heat treatment at 2000 °C delivered an increased capacitance of up to 1.94 mF cm^{-2}. This value is about ×8 larger than that for carbon fibers formed under identical conditions.[516] By combining conductive diamond with these sp^2 carbon materials, enhanced performance has been achieved, compared to that of BDD EDLCs alone. This is attributed partially to further increased surface areas and partially to the addition of the capacitances from the other carbon materials.[417] Porous BDD formed by means of a two-step thermal etching of diamond showed a capacitance of 140 μF cm^{-2}

in aqueous solution.[90] A diamond porous structure obtained *via* the oxidative etching of BDD electrodes within steams or CO_2[93] improved its active surface area by a factor of 20 compared to a planar BDD.[91] The capacitance of a porous conductive diamond network was recorded to be 13.7 F g^{-1} or 17.3 F cm^{-3} at 0.1 V s^{-1} in 0.1 M H_2SO_4.[89] These values are comparable to that (ca. 13 F g^{-1}) of a BDD hollow fiber.[517]

Due to the rich carbon surface chemistry, BDD is also promising as the electrode support to form novel sp^2-sp^3 carbon hybrid films. For example, the direct growth of other sp^2 carbon materials (*e.g.*, CNTs,[518] graphene,[519] carbon nanofibers (CNF),[520] *etc*.) on thin BDD films has been studied. For example, hybrid films of vertically aligned CNFs on BDD (CNF/BDD) have been grown in a thermal CVD reactor; a sputtered copper thin film acted as the catalyst and C_2H_2 as the reaction gas. In 1.0 M H_2SO_4 aqueous solution, the capacitance of a CNF/BDD based EDLC was as high as 137.90 mF cm^{-2} at a current density of 2 mA cm^{-2}.[520] Such a large capacitance is due to the following factors: (i) a large surface area of this CNF/BDD hybrid film due to its porous structure, (ii) high conductivity due to containment of stacked graphene layers inside CNFs and copper metal catalysts inside the CNFs, (iii) high stability, and (iv) free of binder.

Conductive diamond particles (section 2.4) have been applied for the construction of supercapacitors. They are normally annealed at high temperature under vacuum or in an inert atmosphere to form onion-like carbon on the nanodiamond surface.[521] The capacitances of the EDLCs based on these materials were thus found to be dependent on the degree of diamond graphitization, or annealing temperature.[522] For example, through graphitization of detonation nanodiamond powder at 897 - 1867 ^oC, onion-like carbon with varied structure and properties (*e.g.*, surface area and conductivity) was produced.[522] The double layer capacitance was estimated to be about 20 - 40 F g^{-1} and 70 - 100 F g^{-1} in 1.0 M H_2SO_4 acid and 6.0 M KOH alkaline solutions, respectively.[522] By annealing the composite films of graphene oxide and nanodiamond at 1200 ^oC, mesoporous graphene and onion-like carbon were synthesized.[521] These films were flexible, mechanically stable, highly conductive (7400 to 20,300 S m^{-1}), and exhibited a maximal specific surface area of about 420 m^2 g^{-1} with pore size in the range of 2 - 11 nm. The formed EDLCs showed a specific capacitance of 143 F g^{-1} at a discharge current density of 0.2 A g^{-1} in 1.0 M H_2SO_4 aqueous solution.[521] Furthermore, reduced graphene oxide matrices with intercalated conductive diamond particles of different densities have been prepared and further utilized as electrode materials for SC applications. The reduced mass ratio of

graphene oxide to nanodiamond from 10 to 1 provided the maximal capacitance of 186 ± 10 F g^{-1} in 1 M H_2SO_4 with an excellent cycling stability.[523]

4.5.1.2 Conductive Diamond PCs

To construct conductive diamond PCs, BDD films with different doping levels were deposited on TiO_2 (BDD/TiO_2) nanotubes and applied as capacitor electrodes.[524] The measured capacitances of these capacitor electrodes in 0.1 M $NaNO_3$ at a scan rate of 10 mV s^{-1} were 2.10, 4.79, and 7.46 mF cm^{-2} when the concentration ratio of boron to carbon was 2000, 5000, and 10,000, respectively.[525] The enhanced performance of the BDD/TiO_2 nanotube electrodes was explained by the increased surface area, additional capacitance introduced with the presence of TiC and Ti_2O_3, the synergistic effect of TiO_2 treatment in CH_4:H_2 plasma and the high electrical conductivity of BDD.[525]

A more efficient approach to achieve high capacitances of conductive diamond PCs is to use pseudo-capacitive species (*e.g.*, metal oxides, conducting polymers, soluble redox-active couples, *etc.*) combined with BDD as electrodes or dissolved in the aqueous solutions as electrolytes. For instance, the combination of BDD and $RuO_x \cdot nH_2O$ for the construction of SCs has been reported. $RuO_x \cdot nH_2O$ was deposited electrochemically on the BDD film as well as on diamond powders. The specific capacitances obtained in 0.5 M H_2SO_4 were 132 and 324 F g^{-1} for the BDD film and powders, respectively.[503] $Ni(OH)_2$ decorated conductive diamond nanowires have been employed to construct PCs. Due to the reversible redox transitions of nickel hydroxide and nickel oxy-hydroxide groups, a high gravitational *C* of 1601 F g^{-1} (about 80% of the theoretical value) and a *P* of up to 3×10^5 W kg^{-1} have been achieved. This high *P* was explained by fast ion diffusion inside this 3D composite. However, relatively poor cycling stability was noticed (e.g., the capacitance retained only 70-80% of the initial value after 1000 cyclic voltammetric cycles within a 0.5 V potential window at a scan rate of 100 mV s^{-1}).[526]

MnO_2 coated BDD showed varied capacitances as a function of the mass of MnO_2 deposited. At a MnO_2 area density of 24 μg cm^{-2}, a maximum *C* of 326 F g^{-1} (namely 7.82 mF cm^{-2}) or 349 F g^{-1} was obtained from CV at a scan rate of 10 mV s^{-1} or a galvanostatic charging- discharging process at 3 A g^{-1}, respectively. The capacitance retention was only 66% after 1000 charging-discharging cycles at a scan rate of 100 mV s^{-1}.[153] The PC based on conductive diamond NPs embedded in polyaniline (with the weight ratios of 3-28%) showed a stable capacitance of 640 F

g^{-1} in 1.0 M H_2SO_4 for 10 000 cycles. This capacitance was ×3-4 higher than that for activated carbons, and more than ×15 higher than that for onion-like carbon.[527]

As an alternative approach, water-soluble redox couples (*e.g.*, $Fe(CN)_6^{3-/4-}$) dissolved in 1.0 M Na_2SO_4 aqueous solution were used as redox electrolytes to form planar BDD, BDD networks as well as CNF/BDD PCs. For example, when a BDD film was employed as the capacitor electrode, its *C* reached 41.51 mF cm^{-2} at a scan rate of 10 mV s^{-1}.[528] For the BDD network capacitor electrode, its *C* was 73.42 mF cm^{-2} at a charging-discharging current density of 1 mA cm^{-2}.[528] By applying a CNF/BDD hybrid film produced under optimal conditions (*e.g.*, a copper sputtering time of 60 s, a CNF growth time of 60 min in C_2H_2 atmosphere using a thermal CVD technique) a *C* of 232.01 mF cm^{-2} was achieved at a charging-discharging current density of 2.0 mA cm^{-2}.[520]

Conductive diamond SC devices fabricated with two-electrode configurations have also been reported. The prototype SC demonstrated in aqueous electrolyte a gravimetric *C* of 0.688 mF cm^{-2} (0.645 F g^{-1}) per layer with excellent stability (92% of capacitance retention after 20,000 cycles at a current density of 1 mA cm^{-2}).[94] A high specific *P* of 1×10^5 W kg^{-1} has been achieved as well.[94] By applying poly(3,4-(ethylenedioxy)thiophene) (PEDOT) coated BDD diamond overgrown on silicon nanowires as electrodes, the constructed symmetric micro-SC device exhibited a high *C* of 9.5 mF cm^{-2}, as well as high *E* and *P* values of 26 mJ cm^{-2} and 1.3 mW cm^{-2} in a large cell voltage of 2.5 V. The capacitance retention was examined to be 80% after 15,000 galvanostatic charging-discharging cycles at a current density of 1 mA cm^{-2}.[97] When the redox species ($Fe(CN)_6^{3-/4-}$) was introduced in the electrolyte, several two-electrode symmetric SC devices have been constructed using planar diamond, diamond network, CNF/BDD hybrid films as the capacitor electrodes.[528] For example, for a diamond PC device, the maximal *E* and *P* reached 46.96 W h kg^{-1} and 9.87 kW kg^{-1}, respectively, [528] these values increased to 56.5 W h kg^{-1} and 13.7 kW kg^{-1}, respectively, for a diamond network PC device[528] and were found to be 44.1 W h kg^{-1} and 25.3 kW kg^{-1}, respectively for a CNF/BDD PC device. A CNF/BDD EDLC device using inert electrolyte (H_2SO_4), recorded maximal *E* and *P* values of 22.9 W h kg^{-1} and 27.3 kW kg^{-1}, respectively.[520] The performance comparison of these battery-like diamond SCs with capacitors, batteries, and related devices is summarized in **Figure 9B**.[509]

4.1.5.3 Supercapacitor demonstrators

Considering the practical applications, a conductive diamond-based pouch cell was fabricated as a prototype for diamond SCs (**Figure 10A**).[94] The dimension of the pouch was 1.5 × 2 cm^2 using

stainless steel as a current collector. Freestanding conductive diamond paper (section 2.4) was used as the electrode material. Two membranes, the size of the pouch, were integrated in the cell. The porous conductive diamond paper (weight only 3.2 mg) was used as the anode. Aqueous 3 M $NaClO_4$ was used as the electrolyte.

A stand-alone demonstrator based on CNF/BDD EDLC devices has also been fabricated (**Figure 10B**).[520] It consists of three EDLC devices assembled in series, a single-board microcontroller to control the charging-discharging processes, a red light-emitting diode (LED), and a universal serial bus (USB) cable to charge the device. In a CNF/BDD SC device, two CNFs/BDD capacitor electrodes were attached tightly to both sides of the cell. The area of each electrode exposed to the electrolyte was about 0.785 cm^2. A 50 μm Nafion membrane was fixed with two sheets in the middle of the cell and an electrolyte of 1.0 M H_2SO_4 employed. With a high voltage at an initial stage, the LED was very bright. The light lasted for few seconds and became weaker till it ceased.[520]

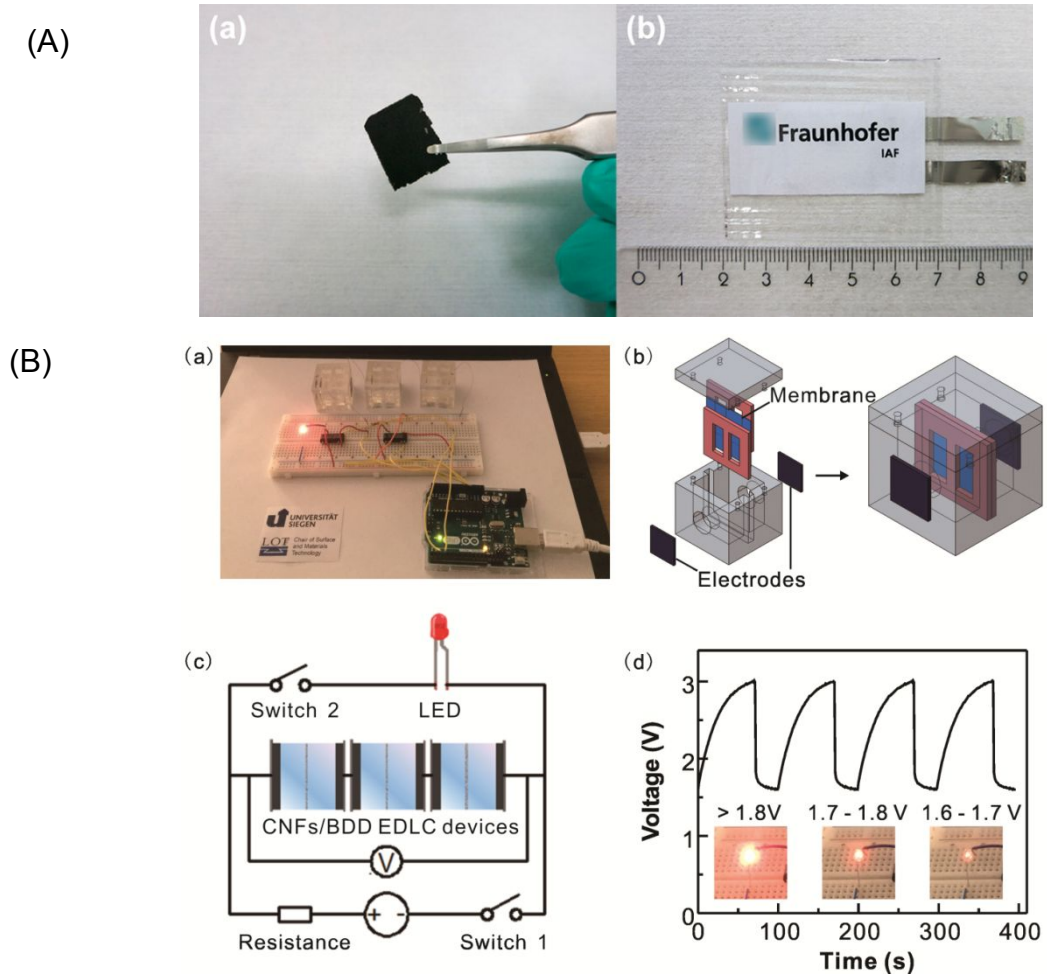

Figure 10. (A) Photos of (a) a piece of free-standing diamond paper with a thickness of ~50 μm;

(b) a diamond pouch cell supercapacitor composed of two pieces of such membranes. The logo of the institute is intentionally blurred for copyright reasons. Reprinted with permission from ref. [94] Copyright 2016, American Chemical Society. (B) A stand-alone CNFs/BDD SC demonstrator: (a) a photograph of the demonstrator consisting of three CNFs/BDD EDLC devices in series, a single-board microcontroller connected to the computer with a USB cable, and a red LED; (b) the design of a CNFs/BDD SC prototype used in the system; (c) the schematic electrical circuit diagram related to (a); (d) typical curves of the voltage as a function of time during the charging-discharging processes. The insets show the variation of light intensity of the red LED in relation to the cell voltage. Reprinted with permission from ref. [520]. Copyright 2018, WILEY-VCH Verlag GmbH & Co. KGaA.

4.5.2 Batteries

Diamond has also been utilized for the construction of lithium ion batteries,[529] and nuclear batteries.[530] For example, UNCD diamond coated natural graphite-copper has been used as the anode material in Li-ion batteries,[531] enhancing the capacity retention by orders of magnitude, compared to graphite-copper anodes.[531] BDD films grown on carbon felt using HFCVD has also been applied as an intercalation electrode for Li-ion batteries.[529] Such composite electrodes contain a BDD layer, leading to higher conductivity and smaller grain sizes. They are richer in boundary or sp^2 sites, presenting a reversible specific capacity that is much larger than that of the substrate alone. Depending on the boron doping level of the diamond layers (10^{19} - 10^{21} cm^{-3}), the capacity of the composite electrode was measured to be 160 - 370 mAh g^{-1}, associated with lithium storage.[529]

Nanodiamonds were used as an electrolyte additive in the presence of lithium ions, in order to produce dendrite-free lithium metal deposits: dendritic growth of Li is a problematic failure mechanism in battery operation. The uniform formation of lithium arrays in the presence of the nanodiamond was postulated due to Li^+ ions preferentially adsorbing onto the nanodiamond surfaces with a low diffusion energy barrier. This behavior **(Figure 11A)** significantly altered the subsequent lithium plating, resulting in an enhanced electrochemical cycling performance. The nanodiamond-modified electrolyte was found to lead to a stable cycling of lithium | lithium symmetrical cells up to 150 and 200 h at 2.0 and 1.0 mA cm^{-2}, respectively (**Figure 11B**).[532]

A high-quality DND thin film was also developed as an interfacial protection layer to reinforce the native solid-electrolyte interphase on a Li metal anode. A unique double-layer nanodiamond design was proposed to enhance the defect tolerance of the artificial interface, ensuring the

macroscopic uniformity of the lithium ion flux. The nanodiamond thin film possessed a hardness of higher than 200 GPa modulus for dendrite suppression **(Figure 11C)**. Significantly improved battery performance was realized in both half and Li-S full cells, which effectively arrested dendrite propagation, resulting in controlled Li deposition, significantly improved cycling efficiency **(Figure 11D)**.[533]

(A)

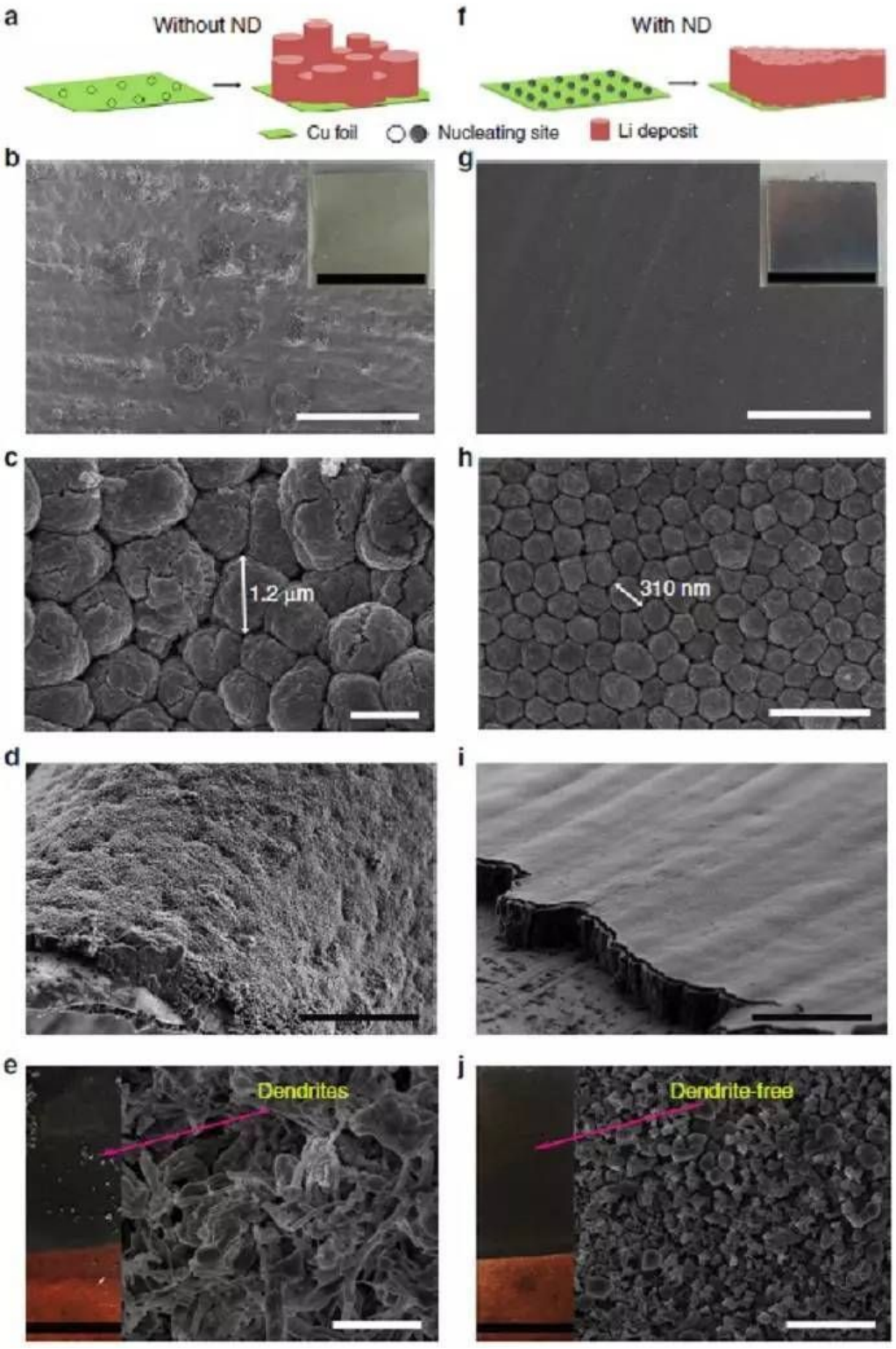

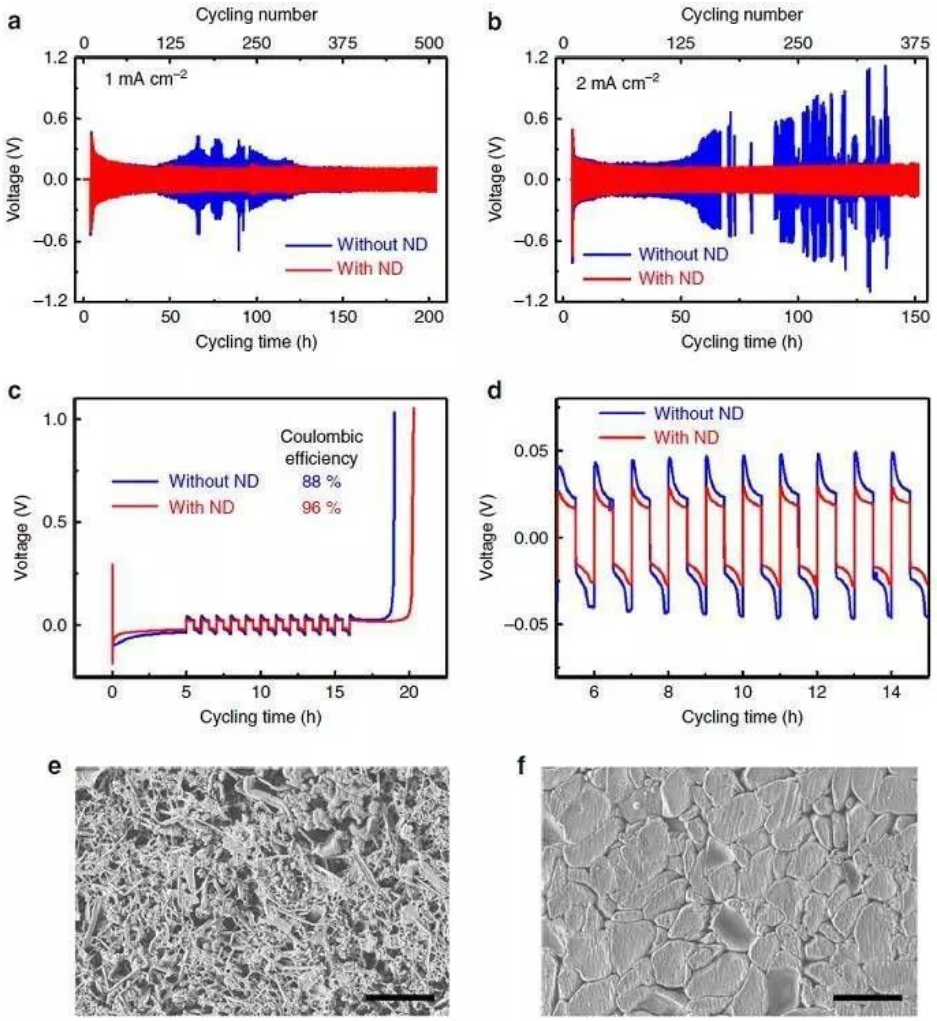
a
Cycling number
0 125 250 375 500
1 mA cm−2
Voltage (V)
1.2 0.6 0.0 −0.6 −1.2
Without ND
With ND
0 50 100 150 200
Cycling time (h)
b
Cycling number
0 125 250 375
2 mA cm−2
Voltage (V)
1.2 0.6 0.0 −0.6 −1.2
Without ND
With ND
0 50 100 150
Cycling time (h)
c
Coulombic efficiency
Without ND 88 %
With ND 96 %
Voltage (V)
1.0 0.5 0.0
0 5 10 15 20
Cycling time (h)
d
Without ND
With ND
Voltage (V)
0.05 0.00 −0.05
6 8 10 12 14
Cycling time (h)
e
f

(C)

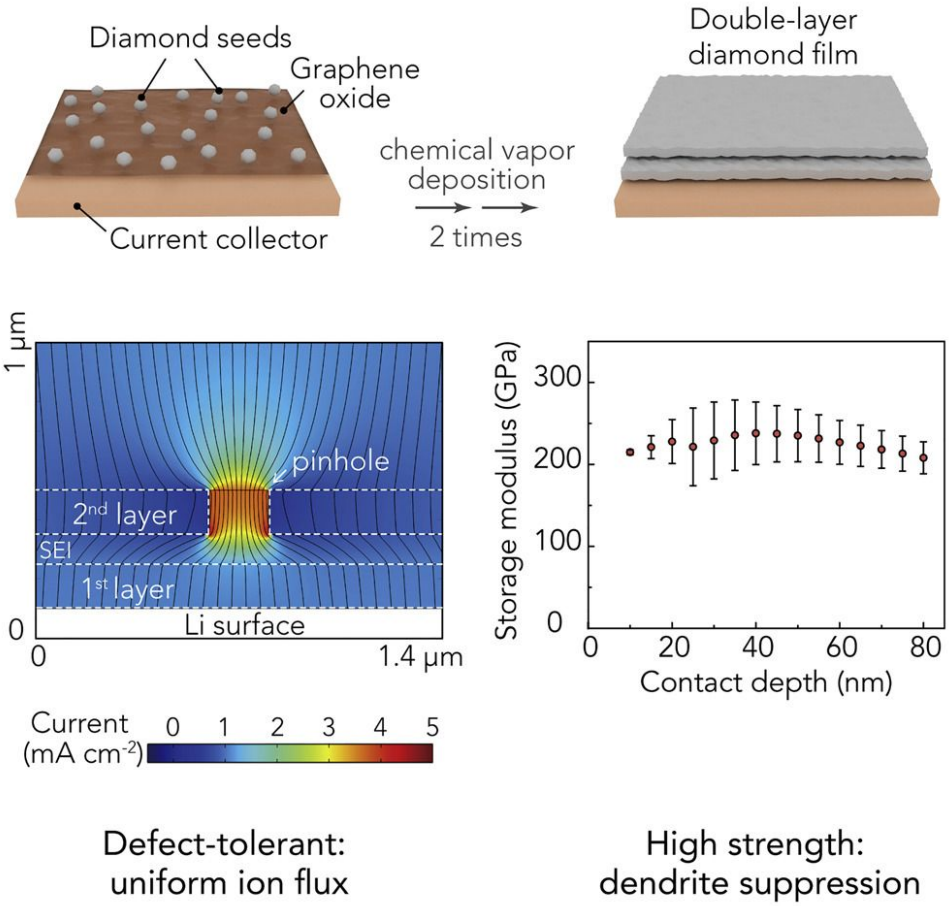
Diamond seeds
Graphene oxide
Current collector
chemical vapor deposition
2 times
Double-layer diamond film
1 μm
pinhole
2nd layer
SEI
1st layer
Li surface
0
0
1.4 μm
Current (mA cm-2)
0 1 2 3 4 5
Storage modulus (GPa)
300
200
100
0
0 20 40 60 80
Contact depth (nm)
Defect-tolerant: uniform ion flux
High strength: dendrite suppression

(D)

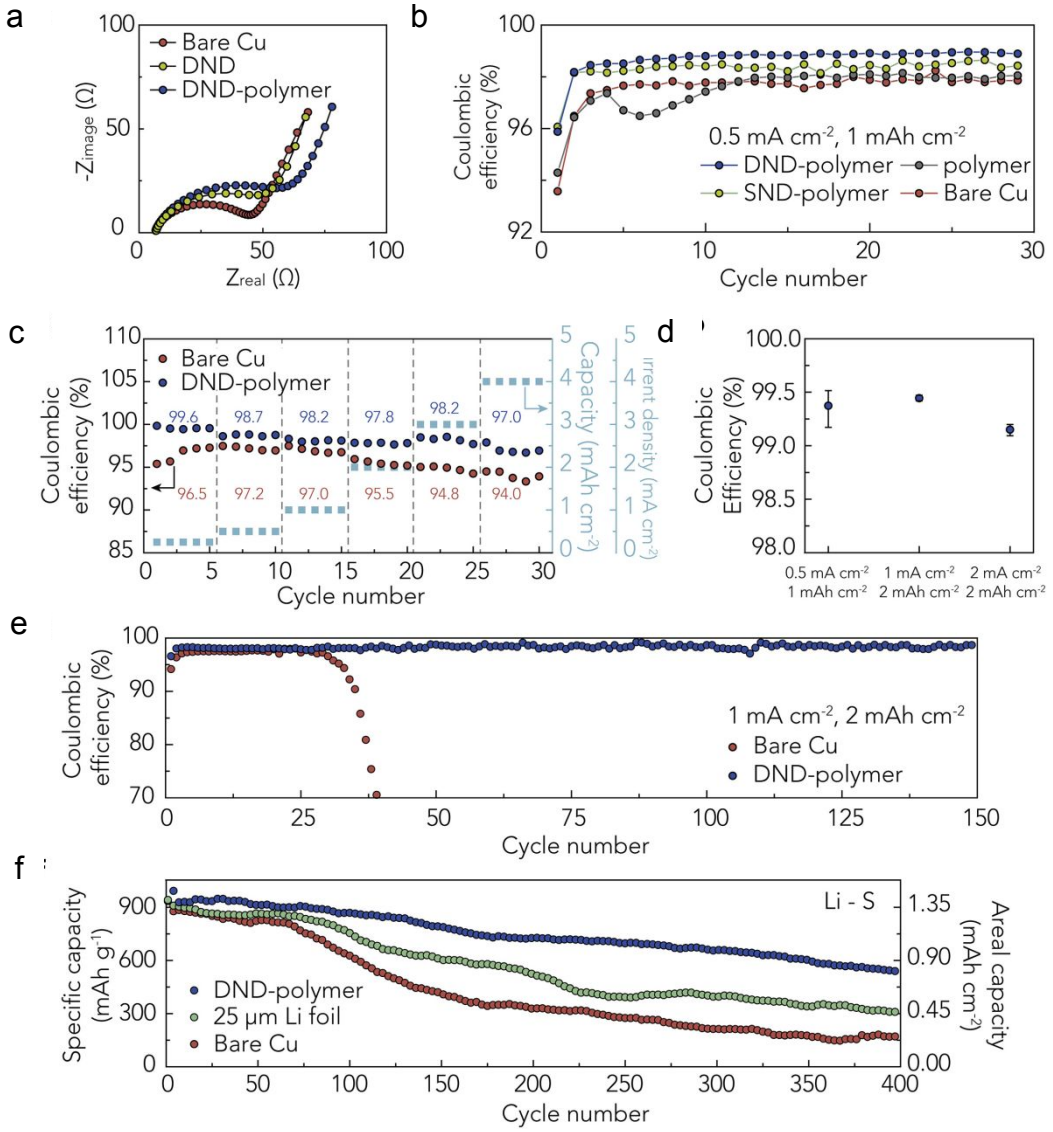

Figure 11. (A) Morphology of Li deposits after galvanostatic plating. Schematic illustration describing Li ion plating behavior in the $LiPF_6$-EC/DEC electrolyte without (a) and with (f) nanodiamond additives. SEM images of b–e Li deposits in $LiPF_6$-EC/DEC electrolyte without nanodiamond additive. SEM images of g–j Li deposits in $LiPF_6$-EC/DEC electrolyte with nanodiamond additives. b–d and g–i Li plating after one time at 0.5 mA cm^{-2} and with plating time of 6 h. e, j Li plating after three cycles at 0.5 mA cm^{-2} and with each step time of 6 h. The insets in e, j are the optical images of the corresponding Li deposits. The scale bars in b and g, c and h, d and i, e and j are 100, 1, 50, 5 μm, respectively. The scale bars in the insets of b, g, e, and i are 1 μm. The word ‘‘ND’’ in the figure is the abbreviation of ‘‘nanodiamond.’’ Reprinted with permission from ref. [532]. Copyright 2017, Nature Publishing Group. (B) Long-term electrochemical cycling stability. Charge-discharge curves of symmetrical Li | Li cells at a 1 mA cm^{-2} and b 2 mA cm^{-2}. Each charge and discharge time is set as 12 min. c Voltage-time curves to calculate the average Coulombic efficiency of Li | Cu cells at 0.5 mA cm^{-2}. d The enlarged view

of c from 5 ~ 15 h. The morphology of a Li deposit cycled at 0.5 mA cm^{-2} in the electrolyte e without and f with the nanodiamond additive. The scale bars in e and f are 10 μm. The word ‘‘ND’’ in the figure is the abbreviation of ‘‘nanodiamond’’. Reprinted with permission from ref. [532]. Copyright 2017, Nature Publishing Group. (C) An ultrastrong double-layer nanodiamond interface for stable lithium metal anodes: schematic plots of experimental steps, simulated defect-tolerant *vs.* uniform ion flex, and high strength *vs.* dendrite suppression. Reprinted with permission from ref. [533]. Copyright 2018, Cell Press. (D) Electrochemical Characterizations of the Nanodiamond Interface. (a) The electrochemical impedance spectra of bare Cu, DND, and DND-polymer electrodes. (b) The CE of different anode architectures cycled at a current density of 0.5 mA cm^{-2} and a capacity of 1 mAh cm^{-2}. (c) The CE of bare Cu and DND-polymer electrodes cycled at varying current densities and capacities. (d) Summary of the 10-cycle average CE of DND-polymer electrode measured according to the method developed by Aurbach et al.[534] (e) Long-term cycling CE of bare Cu and DND-polymer electrodes at a current density of 1 mA cm^{-2} and a capacity of 2 mAh cm^{-2}. (f) Cycling performance of the prototypical Li-S cells at 0.5 C with 25 mm Li foil (ca. 5 mAh cm^{-2}), bare Cu with 5 mAh cm^{-2} electrodeposited Li, or DND-polymer with 5 mAh cm^{-2} electrodeposited Li as the anode. The areal mass loading of the S cathode is 1.5 mg cm^{-2}. The rate is calculated based on the theoretical capacity of S, where 0.5 C is equivalent to 1.25 mA cm^{-2}. Reprinted with permission from ref. [533]. Copyright 2018, Cell Press.

Intrinsic diamond has been proposed as a promising alternative for the development of nuclear batteries, due to its wide band gap (5.5 eV), high radiation resistance, and excellent electronic properties *etc*. For instance, a nuclear microbattery prototype with an active area of 15 cm^2 was fabricated, consisting of 130 single cells based on a Schottky barrier diamond diode. The conversion efficiency of each cell was found to be 4-6%.[535] The performance of the microbattery was characterized using different radioisotope sources (*e.g.*, ^{63}Ni, ^{147}Pm, ^{90}Sr-^{90}Y, and ^{238}Pu). By applying a ^{63}Ni source, the battery exhibited a high energy density of 120 W h kg^{-1} and a total efficiency of only 0.6%. Under irradiation of ^{90}Sr-^{90}Y source, the battery prototype was found to be stable during 1400 hr’s of radiation exposure.[535]

4.5.3 Solar cells

To test the possibility of adopting conductive diamond as an electrode material for solar cell applications, diamond has been functionalized with different molecules (*e.g.*, bithiophene-C_{60},[536] bithiophene-dicyano,[536] manganese phthalocyanine,[537, 538] *etc.*). For example, dye-sensitized

solar cells have been fabricated using polycrystalline BDD foams modified with molecular dyes as electrode.[539] An aqueous solution containing methyl viologen was used as electrolyte. Under white light (20 mW cm^{-2}) illumination, the cathodic photocurrents for a BDD foam electrode were measured to be ca. 500 - 700 nA cm^{-2}, approximately ×3 larger than those on planar BDD. After long-term (1 - 2 days) illumination of the BDD foam electrodes with chopped white light at 1 sun intensity, the photocurrent density was increased to ca. 15 – 22 μA cm^{-2}.[539]

4.6 Other applications

BDD electrodes have been employed to develop a novel *co-reactant-free* electrogenerated chemiluminescence (ECL) system where $Ru(bpy)_3^{2+}$ emission was obtained with an *in situ* generated co-reactant. This method is based on the promoted conversion of inert SO_4^{2-} into the reactive co-reactant $S_2O_8^{2-}$ on BDD electrode at very high oxidation potentials in aqueous solutions. The method is straightforward and does not require any particular electrode geometry.[540] Significant enhancement of the ECL signals from $Ru(bpy)_3^{2+}$ in the presence of tripropylamine was achieved using a BDD nanograss array electrode. This is mainly because of the highly facile oxidation of co-oxidant in the presence of $Ru(bpy)_3^{2+}$, resulting from the superior properties of the BDD nanograss array (*e.g.*, improved electrocatalytic activity and accelerated ET kinetics).[541]

Several new integrated techniques have been developed in combination with BDD electrodes, such as electrochemical-spectroscopy,[542-545] thermal-electrochemical techniques,[546] and BDD platforms for transmission electron microscopy (TEM) - electrochemistry.[547] Many of these adopt a free standing (unsupported) BDD film. In the first area, electrochemical X-ray fluorescence (EC-XRF)[542, 543] and electrochemistry-UV-vis-IR[544, 545] methodologies have been advanced. As an example of combining the power of two technologies in the electrochemical-spectroscopy area, EC-XRF was used to electrochemically preconcentrate soluble heavy metals directly onto the surface of a BDD electrode, in a metallic form, for electrochemical interrogation by the XRF.[515, 516] In this way chemically identification and quantification of heavy metal concentrations (*e.g.*, Ni, Cu, Zn, Hg, and Pb) directly in solution (**Figure 12A**)[542] was proven.

Using an IR laser to locally heat a freestanding BDD film enables local control of the interfacial temperature of a BDD electrode. Temperatures in excess of 100 ^oC could be generated at the electrode – electrolyte interface, importantly under controlled (non-turbulent) mass transport conditions.[548] This approach enabled the study of the effect of temperature on the

electrodeposition of metal nanostructures (Pb/PbO[549] and Pt). For example, laser heating was shown to significantly increase the porosity of electrodeposited Pt NPs, which in turn increased the electrocatalytic activity of these nanostructures, towards oxidation of methanol – an important fuel cell component (**Figure 12B**).[543]

Finally, by producing electron transparent TEM plates from BDD it is possible to follow the morphological dynamics of an electrochemical process, at the level of a single atom. For the proof-of-concept study, the BDD-TEM platform was used to investigate the early stages of electrochemically driven nucleation and growth of a single metal atom to a crystalline metal NP **(Figure 12C)**.[547] Here an identical-location approach was employed whereby after an initial growth period, the BDD-TEM plate was removed from solution and imaged at atom-level resolution in the TEM. The platform was then placed back into solution and growth reinitiated. After removal from solution, imaging again took place in the same location as before, and the process repeated. This procedure thus allowed the growth process to be followed, in the same area, in a series of "time-stamped" images. Using BDD as the TEM grid, compared to conventional sp^2 carbons was found to offer significant advantages including, inherent robustness for repeat measurements, low atomic number, crystallinity, stability, extremely high thermal conductivity and very low Bremsstrahlung backgrounds.

(A)

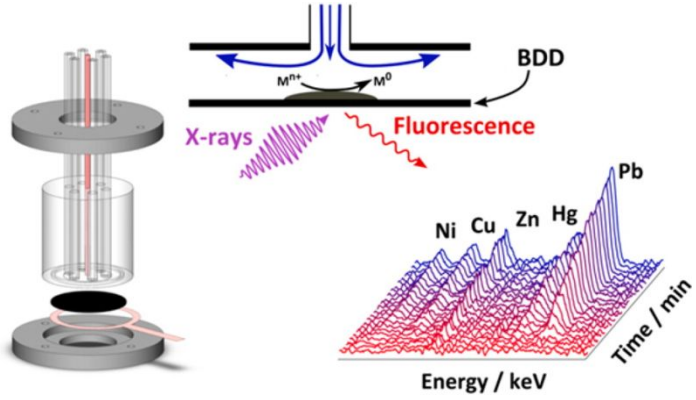

(B)

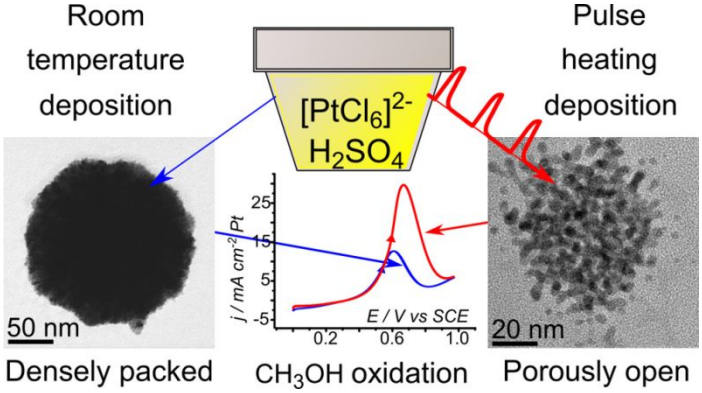

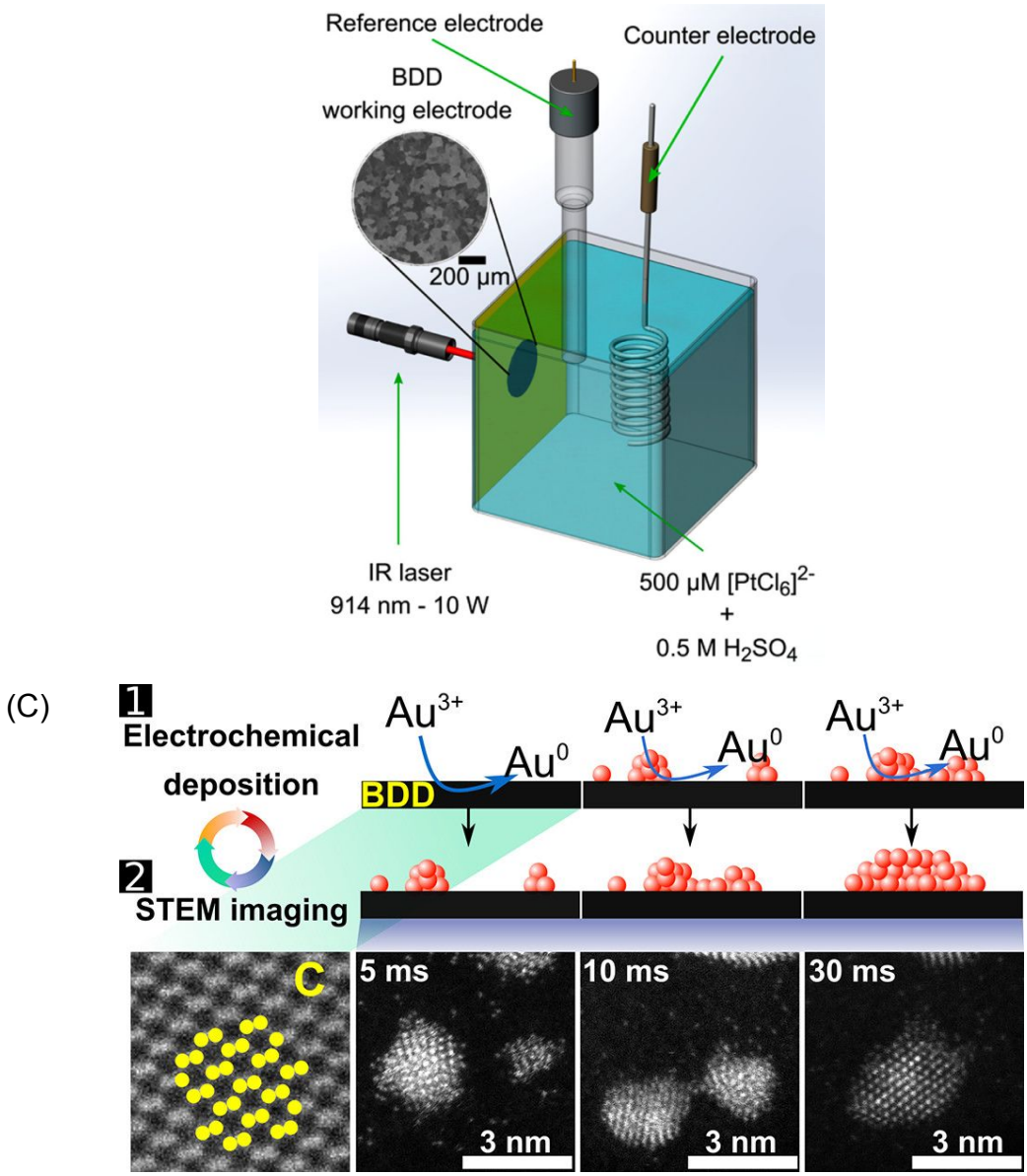

Figure 12. (A) Schematic direct identification and analysis of heavy metals in solution by use of *in situ* EC-XRF. Reprinted with permission from ref. [542] Copyright 2015, American Chemical Society. (B) Electrochemical synthesis of nanoporous platinum NPs for methanol oxidation using laser pulse heating (top) and schematic drawing of the pulsed laser heating experimental setup (bottom). The laser beam is focused by the laser lens onto the back face of the BDD electrode held in the Perspex cell with Kapton tape, which also defines the active electrode area (1 mm disk). The inset image is an FE-SEM image of the BDD electrode surface, where the different colours represent the differently doped grains. Reprinted with permission from ref. [543]. Copyright 2017, American Chemical Society. (C) Tracking metal electrodeposition dynamics from nucleation and growth of a single atom to a crystalline NPs using identical location scanning transmission electron microscopy (STEM) where BDD is served as both an electron-

transparent TEM substrate and electrode. Reprinted with permission from ref. [547]. Copyright 2018, American Chemical Society.

5. Electrochemical devices

In this section, the fabrication of small-dimensional BDD electrodes[274-284.] as well as their ensembles and arrays,[302-311, 313, 314, 317, 318, 550, 551] and scanning probes are summarized.

5.1. Micro- and ultramicroelectrodes

Conductive diamond MEs and UMEs have been fabricated by means of conformal BDD layers on small-diameter metal wires, overgrowing diamond layers on lithographically patterned substrates, or oxygen-based ion beam plasma etching of the bulk conductive diamond material.[235, 280-283] Among them, one frequently applied approach is to coat, by CVD growth, sharpened metal wires with a thin BDD film. The used metals are mainly tungsten (**Figure 13A**)[274-279] and platinum.[235, 280-283] Focused ion beam (FIB) milling can be further applied to improve the exposure areas of the disc-shaped MEs (**Figure 13A**).[279] However, FIB exposure of BDD MEs unavoidably implants Ga^+ ions into the BDD electrode surface as well as the amorphisation of BDD surface layers down to several tens of nanometers.[552]

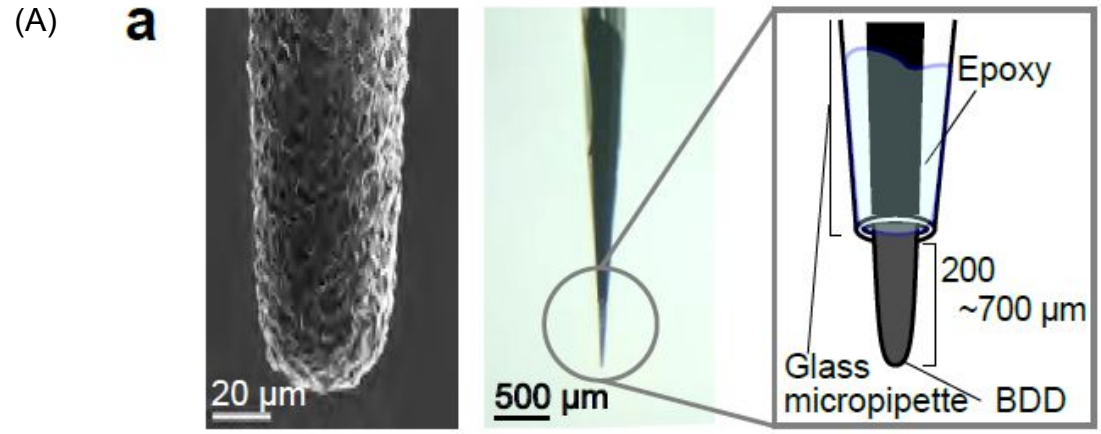

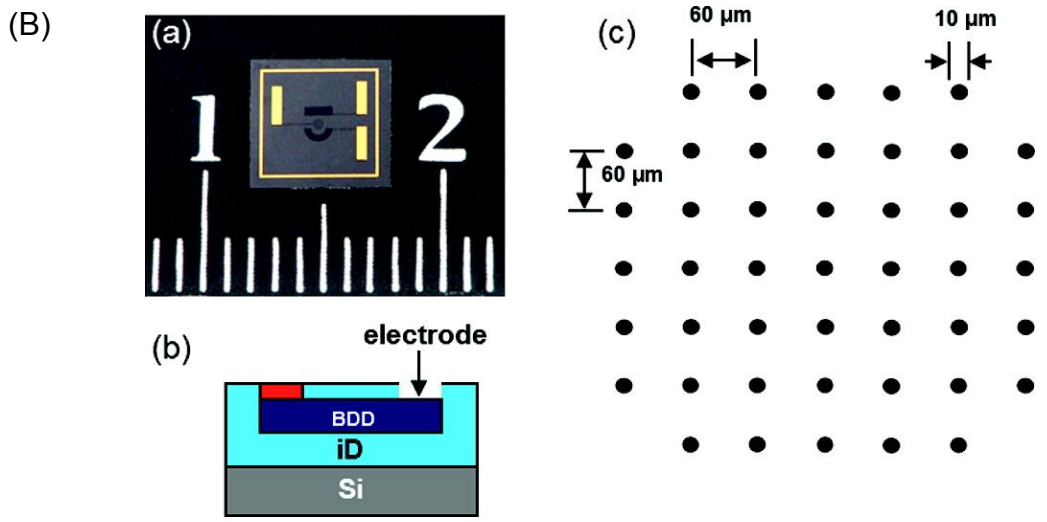

Figure 13. (A) A BDD microsensor. The left panel shows a scanning electron microscopy image of the microsensor tip. The centre and right panels show a stereo-microscope photograph of a microsensor and a schematic illustration, respectively. Reproduced with permission from ref. [235]. Copyright 2017, Nature Publishing Group. (B) (a) Photography of an integrated all-diamond ultramicroelectrode array chip. The yellow parts are metal contacts. The dark part with a semicircle is the counter electrode, the dark rectangle is the quasi-reference electrode, and the center electrode is the working electrode. (b) Schematic plot of the structure of the electrode. (c) Arrangement of the array which is composed of 45 ultramicroelectrodes (10 µm in diameter) in a 500 µm (diameter) circle. Reprinted with permission from ref. [553]. Copyright 2011, American Chemical Society.

These MEs and UMEs have been characterized with various techniques such as scanning electron microscopy, optical microscopy, Raman spectroscopy, and electrochemical techniques (*e.g.*, voltammetry, impedance). [274-283] On BDD MEs, low and stable background currents were obtained.[279, 280] At low scan rates, the cyclic voltammograms for redox probes (*e.g.*, $Ru(NH_3)_6^{3+/2+}$ and $Fe(CN)_6^{3-/4-}$, *etc.*) are sigmoidally shaped, as expected. Electrochemical characterization of BDD UMEs by means of cyclic voltammetry also revealed that the porosity of the film (namely when the BDD grains don't form a contiguous film over the surface of the metal wire tip) affects deleteriously the performance and lifetime of BDD UMEs.[279] EIS has also been applied to investigate the size effect of diamond MEs on their electrochemical properties.[312] By reducing the size (or diameter) of BDD ME/UMEs, formed from UNCD, from 250 µm to 10 µm, the shape of the Nyquist plots changed from linear lines to two arcs,[312] corresponding to the grains of UNCD and grain boundary phases.[312]

5.2. ***Micro- and ultramicroelectrode arrays***

Various diamond MEAs, UMEA, and NEAs have been fabricated. For example, in 2002 Fujishima and coworkers used structured silicon substrates to fabricate BDD MEA,[550] which consisted of 200 micro-disks with diameters between 25 - 30 μm and an electrode spacing of 250 μm. Rychen and coworkers[305] produced BDD UMEAs by depositing a BDD film with a thickness of 5 μm onto patterned silicon nitrite. The diameter of the UMEAs was 5 μm, the distance between UMEs was 150 μm and the number of UMEs was 106. Soh, Swain and co-workers[307-311] produced BDD UMEAs with different shapes, spacing, and number of UMEs. They utilized the "as-grown" diamond surface with randomly micro-structured topology as a planar diamond electrode. They also used a micro-patterning technique to produce a well-defined pyramidal tip-array with a controlled uniformity. In 2005, Compton and coworkers[302-304] realized for the first time all-diamond UMEAs.[284] Here the BDD was machined to reveal pillar structures which were subsequently overgrown with insulating diamond and polished to reveal co-planar structures. The diameters of diamond UMEs are between 10 and 25 μm, with a separation in the range of 100 to 250 μm. Alternatively, it is possible to start from insulating diamond, laser machine the inverse electrode structure into the diamond and overgrow and polish, as shown by Macpherson et al.[195] Using this approach it is possible to produce a wide variety of electrode structures, including microband arrays.[196, 227]

Bergonzo et al.[313] and Carabelli et al.[314] utilized NCD films to generate BDD MEAs. Interconnected and individually addressable diamond (U)MEAs have been also fabricated, including a 10-channel BDD array on polymer based MEA by Hess et al.,[554] a 4-channel NCD MEA by Gao et al.,[555] and a 8×8 multichannel addressable diamond MEA by Bergonzo et al.[556] In 2010, NCD UMEAs were fabricated. They consisted of 2500 BDD nanodiamond elements in a square array surrounded by a layer of thermally grown SiO_2 on a highly doped silicon substrate.[311] In 2011, batch-production of integrated diamond UMEAs has been demonstrated by use of polycrystalline BDD (**Figure 13B**).[306, 312, 318] In the same year, all-diamond NEAs and NEEs were fabricated for the first time using nanocrystalline BDD films.[551] In the diamond NEAs, 18,000 NEs with a radius of 250 nm and separation distance of 10 μm were arranged in a hexagonal order (density = 11×10^5 cm^{-2}).[551] On a BDD NEE, the NEs are randomly distributed. The BDD NE had a radius of ca. 175 nm and a density of ca. 8.5×10^5 cm^{-2}.[551] In 2016, multiple BDD nanodisc and nanoband NEA platforms were fabricated using e-beam lithography where the NE had a diameter of 150 ± 10 nm and separation distance (NE-NE) of 3 μm.[557]

Voltammetry and impedance have been extensively applied to electrochemically characterize diamond MEAs, UMEAs, NEAs, and NEEs. Again as the quality (NDC content) of the BDD employed varies depending on the growth procedures adopted, such factors must be taken into account when interpreting the data. A 64-channel diamond MEA was characterized using cyclic voltammetry and EIS,[556] and relatively fast ET rate constants up to 0.05 $cm \cdot s^{-1}$ was reported. Voltammetry has also been applied to investigate the effect of surface termination, boron doping concentrations, electrolyte composition, and scan rates on the faradaic response of mediators such as the outer sphere couple $Ru(NH)_6^{3+/2+}$, and surface sensitive species $Fe(CN)_6^{3-/4-}$ on conductive diamond UMEAs.[195, 306, 318] Hydrogen terminated BDD UMEAs with boron-concentration of $4.2(\pm2)\times10^{20}$ cm^{-3} showed higher faradaic current (steady-state current at slow scan rates) than oxygen terminated ones, indicating faster ET kinetics.[279] Variation of supporting electrolyte did not affect significantly the capacitive currents but altered dramatically the Faradaic currents.[279] A higher ratio of faradaic current to capacitive current was achieved at a slower scan rate. Much improved sensitivity for sensing applications is expected for diamond UMEAs.[306, 318] BDD MEAs with four different geometries (*e.g.*, size and spacing between MEs) have been characterized using EIS.[310] Together with the results from cyclic voltammetry, it was reported that the charge transfer resistance increases while the double layer capacitance decreases as the MEs are further spaced from one another.[310] BDD MEAs spaced further from one another gave better resolution from the background signal in fast scan cyclic voltammetric measurements of soluble targets (*e.g.*, dopamine).[312, 558] Other techniques have been also applied to characterize conductive diamond array electrodes, including electron and optical microscopy, conductive atomic force microscopy (AFM),[551] Raman spectroscopy,[311] electrochemical methods,[551] SECM[559] and ECL mapping.[557]

5.3. Scanning probes

Conductive diamond has been utilized for the fabrication of scanning probe microscopy (SPM) tips, including AFM, SECM, and scanning tunneling microscopy (STM) tips. The reason for adopting diamond results from the chemical stability of diamond, extreme hardness, its robustness and chemical inertness in different chemical environments. Due to state-of-art developments in material processing at the nanoscale, conductive diamond nanostructures with different sizes and radius can now be routinely fabricated, which has greatly accelerated the usage of diamond in SPM.[560]

BDD UMEs have been employed as the tips for SECM to provide high resolution spatial and

temporal resolution electrochemical measurements.[279, 284] Besides SECM tips,[277-279] BDD MEs and UMEs have also been integrated into AFM-SECM probes where the AFM component provides a non-electrochemical measure of surface topography. For example, a conically shaped BDD-AFM-SECM probe has been fabricated from commercially available AFM probes, using reactive ion etching (RIE) and FIB processing.[561] Unfortunately, such a probe exhibited a relatively high capacitive current even at a scan rate of 10 mV s^{-1}. Later, BDD-AFM-SECM probes with recessed electrodes were fabricated[553, 562] to record AFM and SECM images of an electrode at the same time.[562]

The first conductive diamond STM tip was fabricated through diamond polishing, followed by boron ion implantation. The tip was sharpened to a radius of about 100 nm and used repeatedly even after contact with the sample surface.[563] An STM tip with a tip radius less than 12 nm was later fabricated through conventional polishing of a heavily BDD layer epitaxially grown on an insulating natural diamond substrate using HFCVD.[564] By use of such a tip, atomic resolution images of graphite surfaces were obtained in air. Diamond coated STM tips were also fabricated *via* MWCVD growth of diamond grains on an electrochemically etched tungsten probe (radius less than 100 nm).[565] The apexes on cubo-octahedral diamond micro-particles bound by {100} and {111} facets were effectively used as STM tips. These diamond micro-particles were grown on etched tungsten wires by use of a MWCVD process.[566] In 2007, STM tips with pyramid-shaped nanoprobes of ~80 nm apex were fabricated using BDD particles sized at around 0.5 mm with octahedral habit.[567] Later, BDD single crystals grown by the temperature gradient method were used for STM.[568, 569] Very recently, a heavily boron-doped (metal-like) diamond single crystal (with boron concentration from 5.0×10^{20} to 3.0×10^{21} cm^{-3}) synthesized by the temperature gradient method under HPHT conditions was used as a material for the fabrication of STM tips. These single crystalline conductive BDD probes are believed to record STM imaging with sub-Ångström lateral resolution.[570]

6. Summary and outlook

Various conductive diamond films have been grown by use of numerous chemical vapour deposition techniques. They exhibit unique electrochemical properties, such as low and stable capacitive currents, wide electrochemical potential windows, and varied electrochemical response toward different electroactive species. Moreover, by manipulating the surface termination, conductive diamond films can be modified photochemically, electrochemically, and thermally, resulting in a wide variety of functional interfaces on which required target

compounds (*e.g.*, DNA, enzyme, bacteria, *etc.*) can be grafted.

With the aid of electrochemical, photochemical, and optical techniques, unmodified and modified conductive diamond films are being employed in many different applied technological and scientific fields of interest:

(i) chemical and biochemical sensing of electroactive and non-electroactive molecules
(ii) advanced electrochemical oxidation or degradation of organic pollutants, synthetic dyes and real wastewater,
(iii) anodic and cathodic electrosynthesis of different compounds,
(iv) electrocatalytic reactions for CO_2 reduction and for fuel cells,
(v) the construction of various energy storage devices,
(vi) the production of electrochemical tools and demonstrators.

Conductive diamond exhibits varied electrochemical behavior, depending on its material properties (*e.g.*, dopant concentration, structural defects, NDC impurities or sp^2 hybridized carbon, crystallographic orientation, surface termination and chemistry, and fraction of grain boundaries, *etc.*). For many applications high quality conductive diamond is required, whereas for others more defective material may be suitable (the latter which is often easier and more cost efficient to grow). Hence for each application, the material requirements must be known and suitably assessed. As our demands on higher specification conductive diamond increases, this drives the requirements for *cost-effective* improvements in growth and material processing at larger scales. We envisage this will be one of the main future research focuses for conductive diamond. Moreover, as applications advance, more complex conductive diamond architectures will be required which challenge growth and processing, e.g. ultra-thin conductive films, flexible structures, nanostructured material, such as diamond nanopore electrodes. Chemical vapour deposition of multi-component conductive diamond films (*e.g.*, diamond/SiC, diamond/graphene, diamond/CNT composite films) will also be attractive since these films possess the features of both components and thus expand the applications of conductive films into more applied fields.

However, even now there are clearly many promising, potential applications of conductive diamond:

(i) In the sensing field, BDD electrodes are proving to be incredibly robust, outperforming other electrode materials, for longevity, stability, sensitivity and reliability for the detection of analytes in complex environments. Single molecular detection (*e.g.*, DNA sequencing),

will be possible once *e.g.* the methods to grow ultra-thin conductive diamond films embedded within thru-hole nanopore become available;[571, 572]

(ii) As for environmental degradation, although the concept is proven, the need is now on the lower cost production of large area BDD electrodes. Whilst it is known, modification or immobilization of different modifiers (*e.g.*, biocompatible materials) on BDD surface can promote electrocatalytic activity and enhance the degradation performance for contamination control, more research is needed on the long term viability of placing less robust species onto the conductive diamond surface;

(iii) In terms of electrosynthesis, the methods or the interfaces (especially those with decoration) to generate radicals at low potentials or current densities but with high efficiencies are needed. Combination with metal particles or metal oxides as co-catalysts might be a promising approach to start. Although anodically-driven direct radical formation was proven, no evidence of radical formation was reported in the indirect reduction reaction. With those proposed reaction mechanisms, further investigation of the mechanisms in cathodic reactions is necessary; Scaling up to compete with chemical approaches and the cost implications, how to get grow cheaper, high quality BDD, and the development of new set-ups to achieve efficient mass transport in the electrosynthesis systems need to be carried out.

(iv) Electrocatalysis using conductive diamond before and after modifying with different functional groups or molecules for various electrochemical reductions including CO_2 reduction into useful chemicals, ammoniation from nitrogen gas, cathodic generation of chlorine gas, and highly efficient water electrolysis could be possible once conductive diamond films are sufficiently heavily doped or co-doped with nitrogen and phosphorus; The electrocatalytic functions of different dopants or NDC sites as well as the effect of the density and location of dopants and NDC sites on the electrocatalytic performance should be clarified from experimental and theoretical aspects.

(v) With respect to electrochemical energy storage using conductive diamond, diamond energy devices (*e.g.*, supercapacitors) with further improved performance can be expected by addressing the following challenges: decreasing of series resistance *via* deposition of metal particles or highly conductive species; production of novel

architectures with conductive diamond NPs and nanostructures; combination of surface-coated multi-layered redox species with soluble redox electrolytes in solution.

(vi) Regarding small-scale diamond electrodes, for these to be widely implemented there needs to be a simplification of the fabrication processes to produce price-reduced and high quality small dimensional electrodes and electrode arrays. Also when moving to non-planar substrate, there needs to be an improvement in the reproducibility of highly conductive and conformal diamond films on fibrous substrates *(e.g.*, metal wires, *etc.*), and better control over dopant levels and NDC impurity content.

In conclusion, as this review shows we believe the future is bright for conductive diamond. Excitingly, the community continues to grow, driven by the prospects of so many applications in a wide range of diverse fields. In doing so this drives the impetus in pushing the boundaries in the growth and processing capabilities of this unique substance and its integration with other materials.

Acknowledgments

N.Y. thanks the financial support from German Research Foundation (DFG) under the project (YA344/1-1, N.Y.), S.Y. acknowledges the financial support from the China Scholarship Council (Award no. 201408080015), J.V.M. thanks the Royal Society for an Industry Fellowship (INF/R1/180026), G.Z. thanks the National Natural Science Foundation of China (21537003, 21677106, G.Z), G.M.S. acknowledges financial support by the Army Research Office through award W911NF-12-R-0011.

References

1. R. B. Weisman, *Electrochem. Soc. Interface*, 2013, **22**, 49.

2. R. L. McCreery, *Chem. Rev.*, 2008, **108**, 2646-2687.

3. H. W. Kroto, J. R. Heath, S. C. O'Brien, R. F. Curl and R. E. Smalley, *Nature*, 1985, **318**, 162-163.

4. S. Iijima, *Nature*, 1991, **354**, 56-58.

5. M. Valcárcel, S. Cárdenas and B. M. Simonet, *Anal. Chem.*, 2007, **79**, 4788-4797.

6. K. S. Novoselov, A. K. Geim, S. V. Morozov, D. Jiang, Y. Zhang, S. V. Dubonos, I. V. Grigorieva and A. A. Firsov, *Science*, 2004, **306**, 666-669.

7. X. Yu, H. Cheng, M. Zhang, Y. Zhao, L. Qu and G. Shi, *Nat. Rev. Mater.*, 2017, **2**, 17046.

8. R. N. Adams, *Anal. Chem.*, 1976, **48**, 1126A-1138A.

9. M. Iwaki, S. Sato, K. Takahashi and H. Sakairi, *Nucl. Instrum. Methods Phys. Res.* , 1983, **209-210**, 1129-1133.

10. Y. V. Pelskov, A. Y. Sakharova, M. D. Krotova, L. L. Bouilov and B. V. Spitsyn, *J. Electroanal. Chem. Interfacial Electrochem.*, 1987, **228**, 19-27.

11. K. Patel, K. Hashimoto and A. Fujishima, *J. Photochem. Photobio. A: Chem.*, 1992, **65**, 419-429.

12. K. Patel, K. Hashimoto and A. Fujishima, *Denki Kagaku*, 1992, **60**, 659-661.

13. R. Tenne, K. Patel, K. Hashimoto and A. Fujishima, *J. Electroanal. Chem.*, 1993, **347**, 409-415.

14. G. M. Swain and R. Ramesham, *Anal. Chem.*, 1993, **65**, 345-351.

15. R. Ramesham, R. F. Askew, M. F. Rose and B. H. Loo, *J. Electrochem. Soc.*, 1993, **140**, 3018-3020.

16. B. Miller, R. Kalish, L. C. Feldman, A. Katz, N. Moriya, K. Short and A. E. White, *J. Electrochem. Soc.*, 1994, **141**, L41-L43.

17. J. J. Carey, C. S. Christ and S. N. Lowery, *US Patent*, 1995, **399**, 247.

18. A. Fujishima, Y. Einaga, T. N. Rao and D. A. Tryk, (eds.), *Diamond Electrochemistry*, Elsevier and BKC, 2005.

19. N. Yang, G. M. Swain and X. Jiang, *Electroanalysis*, 2016, **28**, 27-34.

20. H. B. Martin, A. Argoitia, U. Landau, A. B. Anderson and J. C. Angus, *J. Electrochem. Soc.*, 1996, **143**, L133-L136.

21. S. J. Cobb, Z. J. Ayres and J. V. Macpherson, *Annu. Rev. Anal. Chem.*, 2018, **11**, 463-484.

22. T. A. Ivandini and Y. Einaga, *Chem. Commun.*, 2017, **53**, 1338-1347.

23. N. Yang, J. S. Foord and X. Jiang, *Carbon*, 2016, **99**, 90-110.

24. Y. Zhou and J. Zhi, *Talanta*, 2009, **79**, 1189-1196.

25. R. Linares, P. Doering and B. Linares, *Stud. Health Technol. Inform.*, 2009, **149**, 284-296.

26. V. Vermeeren, S. Wenmackers, P. Wagner and L. Michiels, *Sensors*, 2009, **9**, 5600-5636.

27. G. Zhao, Y. Tang, M. Liu, Y. Lei and X. Xiao, *Chin. J. Chem.*, 2007, **25**, 1445-1450.

28. M. Li, G. Zhao, R. Geng and H. Hu, *Bioelectrochemistry*, 2008, **74**, 217-221.

29. H. Ke, M. Liu, L. Zhuang, Z. Li, L. Fan and G. Zhao, *Electrochim. Acta*, 2014, **137**, 146-153.

30. R. Geng, G.-H. Zhao, M.-C. Liu and Y.-Z. Lei, *Acta Phys-Chim Sin.*, 2010, **26**, 1493-1498.

31. F. P. Bundy, H. T. Hall, H. M. Strong and R. H. Wentorf Jun, *Nature*, 1955, **176**, 51.

32. J. Angus, *Synthetic Diamond: Emerging CVD Science and Technology*, K. Spear and J. Dismukes (eds.), New York: John Wiley & Sons, Inc., 1994, 21-39.

33. J. C. Angus, H. A. Will and W. S. Stanko, *J. Appl. Phys.*, 1968, **39**, 2915-2922.

34. D. J. Poferl, N. C. Gardner and J. C. Angus, *J. Appl. Phys.*, 1973, **44**, 1428-1434.

35. S. P. Chauhan, J. C. Angus and N. C. Gardner, *J. Vac. Sci. Tech.*, 1974, **11**, 423.

36. S. P. Chauhan, J. C. Angus and N. C. Gardner, *J. Appl. Phys.*, 1976, **47**, 4746-4754.

37. B. V. Derjaguin, D. V. Fedoseev, V. M. Lukyanovich, B. V. Spitzin, V. A. Ryabov and A. V. Lavrentyev, *J. Cryst. Growth*, 1968, **2**, 380-384.

38. B. V. Deryagin and D. V. Fedoseev, *Russ. Chem. Rev.*, 1970, **39**, 783-788.

39. B. V. Spitsyn, L. L. Bouilov and B. V. Derjaguin, *J. Cryst. Growth*, 1981, **52**, 219-226.

40. S. Matsumoto, Y. Sato, M. Kamo and N. Setaka, *Jpn. J. Appl. Phys.*, 1982, **21 (part 2)**, L183-L185.

41. S. Matsumoto, Y. Sato, M. Tsutsumi and N. Setaka, *J. Mater. Sci.*, 1982, **17**, 3106-3112.

42. M. Kamo, Y. Sato, S. Matsumoto and N. Setaka, *J. Crys. Growth*, 1983, **62**, 642-644.

43. S. Matsumoto, *J. Mater. Sci. Lett.*, 1985, **4**, 600-602.

44. S. Matsumoto, M. Hino and T. Kobayashi, *Appl. Phys. Lett.*, 1987, **51**, 737-739.

45. Y. Matsui, S. Matsumoto and N. Setaka, *J. Mater., Sci. Lett.*, 1983, **2**, 532-534.

46. J. J. Gracio, Q. H. Fan and J. C. Madaleno, *J. Phys. D: Appl. Phys.*, 2010, **43**, 374017.

47. C. I. Pakes, J. A. Garrido and H. Kawarada, *MRS Bulletin*, 2014, **39**, 542-548.

48. C. E. Nebel, B. Rezek, B. Shin and H. Watanabe, *Phys. Status Solidi A*, 2006, **203**, 3273-3298.

49. A. V. D. Drift, *Phillips Res. Rep.*, 1967, **22**, 267.

50. D. M. Gruen, *MRS Bull.*, 2013, **23**, 32-35.

51. D. M. Gruen, *Annu. Rev. Mater. Sci.*, 1999, **29**, 211-259.

52. J. Birrell, J. E. Gerbi, O. Auciello, J. M. Gibson, D. M. Gruen and J. A. Carlisle, *J. Appl. Phys.*, 2003, **93**, 5606-5612.

53. D. Zhou, D. M. Gruen, L. C. Qin, T. G. McCauley and A. R. Krauss, *J. Appl. Phys.*, 1998, **84**, 1981-1989.

54. J. Birrell, J. E. Gerbi, O. Auciello, J. M. Gibson, J. Johnson and J. A. Carlisle, *Diam. Rel. Mater.*, 2005, **14**, 86-92.

55. Q. Chen, D. M. Gruen, A. R. Krauss, T. D. Corrigan, M. Witek and G. M. Swain, *J. Electrochem. Soc.*, 2001, **148**, E44-E51.

56. J. E. Butler and A. V. Sumant, *Chem. Vap. Dep.*, 2008, **14**, 145-160.

57. S. Wang, V. M. Swope, J. E. Butler, T. Feygelson and G. M. Swain, *Diam. Relat. Mater.*, 2009, **18**, 669-677.

58. Y. V. Pleskov, M. D. Krotova, V. G. Ralchenko, A. V. Saveliev and A. D. Bozhko, *Russ. J. Electrochem.*, 2007, **43**, 827-836.

59. W. Zhao, J.-J. Xu, Q.-Q. Qiu and H.-Y. Chen, *Biosens. Bioelectron.*, 2006, **22**, 649-655.

60. A. E. Fischer, Y. Show and G. M. Swain, *Anal. Chem.*, 2004, **76**, 2553-2560.

61. K. Haenen, K. Meykens, M. Nesládek, G. Knuyt, L. M. Stals, T. Teraji, S. Koizumi and E. Gheeraert, *Diamond Relat. Mater.*, 2001, **10**, 439-443.

62. S. J. Sque, R. Jones, J. P. Goss and P. R. Briddon, *Phys. Rev. Lett.* , 2004, **92**, 017402.

63. Y. Liu, Y. Zhang, K. Cheng, X. Quan, X. Fan, Y. Su, S. Chen, H. Zhao, Y. Zhang, H. Yu and M. R. Hoffmann, *Angew. Chem. Int. Ed.*, 2017, **56**, 15607-15611.

64. G. M. Swain, in *Electroanalytical Chemistry*, A. J. Bard and I. Rubinstein (eds.), Dekker: New York, 2004, vol. 22.

65. J. P. Lagrange, A. Deneuville and E. Gheeraert, *Diamon Relat. Mater.*, 1998, **7**, 1390-1393.

66. A. Kraft, *Int. J. Electrochem. Soc.*, 2007, **2**, 355-385.

67. P. Achatz, W. Gajewski, E. Bustarret, C. Marcenat, R. Piquerel, C. Chapelier, T. Dubouchet, O. A. Williams, K. Haenen and J. A. Garrido, *Phys. Rev. B: Condens. Matter*, 2009, **79**, 201203.

68. E. A. Ekimov, V. A. Sidorov, E. D. Bauer, N. N. Mel'nik, N. J. Curro, J. D. Thompson and S. M. Stishov, *Nature*, 2004, **428**, 542.

69. K. W. Lee and W. E. Pickett, *Phys. Rev. Lett.*, 2004, **93**, 237003.

70. M. Ortolani, S. Lupi, L. Baldassarre, U. Schade, P. Calvani, Y. Takano, M. Nagao, T. Takenouchi and H. Kawarada, *Phys. Rev. Lett.*, 2006, **97**, 097002.

71. H. Mukuda, T. Tsuchida, A. Harada, Y. Kitaoka, T. Takenouchi, Y. Takano, M. Nagao, I. Sakaguchi, T. Oguchi and H. Kawarada, *Phys. Rev. B*, 2007, **75**, 033301.

72. K. Ishizaka, R. Eguchi, S. Tsuda, T. Yokoya, A. Chainani, T. Kiss, T. Shimojima, T. Togashi, S. Watanabe and C. T. Chen, *Phys. Rev. Lett.*, 2007, **98**, 047003.

73. Y. Takano, T. Takenouchi, S. Ishii, S. Ueda, T. Okutsu, I. Sakaguchi, H. Umezawa, H. Kawarada and M. Tachiki, *Diam. Relat. Mater.*, 2007, **16**, 911-914.

74. T. Yokoya, E. Ikenaga, M. Kobata, H. Okazaki, K. Kobayashi, A. Takeuchi, A. Awaji, Y. Takano, M. Nagao and I. Sakaguchi, *Phys. Rev. B*, 2007, **75**, 205117.

75. M. Hoesch, T. Fukuda, T. Takenouchi, J. P. Sutter, S. Tsutsui, A. Q. R. Baron, M. Nagao, Y. Takano, H. Kawarada and J. Mizuki, *Phys. Rev. B*, 2007, **75**, 140508.

76. S. Mandal, T. Bautze, O. A. Williams, C. Naud, É. Bustarret, F. Omnès, P. Rodière, T. Meunier, C. Bäuerle and L. Saminadayar, *ACS Nano*, 2011, **5**, 7144-7148.

77. R. Torz-Piotrowska, A. Wrzyszczyński, K. Paprocki and E. Staryga, *Opt. Mater.*, 2009, **31**, 1870-1872.

78. J. Shalini, Y.-C. Lin, T.-H. Chang, K. J. Sankaran, H.-C. Chen, I. N. Lin, C.-Y. Lee and N.-H. Tai, *Electrochem. Acta*, 2013, **92**, 9-19.

79. S. Raina, W. P. Kang and J. L. Davidson, *Diam. Relat. Mater.*, 2009, **18**, 574-577.

80. Q. Zhang, Y. Liu, S. Chen, X. Quan and H. Yu, *J. Hazard. Mater.*, 2014, **265**, 185-190.

81. W. Yuan, L. Fang, Z. Feng, Z. Chen, J. Wen, Y. Xiong and B. Wang, *J. Mater. Chem. C*, 2016, **4**, 4778-4785.

82. S.-S. Yan, H.-Y. Peng, Z.-B. Zhao, M.-M. Pan, D.-L. Yang, J.-H. A, G.-L. Ye, C.-T. Wang and X.-W. Guo, *J. Inorganic Mater.*, 2018, **33**, 565-569.

83. Y. Mukuda, T. Watanabe, A. Ueda, Y. Nishibayashi and Y. Einaga, *Electrochim. Acta*, 2015, **179**, 599-603.

84. Z. Vlckova Zivcova, O. Frank, S. Drijkoningen, K. Haenen, V. Mortet and L. Kavan, *RSC Adv.*, 2016, **6**, 51387-51393.

85. M. I. Landstrass and K. V. Ravi, *Appl. Phys. Lett.*, 1989, **55**, 975-977.

86. F. Maier, M. Riedel, B. Mantel, J. Ristein and L. Ley, *Phys. Rev. Lett.*, 2000, **85**, 3472-3475.

87. Y. Yu, L. Wu and J. Zhi, *Angew. Chem. Int. Ed.*, 2014, **53**, 14326-14351.

88. S. Szunerits, Y. Coffinier and R. Boukherroub, *Sensors*, 2015, **15**, 12573-12593.

89. H. Zhuang, N. Yang, H. Fu, L. Zhang, C. Wang, N. Huang and X. Jiang, *ACS Appl. Mater. Interfaces*, 2015, **7**, 5384-5390.

90. T. Kondo, Y. Kodama, S. Ikezoe, K. Yajima, T. Aikawa and M. Yuasa, *Carbon*, 2014, **77**, 783-789.

91. T. Ohashi, J. Zhang, Y. Takasu and W. Sugimoto, *Electrochim. Acta*, 2011, **56**, 5599-5604.

92. J. Zhang, T. Nakai, M. Uno, Y. Nishiki and W. Sugimoto, *Carbon*, 2013, **65**, 206-213.

93. J. Zhang, T. Nakai, M. Uno, Y. Nishiki and W. Sugimoto, *Carbon*, 2014, **70**, 207-214.

94. F. Gao and C. E. Nebel, *ACS Appl. Mater. Interfaces* 2016, **8**, 28244-28254.

95. H. Masuda, M. Watanabe, K. Yasui, D. Tryk, T. Rao and A. Fujishima, *Adv. Mater.*, 2000, **12**, 444-447.

96. V. Petrák, Z. Vlčková Živcová, H. Krýsová, O. Frank, A. Zukal, L. Klimša, J. Kopeček, A. Taylor, L. Kavan and V. Mortet, *Carbon*, 2017, **114**, 457-464.

97. D. Aradilla, F. Gao, G. Lewes-Malandrakis, W. Müller-Sebert, P. Gentile, M. Boniface, D. Aldakov, B. Iliev, T. J. S. Schubert, C. E. Nebel and G. Bidan, *ACS Appl. Mater. Interfaces*, 2016, **8**, 18069-18077.

98. J. Shalini, K. J. Sankaran, C.-L. Dong, C.-Y. Lee, N.-H. Tai and I. N. Lin, *Nanoscale*, 2013, **5**, 1159-1167.

99. S. A. Skoog, P. R. Miller, R. D. Boehm, A. V. Sumant, R. Polsky and R. J. Narayan, *Diam. Related Mater.*, 2015, **54**, 39-46.

100. Y. Liu, S. Chen, X. Quan, X. Fan, H. Zhao, Q. Zhao and H. Yu, *Appl. Catal. B Environ.*, 2014, **154-155**, 206-212.

101. G. Bhattacharya, K. Jothiramalingam Sankaran, S. B. Srivastava, J. P. Thomas, S. Deshmukh, P. Pobedinskas, S. P. Singh, K. T. Leung, M. K. Van Bael, K. Haenen and S. S. Roy, *Electrochim. Acta*, 2017, **246**, 68-74.

102. A. Krüger, F. Kataoka, M. Ozawa, T. Fujino, Y. Suzuki, A. E. Aleksenskii, A. Y. Vul' and E. Ōsawa, *Carbon*, 2005, **43**, 1722-1730.

103. A. E. Fischer and G. M. Swain, *J. Electrochem. Soc.*, 2005, **152**, B369-B375.

104. A. Ay, V. M. Swope and G. M. Swain, *J. Electrochem. Soc.*, 2008, **155**, B1013-B1022.

105. L. Guo, V. M. Swope, B. Merzougui, L. Protsailo, M. Shao, Q. Yuan and G. M. Swain, *J. Electrochem. Soc.*, 2010, **157**, A19-A25.

106. I. Sasaki, V. M. Swope, A. Ay, D. Y. Kim and G. M. Swain, *J. Electrochem. Soc.*, 2011, **158**, B1446-B1452.

107. D. Y. Kim, B. Merzougui and G. M. Swain, *Chem. Mater.*, 2009, **21**, 2705-2713.

108. O. A. Williams, (ed.), *Nanodiamond*, RSC Publisher, 2014.

109. S. Heyer, W. Janssen, S. Turner, Y.-G. Lu, W. S. Yeap, J. Verbeeck, K. Haenen and A. Krueger, *ACS Nano*, 2014, **8**, 5757-5764.

110. E. Brillas and C. A. Martinez-Huitle, (eds.), *Synthetic Diamond Films: Preparation, Electrochemistry, Characterization, and Applications*, Wiley, 2011.

111. P. N. Bartlett, *Electrochemistry of Carbon Electrodes (Band 16)* in *Advances in Electrochemical Sciences and Engineering* C. Richard and J. Lipkowski (eds.), Wiley-VCH, Weinheim, 2015.

112. Y. S. Zou, Y. Yang, W. J. Zhang, Y. M. Chong, B. He, I. Bello and S. T. Lee, *Appl. Phys. Lett.*, 2008, **92**, 053105.

113. N. Yang, H. Uetsuka, E. Osawa and C. E. Nebel, *Nano Lett.*, 2008, **8**, 3572-3576.

114. C. E. Nebel, N. Yang, H. Uetsuka, E. Osawa, N. Tokuda and O. Williams, *Diam. Relat. Mater.*, 2009, **18**, 910-917.

115. W. Smirnov, A. Kriele, N. Yang and C. E. Nebel, *Diam. Relat. Mater.*, 2010, **19**, 186-189.

116. R. Hoffmann, A. Kriele, H. Obloh, J. Hees, M. Wolfer, W. Smirnov, N. Yang and C. E. Nebel, *Appl. Phys. Lett.*, 2010, **97**, 073117.

117. E. Vanhove, J. de Sanoit, J. C. Arnault, S. Saada, C. Mer, P. Mailley, P. Bergonzo and M. Nesladek, *Phys. Status Solidi A*, 2007, **204**, 2931-2939.

118. G. R. Salazar-Banda, L. S. Andrade, P. A. P. Nascente, P. S. Pizani, R. C. Rocha-Filho and L. A. Avaca, *Electrochim. Acta*, 2006, **51**, 4612-4619.

119. I. Yagi, H. Notsu, T. Kondo, D. A. Tryk and A. Fujishima, *J. Electroanal. Chem.*, 1999, **473**, 173-178.

120. F. B. Liu, J. D. Wang, B. Liu, X. M. Li and D. R. Chen, *Diam. Relat. Mater.*, 2007, **16**, 454-460.

121. R. Boukherroub, X. Wallart, S. Szunerits, B. Marcus, P. Bouvier and M. Mermoux, *Electrochem. Commun.*, 2005, **7**, 937-940.

122. L. Ostrovskaya, V. Perevertailo, V. Ralchenko, A. Dementjev and O. Loginova, *Diam. Relat. Mater.*, 2002, **11**, 845-850.

123. L. A. Hutton, J. G. Iacobini, E. Bitziou, R. B. Channon, M. E. Newton and J. V. Macpherson, *Anal. Chem.*, 2013 **85**, 7230-7240.

124. H. Notsu, I. Yagi, T. Tatsuma, D. A. Tryk and A. Fujishima, *J. Electroanal. Chem.*, 2000, **492** 31-37.

125. I. Duo, C. Levy-Clement, A. Fujishima and C. Comninellis, *J. Appl. Electrochem.*, 2004, **34**, 935-943.

126. H. A. Girard, N. Simon, D. Ballutaud, E. de La Rochefoucauld and A. Etcheberry, *Diam. Relat. Mater.*, 2007, **16**, 888-891

127. C. H. Goeting, F. Marken, A. Gutie´rrez-Sosa, R. G. Compton and J. S. Foord, *Diam. Relat. Mater.*, 2000, **9**, 390-396.

128. J. V. Macpherson, *Phys. Chem. Chem. Phys.*, 2015, **17**, 2935-2949.

129. K. Larsson and S. Lunell, *J. Phys. Chem. A*, 1997, **101**, 76-82.

130. G.-J. Zhang, K.-W. Song, Y. Nakamura, T. Ueno, T. Funatsu, I. Ohndomari and H. Kawarada, *Langmuir*, 2006, **22**, 3728-3734.

131. L. Mayrhofer, G. Moras, N. Mulakaluri, S. Rajagopalan, P. A. Stevens and M. Moseler, *J. Am. Chem. Soc.*, 2016, **138**, 4018-4028.

132. A. K. Tiwari, J. P. Goss, P. R. Briddon, N. G. Wright, A. B. Horsfall, R. Jones, H. Pinto and M. J. Rayson, *Phys. Status Solidi A,* , 2011, **209**, 1709-1714.

133. J. B. Miller, *Surf. Sci.*, 1999, **439**, 21-33.

134. S. Kuga, J.-H. Yang, H. Takahashi, K. Hirama, T. Iwasaki and H. Kawarada, *J. Am. Chem. Soc. Chem.*, 2008, **130**, 13251-13263.

135. L. Lai and A. S. Barnard, *J. Phys. Chem. C.*, 2011, **115**, 6218-6228.

136. J.-P. Chou, A. Retzker and A. Gali, *Nano Lett.*, 2017, **17**, 2294-2298.

137. N. Yang, J. Yu, H. Uetsuka and C. E. Nebel, *Electrochem. Commun.*, 2009, **11**, 2237-2240.

138. R. Hoffmann, H. Obloh, N. Tokuda, N. Yang and C. E. Nebel, *Langmuir*, 2012, **28**, 47-50.

139. S. Szunerits and R. Boukherroub, *J. Solid State Electrochem.*, 2008, **12** 1205-1218.

140. S. Szunerits, C. E. Nebel and R. J. Hamers, *MRS Bull.*, 2014, **39**, 517-524.

141. J. Svítková, T. Ignat, Ľ. Švorc, J. Labuda and J. Barek, *Crit. Rev. Anal. Chem.*, 2016, **46**, 248-256.

142. H. Wang, J.-P. Griffiths, R. G. Egdell, M. G. Moloney and J. S. Foord, *Langmuir* 2008, **24**, 862-868.

143. M. Hoeb, M. Auenhammer, S. J. Schoell, M. S. Brandt, J. A. Garrido, M. Stutzmann and I. D. Sharp, *Langmuir* 2010, **64**, 18862-18867.

144. N. Yang, H. Uetsuka, H. Watanabe, T. Nakamura and C. E. Nebel, *Chem. Mater.*, 2007, **19**, 2852-2859.

145. T. Kondo, Y. Niwano, A. Tamura, J. Imai, K. Honda, Y. Einaga, D. A. Tryk, A. Fujishima and T. Kawai, *Electrochim. Acta*, 2009, **54**, 2312-2319.

146. C. E. Nebel, D. Shin, D. Takeuchi, T. Yamamoto, H. Watanabe and T. Nakamura, *Diam. Relat. Mater.*, 2006, **15**, 1107-1112.

147. W. Yang, O. Auciello, J. E. Butler, W. Cai, J. A. Carlisle, J. Gerbi, D. M. Gruen, T. Knickerbocker, T. L. Lasseter, J. N. Russell, L. M. Smith and R. J. Hamers, *Nat. Mater.*, 2002, **1**, 253-257.

148. T. C. Kuo, R. L. McCreery and G. M. Swain, *Electrochem. Solid-State Lett.*, 1999, **2**, 288-290.

149. J. Wang and J. A. Carlisle, *Diam. Relat. Mater.*, 2006, **15**, 279-284.

150. Ĺ. Švorc, D. Jambrec, M. Vojs, S. Barwe, J. Clausmeyer, P. Michniak, M. Marton and W. Schuhmann, *ACS Appl. Mater. Interfaces*, 2015, **7**, 18949-18956.

151. J. Wang, M. A. Firestone, O. Auciello and J. A. Carlisle, *Langmuir*, 2004, **20**, 11450-11456.

152. C. E. Nebel, B. Rezek, D. Shin, H. Uetsuka and N. Yang, *J. Phys. D: Appl. Phys.*, 2007, **40**, 6443-6466.

153. S. Yu, N. Yang, H. Zhuang, J. Meyer, S. Mandal, O. A. Williams, I. Lilge, H. Schönherr and X. Jiang, *J. Phys. Chem. C*, 2015, **119**, 18918-18926.

154. H. V. Patten, K. E. Meadows, L. A. Hutton, J. G. Iacobini, D. Battistel, K. McKelvey, A. W. Colburn, M. E. Newton, J. V. Macpherson and P. R. Unwin, *Angew. Chem. Int. Ed.*, 2012, **51**, 7002-7006.

155. A. J. Lucio, S. K. Shaw, J. Zhang and A. M. Bond, *J. Phys. Chem. C*, 2018, **122**, 11777-11788.

156. B. A. Patel, X. C. Bian, V. Quaiserova-Mocko, J. J. Galligan and G. M. Swain, *Analyst*, 2007, **132**, 41-47.

157. N. Yang, J. Hees and C. E. Nebel, in *Novel Aspects of Diamond*, N. Yang (ed.), Springer, 2015, 273-293.

158. Y. Pleskov, in *Synthetic Diamond Films*, E. Brillas and C. A. Martinez-Huitle (eds.), Wiley, 2011, 79-108.

159. M. Hupert, A. Muck, R. Wang, J. Stotter, Z. Cvackova, S. Haymond, Y. Show and G. M. Swain, *Diam. Relat. Mater.*, 2003, **12**, 1940-1949.

160. M. C. Granger, J. Xu, J. W. Strojek and G. M. Swain, *Anal. Chim. Acta*, 1999, **397**, 145-161.

161. R. Jarošová, P. M. De Sousa Bezerra, C. Munson and G. M. Swain, *Phys. Status Solidi A*, 2016, **213**, 2087-2098.

162. S.-y. Tan, P. R. Unwin, J. V. Macpherson, J. Zhang and A. M. Bond, *Anal. Chem.*, 2017, **89**, 2830-2837.

163. S.-y. Tan, R. A. Lazenby, K. Bano, J. Zhang, A. M. Bond, J. V. Macpherson and P. R. Unwin, *Phys. Chem. Chem. Phys.*, 2017, **19**, 8726-8734.

164. D. Shin, H. Watanabe and C. E. Nebel, *J. Am. Chem. Soc.*, 2005, **127**, 11236-11237.

165. S. Raina, W. P. Kang and J. L. Davidson, *Diam. Relat. Mater.*, 2009, **18**, 718-721.

166. J. A. Bennett, J. Wang, Y. Show and G. M. Swain, *J. Electrochem. Soc.*, 2004, **151**, E306-E313.

167. Y. Show, V. M. Swope and G. M. Swain, *Diam. Relat. Mater.*, 2009, **18**, 1426-1434.

168. S. Garcia-Segura, E. Vieira dos Santos and C. A. Martínez-Huitle, *Electrochem. Commun.*, 2015, **59**, 52-55.

169. D. Medeiros de Araújo, P. Cañizares, C. A. Martínez-Huitle and M. A. Rodrigo, *Electrochem. Commun.*, 2014, **47**, 37-40.

170. A. N. Patel, S.-Y. Tan, T. S. Miller, J. V. Macpherson and P. R. Unwin, *Anal. Chem.*, 2013, **85**, 11755-11764.

171. Z. J. Ayres, S. J. Cobb, M. E. Newton and J. V. Macpherson, *Electrochem. Commun.*, 2016, **72**, 59-63.

172. Z. J. Ayres, J. C. Newland, M. E. Newton, S. Mandal, O. A. Williams and J. V. Macpherson, *Carbon*, 2017, **121**, 434-442.

173. E. Mahe, D. Devilliers and C. Comninellis, *Electrochem. Commun.*, 2005, **20**, 2263.

174. Y. V. Pleskov, Y. E. Evstefeeva, V. P. Varnin and I. G. Teremetskaya, *Electrokhimiya*, 2005, **41**, 1023.

175. Y. V. Pleskov, M. D. Krotova, V. P. Varnin and I. G. Teremetskaya, *J. Electroanal. Chem.*, 2006, **595**, 168-174.

176. P. Y. lim, F. Y. Lin, H. S. Shih, V. G. Ralchenko, V. P. Varin, Y. V. Pleskov, S. F. Hu, S. S. Chou and P. L. Hsu, *Thin Solid Films*, 2008, **516**, 6125.

177. A. J. Bard, *J. Am. Chem. Soc.*, 2010, **132**, 7559-7567.

178. M. Pumera, *Chem. Euro. J.*, 2009, **15**, 4970-4978.

179. I. Dumitrescu, P. R. Unwin and J. V. Macpherson, *Chem. Commun.*, 2009, 6886-6901.

180. A. Ambrosi, C. K. Chua, A. Bonanni and M. Pumera, *Chem. Rev.*, 2014, **114**, 7150-7188.

181. P. R. Unwin, A. G. Güell and G. Zhang, *Acc. Chem. Res.*, 2016, **49**, 2041-2048.

182. J. Xu and G. M. Swain, *Anal. Chem.*, 1998, **70**, 1502-1510.

183. M. D. Koppang, M. Witek, J. Blau and G. M. Swain, *Anal. Chem.*, 1999, **71**, 1188-1195.

184. M. A. Witek and G. M. Swain, *Anal. Chim. Acta*, 2002, **440**, 119-129.

185. M. Witek, M. D. Koppang and G. M. Swain, *Electroanal.*, 2016, **28**, 151-160.

186. S. Kasahara, K. Natsui, T. Watanabe, Y. Yokota, Y. Kim, S. Iizuka, Y. Tateyama and Y. Einaga, *Anal. Chem.*, 2017, **89**, 11341-11347.

187. H. Notsu, I. Yagi, T. Tatsuma, D. A. Tryk and A. Fujishima, *Electrochem. Solid State Lett.*, 1999, **2**, 522-524.

188. Irkham, T. Watanabe and Y. Einaga, *Anal. Chem.*, 2017, **89**, 7139-7144.

189. T. A. Ivandini, T. N. Rao, A. Fujishima and Y. Einaga, *Anal. Chem.*, 2006, **78**, 3467-3471.

190. R. Trouillon and D. O. Hare, *Electrochim. Acta* 2010, **55**, 6586-6595.

191. R. E. Wilson, I. Stoianov and D. O. Hare, *Electrochem. commun.*, 2016, **71**, 79–83.

192. B. Marselli, J. Garcia-Gomez, P.-A. Michaud, M. A. Rodrigo and C. Comninellis, *J. Electrochem. Soc.*, 2003, **150**, D79-D83.

193. R. Kiran, E. Scorsone, J. de Sanoit, J.-C. Arnault, P. Mailley and P. Bergonzo, *J. Electrochem. Soc.*, 2012, **160**, H67-H73.

194. J. Ruzicka and E. H. Hansen, *Anal. Chem.*, 2000, **72**, 212A-217A.

195. M. B. Joseph, E. Bitziou, T. L. Read, L. Meng, N. L. Palmer, T. P. Mollart, M. E. Newton and J. V. Macpherson, *Anal. Chem.*, 2014, **86**, 5238-5244.

196. R. B. Channon, M. B. Joseph, E. Bitziou, A. W. T. Bristow, A. D. Ray and J. V. Macpherson, *Anal. Chem.*, 2015, **87**, 10064-10071.

197. T. Watanabe, S. Shibano, H. Maeda, A. Sugitani, M. Katayama, Y. Matsumoto and Y. Einaga, *Electrochim. Acta*, 2016, **197**, 159-166.

198. P. Forsberg, E. O. Jorge, L. Nyholm, F. Nikolajeff and M. Karlsson, *Diam. Relat. Mater.*, 2011, **20**, 1121-1124.

199. M. Ensch, V. Y. Maldonado, G. M. Swain, R. Rechenberg, M. F. Becker, T. Schuelke and C. A. Rusinek, *Anal. Chem.*, 2018, **90**, 1951-1958.

200. E. A. McGaw and G. M. Swain, *Anal. Chim. Acta*, 2006, **575**, 180-189.

201. K. Pecková, J. Musilová and J. Barek, *Crit. Rev. Anal. Chem.*, 2009, **39**, 148-172.

202. Y. Lei, G. Zhao, M. Liu, X. Xiao, Y. Tang and D. Li, *Electroanalysis*, 2007, **19**, 1933-1938.

203. G. Zhao, Y. Qi and Y. Tian, *Electroanalysis*, 2006, **18**, 830-834.

204. C. D. Souza, O. C. Braga, I. C. Vieira and A. Spinelli, *Sensors Actuators, B Chem.*, 2008, **135**, 66-73.

205. R. Šelešovská, L. Janíková-Bandžuchová and J. Chýlková, *Electroanalysis*, 2015, **27**, 42-51.

206. B. C. Lourenção, R. A. Medeiros, R. C. Rocha-Filho, L. H. Mazo and O. Fatibello-Filho, *Talanta*, 2009, **78**, 748-752.

207. A. Suzuki, T. A. Ivandini, K. Yoshimi, A. Fujishima, G. Oyama, T. Nakazato, N. Hattori, S. Kitazawa and Y. Einaga, *Anal. Chem.*, 2007, **79**, 8608-8615.

208. A. G. Güell, K. E. Meadows, P. R. Unwin and J. V. Macpherson, *Phys. Chem. Chem. Phys.*, 2010, **12**, 10108-10114.

209. J. Sochr, Ľ. Švorc, M. Rievaj and D. Bustin, *Diam. Relat. Mater.*, 2014, **43**, 5-11.

210. R. Hoffmann, A. Kriele, H. Obloh, N. Tokuda, W. Smirnov, N. Yang and C. E. Nebel, *Biomaterials*, 2011, **32**, 7325-7332.

211. N. Yang, R. Hoffmann, W. Smirnov, A. Kriele and C. E. Nebel, *Electrochem. Commun.*, 2010, **12**, 1218-1221.

212. K. Asai, T. A. Ivandini and Y. Einaga, *Sci. Rep.*, 2016, **6**, 32429.

213. T. Watanabe, Y. Honda, K. Kanda and Y. Einaga, *Phy. Status Solidi A*, 2014, **211**, 2709-2717.

214. Z. J. Ayres, A. J. Borrill, J. C. Newland, M. E. Newton and J. V. Macpherson, *Anal. Chem.*, 2016, **88**, 974-980.

215. F. Picollo, A. Battiato, E. Carbone, L. Croin, E. Enrico, J. Forneris, S. Gosso, P. Olivero, A. Pasquarelli and V. Carabelli, *Sensors*, 2015, **15**, 515-528.

216. R. E. P. Meyler, M. A. Edwards and J. V. Macpherson, *Electrochem. commun.*, 2018, **86**, 21-25.

217. B. C. Lourencao, T. A. Silva, H. Zanin, P. W. May, E. J. Corat and O. Fatibello-Filho, *J. Solid State Electrochem.*, 2016, **20**, 2403-2409.

218. B. C. Lourencao, R. A. Pinheiro, T. A. Silva, E. J. Corat and O. Fatibello-Filho, *Diam. Relat. Mater.*, 2017, **74**, 182-190.

219. K. E. Toghill and R. G. Compton, *Electroanalysis*, 2010, **22**, 1947-1956.

220. F. Gao, N. Yang and C. E. Nebel, *Electrochim. Acta*, 2013, **112**, 493-499.

221. F. Gao, N. Yang, H. Obloh and C. E. Nebel, *Electrochem. Commun.*, 2013, **30**, 55-58.

222. F. Gao, N. Yang, W. Smirnov, H. Obloh and C. E. Nebel, *Electrochim. Acta*, 2013, **90**, 445-451.

223. N. Yang, W. Smirnov and C. E. Nebel, *Electrochem. Commun.*, 2013, **23**, 89-91.

224. B. Channon Robert, C. Newland Jonathan, W. T. Bristow Anthony, D. Ray Andrew and V. Macpherson Julie, *Electroanalysis*, 2013, **25**, 2613-2619.

225. S. Nantaphol, O. Chailapakul and W. Siangproh, *Anal. Chim. Acta*, 2015, **891**, 136-143.

226. A. Sugitani, T. Watanabe, T. A. Ivandini, T. Iguchi and Y. Einaga, *Phys. Chem. Chem. Phys.*, 2013, **15**, 142-147.

227. E. Bitziou, M. B. Joseph, T. L. Read, N. Palmer, T. Mollart, M. E. Newton and J. V. Macpherson, *Anal. Chem.*, 2014, **86**, 10834-10840.

228. T. L. Read, E. Bitziou, M. B. Joseph and J. V. Macpherson, *Anal. Chem.*, 2014, **86**, 367-371.

229. T. L. Read, M. B. Joseph and J. V. Macpherson, *Chem. Commun.*, 2016, **52**, 1-4.

230. P. A. Nistor and P. W. May, *J. R. Soc. Interface,*, 2017, **14**, 20170382.

231. J. Garrett David, L. Saunders Alexia, C. McGowan, J. Specks, K. Ganesan, H. Meffin, A. Williams Richard and A. X. Nayagam David, *J. Biomed. Mater. Res. - Part B Appl. Biomater.*, 2016, **104**, 19-26.

232. M. Alcaide, A. Taylor, M. Fjorback, V. Zachar and C. P. Pennisi, *Front. Neurosci.*, 2016, **10**, 1-9.

233. M. Liu, G. Zhao and Y. Qi, *Int. J. Environ. Anal. Chem.*, 2012, **92**, 534-547.

234. R. Geng, G. Zhao, M. Liu and M. Li, *Biomaterials*, 2008, **29**, 2794-2801.

235. G. Ogata, Y. Ishii, K. Asai, Y. Sano, F. Nin, T. Yoshida, T. Higuchi, S. Sawamura, T. Ota, K. Hori, K. Maeda, S. Komune, K. Doi, M. Takai, I. Findlay, H. Kusuhara, Y. Einaga and H. Hibino, *Nat. Biomed. Engineer.*, 2017, **1**, 654-666.

236. Y. S. Singh, L. E. Sawarynski, H. M. Michael, R. E. Ferrell, M. A. Murphey-Corb, G. M. Swain, B. A. Patel and A. M. Andrews, *ACS Chem. Neurosci.*, 2010, **1**, 49-64.

237. S. Meijs, M. Alcaide, C. Sørensen, M. McDonald, S. Sørensen, K. Rechendorff, A. Gerhardt, M. Nesladek, N. J. M. Rijkhoff and C. P. Pennisi, *J. Neural Eng.*, 2016, **13**, 056011.

238. M. Becker, C. A. Rusinek, B. Fan, W. Li, G. Y. and R. Rechenberg, http://ma.ecsdl.org/content/MA2017-02/55/2319.abstract, *ECS Meeting*, 2018

239. T. Watanabe, T. K. Shimizu, Y. Tateyama, Y. Kim, M. Kawai and Y. Einaga, *Diam. Relat. Mater.*, 2010, **19**, 772-777.

240. R. J. Hamers, *Nature*, 2008, **454**, 708-709.

241. D. Nidzworski, K. Siuzdak, P. Niedziałkowski, R. Bogdanowicz, M. Sobaszek, J. Ryl, P. Weiher, M. Sawczak, E. Wnuk, W. A. Goddard, A. Jaramillo-Botero and T. Ossowski, *Sci. Rep.*, 2017, **7**, 1-10.

242. T. Matsubara, M. Ujie, T. Yamamoto, M. Akahori, Y. Einaga and T. Sato, *Proc. Natl. Acad. Sci.*, 2016, **113**, 8981-8984.

243. M. Braiek, Y. Yang, C. Farre, C. Chaix, F. Bessueille, A. Baraket, A. Errachid, A. Zhang and N. Jaffrezic-Renault, *Electroanalysis*, 2016, **28**, 1810-1816.

244. D. Meziane, A. Barras, A. Kromka, J. Houdkova, R. Boukherroub and S. Szunerits, *Anal. Chem.*, 2012, **84**, 194-200.

245. S. Yeap Weng, S. Murib Mohammed, W. Cuypers, X. Liu, B. van Grinsven, M. Ameloot, M. Fahlman, P. Wagner, W. Maes and K. Haenen, *ChemElectroChem*, 2014, **1**, 1145-1154.

246. H. Gu, X. d. Su and K. P. Loh, *J. Phys. Chem. B*, 2005, **109**, 13611-13618.

247. N. Yang, H. Uetsuka, E. Osawa and C. E. Nebel, *Angew. Chem. Int. Ed.*, 2008, **47**, 5183-5185.

248. N. Yang, H. Uetsuka and C. E. Nebel, *Adv. Funct. Mater.*, 2009, **19**, 887-893.

249. S. Wenmackers, V. Vermeeren, M. VandeVen, M. Ameloot, N. Bijnens, K. Haenen, L. Michiels and P. Wagner, *Phys. Status Solidi A*, 2009, **206**, 391-408.

250. W. Yang, O. Auciello, J. E. Butler, W. Cai, J. A. Carlisle, J. E. Gerbi, D. M. Gruen, T. Knickerbocker, T. L. Lasseter, J. N. Russell Jr, L. M. Smith and R. J. Hamers, *Nat. Mater.*, 2002, **1**, 253-257.

251. M. Dankerl, V. Hauf Moritz, M. Stutzmann and A. Garrido Jose, *Phy. Status Solidi A*, 2012, **209**, 1631-1642.

252. H. Kawarada, Y. Araki, T. Sakai, T. Ogawa and H. Umezawa, *Phy. Status Solidi A*, 2001, **185**, 79-83.

253. J. A. Garrido, A. Härtl, S. Kuch, M. Stutzmann, O. A. Williams and R. B. Jackmann, *Appl. Phys. Lett.*, 2005, **86**, 073504.

254. M. Dankerl, A. Reitinger, M. Stutzmann and J. A. Garrido, *Phys. Status Solidi RRL*, 2007, **2**, 31-33.

255. A. Härtl, J. A. Garrido, S. Nowy, R. Zimmermann, C. Werner, D. Horinek, R. Netz and M. Stutzmann, *J. Am. Chem. Soc.*, 2007, **129**, 1287-1292.

256. M. Dankerl, A. Lippert, S. Birner, E. U. Stützel, M. Stutzmann and J. A. Garrido, *Phys. Rev. Lett.*, 2011, **106**, 196103.

257. K.-S. Song, G.-J. Zhang, Y. Nakamura, K. Furukawa, T. Hiraki, J.-H. Yang, T. Funatsu, I. Ohdomari and H. Kawarada, *Phys. Rev. E* 2006, **74**, 041919.

258. M. V. Hauf, L. H. Hess, J. Howgate, M. Dankerl, M. Stutzmann and J. A. Garrido, *Appl. Phys. Lett.*, 2010, **97**, 093504.

259. K.-S. Song, Y. Nakamura, Y. Sasaki, M. Degawa, J.-H. Yang and H. Kawarada, *Anal. Chim. Acta*, 2006, **573-574**, 3-8.

260. H. Kawarada and A. R. Ruslinda, *Phy. Status Solidi A*, 2011, **208**, 2005-2016.

261. M. Dankerl, S. Eick, B. Hofmann, M. Hauf, S. Ingebrandt, A. Offenhäusser, M. Stutzmann and A. Garrido Jose, *Adv. Funct. Mater.*, 2009, **19**, 2915-2923.

262. A. Härtl, B. Baur, M. Stutzmann and J. A. Garrido, *Langmuir*, 2008, **24**, 9898-9906.

263. C. E. Nebel, D. Shin, D. Takeuchi, T. Yamamoto, H. Watanabe and T. Nakamura, *Langmuir*, 2006, **22**, 5645-5653.

264. C. E. Nebel, D. Shin, B. Rezek, N. Tokuda, H. Uetsuka and H. Watanabe, *J. R. Soc. Interface*, 2007, **4**, 439-461.

265. N. R. Wilson, S. L. Clewes, M. E. Newton, P. R. Unwin and J. V. Macpherson, *J. Phys. Chem. B*, 2006, **110**, 5639-5646.

266. R. Tenne and C. Lévy-Clément, *Israel J. Chem.*, 1998, **38**, 57-73.

267. G. M. Swain, A. B. Anderson and J. C. Angus, *MRS Bull.*, 2013, **23**, 56-60.

268. Y. V. Pleskov, *Russ. Chem. Rev.*, 1999, **68**, 381-392.

269. O. Chailapakul, W. Siangproh and D. A. Tryk, *Sens. Lett.*, 2006, **4**, 99-119.

270. X.-J. Huang, A. M. O'Mahony and R. G. Compton, *Small*, 2009, **5**, 776-788.

271. D. W. M. Arrigan, *Analyst*, 2004, **129**, 1157-1165.

272. R. G. Compton, G. G. Wildgoose, N. V. Rees, I. Streeter and R. Baron, *Chem. Phys. Lett.*, 2008, **459**, 1-17.

273. O. Ordeig, J. del Campo, F. X. Muñoz, E. Banks Craig and G. Compton Richard, *Electroanalysis*, 2007, **19**, 1973-1986.

274. J. B. Cooper, S. Pang, S. Albin, J. Zheng and R. M. Johnson, *Anal. Chem.*, 1998, **70**, 464-467.

275. B. V. Sarada, T. N. Rao, D. A. Tryk and A. Fujishima, *J. Electrochem. Soc.*, 1999, **146**, 1469-1471.

276. B. Duran, R. F. Brocenschi, M. France, J. J. Galligan and G. M. Swain, *Analyst*, 2014, **139**, 3160-3166.

277. K. B. Holt, J. Hu and J. S. Foord, *Anal. Chem.*, 2007, **79**, 2556-2561.

278. J. Hu, J. S. Foord and K. B. Holt, *Phys. Chem. Chem. Phys.*, 2007, **9**, 5469-5475.

279. J. Hu, K. B. Holt and J. S. Foord, *Anal. Chem.*, 2009, **81**, 5663-5670.

280. J. Cvačka, V. Quaiserová, J. Park, Y. Show, A. Muck and G. M. Swain, *Anal. Chem.*, 2003, **75**, 2678-2687.

281. J. Park, Y. Show, V. Quaiserova, J. J. Galligan, G. D. Fink and G. M. Swain, *J. Electroanal. Chem.*, 2005, **583**, 56-68.

282. J. M. Halpern, S. Xie, G. P. Sutton, B. T. Higashikubo, C. A. Chestek, H. Lu, H. J. Chiel and H. B. Martin, *Diam. Relat. Mater.*, 2006, **15**, 183-187.

283. S. Xie, G. Shafer, C. G. Wilson and H. B. Martin, *Diam. Relat. Mater.*, 2006, **15**, 225-228.

284. A. L. Colley, C. G. Williams, U. D'Haenens Johansson, M. E. Newton, P. R. Unwin, N. R. Wilson and J. V. Macpherson, *Anal. Chem.*, 2006, **78**, 2539-2548.

285. J. Park, J. J. Galligan, G. D. Fink and G. M. Swain, *Anal. Chem.*, 2006, **78**, 6756-6764.

286. Y. Ishii, T. A. Ivandini, K. Murata and Y. Einaga, *Anal. Chem.*, 2013, **85**, 4284-4288.

287. T. Ochiai, Y. Ishii, S. Tago, M. Hara, T. Sato, K. Hirota, K. Nakata, T. Murakami, Y. Einaga and A. Fujishima, *ChemPhysChem*, 2013, **14**, 2094-2096.

288. K. Yoshimi, Y. Naya, N. Mitani, T. Kato, M. Inoue, S. Natori, T. Takahashi, A. Weitemier, N. Nishikawa, T. McHugh, Y. Einaga and S. Kitazawa, *Neuroscience Res.*, 2011, **71**, 49-62.

289. E. L. Silva, A. C. Bastos, M. A. Neto, R. F. Silva, M. L. Zheludkevich, M. G. S. Ferreira and F. J. Oliveira, *Electrochim. Acta*, 2012, **76**, 487-494.

290. S. F. Peteu, B. W. Whitman, J. J. Galligan and G. M. Swain, *Analyst*, 2016, **141**, 1796-1806.

291. D. Khamis, E. Mahé, F. Dardoize and D. Devilliers, *J. Appl. Electrochem.*, 2010, **40**, 1829-1838.

292. E. Popa, H. Notsu, T. Miwa, D. A. Tryk and A. Fujishima, *Electrochem. Sol. Stat. Lett.*, 1999, **2**, 49-51.

293. A. Fujishima, T. N. Rao, E. Popa, B. V. Sarada, I. Yagi and D. A. Tryk, *J. Electroanal. Chem.*, 1999, **473**, 179-185.

294. D. Sopchak, B. Miller, R. Kalish, Y. Avyigal and X. Shi, *Electroanalysis*, 2002, **14**, 473-478.

295. P. S. Siew, K. P. Loh, W. C. Poh and H. Zhang, *Diam. Relat. Mater.*, 2005, **14**, 426-431.

296. M. Wei, C. Terashima, M. Lv, A. Fujishima and Z.-Z. Gu, *Chem. Commun.*, 2009, 3624-3626.

297. G. W. Muna, V. Quaiserová-Mocko and G. M. Swain, *Anal. Chem.*, 2005, **77**, 6542-6548.

298. R. Oyobiki, T. Kato, M. Katayama, A. Sugitani, T. Watanabe, Y. Einaga, Y. Matsumoto, K. Horisawa and N. Doi, *Anal. Chem.*, 2014, **86**, 9570-9575.

299. L. A. Hutton, M. Vidotti, J. G. Iacobini, C. Kelly, M. E. Newton, P. R. Unwin and J. V. Macpherson, *Anal. Chem.*, 2011, **83**, 5804-5808.

300. E. L. Silva, C. P. Gouvêa, M. C. Quevedo, M. A. Neto, B. S. Archanjo, A. J. S. Fernandes, C. A. Achete, R. F. Silva, M. L. Zheludkevich and F. J. Oliveira, *Anal. Chem.*, 2015, **87**, 6487-6492.

301. J. M. Halpern, M. J. Cullins, H. J. Chiel and H. B. Martin, *Diam. Relat. Mater.*, 2010, **19**, 178-181.

302. M. Pagels, C. E. Hall, N. S. Lawrence, A. Meredith, T. G. J. Jones, H. P. Godfried, C. S. J. Pickles, J. Wilman, C. E. Banks, R. G. Compton and L. Jiang, *Anal. Chem.*, 2005, **77**, 3705-3708.

303. A. O. Simm, C. E. Banks, S. Ward-Jones, T. J. Davies, N. S. Lawrence, T. G. J. Jones, L. Jiang and R. G. Compton, *Analyst*, 2005, **130**, 1303-1311.

304. N. S. Lawrence, M. Pagels, A. Meredith, T. G. J. Jones, C. E. Hall, C. S. J. Pickles, H. P. Godfried, C. E. Banks, R. G. Compton and L. Jiang, *Talanta*, 2006, **69**, 829-834.

305. C. Provent, W. Haenni, E. Santoli and P. Rychen, *Electrochim. Acta* 2004, **49**, 3737-3744.

306. N. Yang, W. Smirnov, J. Hees, R. Hoffmann, A. Kriele, H. Obloh, W. Müller-Sebert and C. E. Nebel, *Phys. Status Solidi A*, 2011, **208**, 2087-2092.

307. K. L. Soh, W. P. Kang, J. L. Davidson, Y. M. Wong, A. Wisitsora-at, G. Swain and D. E. Cliffel, *Sens. Actuators B*, 2003, **91**, 39-45.

308. K. L. Soh, W. P. Kang, J. L. Davidson, S. Basu, Y. M. Wong, D. E. Cliffel, A. B. Bonds and G. M. Swain, *Diam. Relat. Mater.*, 2004, **13**, 2009-2015.

309. K. L. Soh, W. P. Kang, J. L. Davidson, Y. M. Wong, D. E. Cliffel and G. M. Swain, *Diam. Relat. Mater.*, 2008, **17**, 240-246.

310. K. L. Soh, W. P. Kang, J. L. Davidson, Y. M. Wong, D. E. Cliffel and G. M. Swain, *Diam. Relat. Mater.*, 2008, **17**, 900-905.

311. S. Raina, W. P. Kang and J. L. Davidson, *Diam. Relat. Mater.*, 2010, **19**, 256-259.

312. G. Dutta, S. Siddiqui, H. Zeng, J. A. Carlisle and P. U. Arumugam, *J. Electroanal. Chem.*, 2015, **756**, 61-68.

313. M. Bonnauron, S. Saada, L. Rousseau, G. Lissorgues, C. Mer and P. Bergonzo, *Diam. Relat. Mater.*, 2008, **17**, 1399-1404.

314. M. Bonnauron, S. Saada, C. Mer, C. Gesset, O. A. Williams, L. Rousseau, E. Scorsone, P. Mailley, M. Nesladek, J. C. Arnault and P. Bergonzo, *Phys. Status Solidi A*, 2008, **205**, 2126-2129.

315. V. Carabelli, A. Marcantoni, F. Picollo, A. Battiato, E. Bernardi, A. Pasquarelli, P. Olivero and E. Carbone, *ACS Chem. Neurosci.*, 2017, **8**, 252-264.

316. D. J. Garrett, W. Tong, D. A. Simpson and H. Meffin, *Carbon*, 2016, **102**, 437-454.

317. V. Carabelli, S. Gosso, A. Marcantoni, Y. Xu, E. Colombo, Z. Gao, E. Vittone, E. Kohn, A. Pasquarelli and E. Carbone, *Biosens. Bioelectron.*, 2010, **26**, 92-98.

318. W. Smirnov, N. Yang, R. Hoffmann, J. Hees, H. Obloh, W. Müller-Sebert and C. E. Nebel, *Anal. Chem.*, 2011, **83**, 7438-7443.

319. C. Dincer, R. Ktaich, E. Laubender, J. J. Hees, J. Kieninger, C. E. Nebel, J. Heinze and G. A. Urban, *Electrochim. Acta*, 2015, **185**, 101-106.

320. J. Hees, R. Hoffmann, N. Yang and C. E. Nebel, *Chem. Euro. J.* , 2013, **19**, 11287-11292.

321. K. Ganesan, D. J. Garrett, A. Ahnood, M. N. Shivdasani, W. Tong, A. M. Turnley, K. Fox, H. Meffin and S. Prawer, *Biomaterials*, 2014, **35**, 908-915.

322. L. Rousseau, E. Scorsone, A. Bendali, M. Djilas, H. Girard, M. Cottance, S. Joucla, E. Dubus, J. Degardin, B. Yvert, G. Lissorgues, P. Bergonzo and S. Picaud, *2013 Transducers Eurosensors XXVII 17th Int. Conf. Solid-State Sensors, Actuators Microsystems, TRANSDUCERS EUROSENSORS*, 2013, 1227-1230.

323. A. Bendali, L. Rousseau, G. Lissorgues, E. Scorsone, M. Djilas, J. Dégardin, E. Dubus, S. Fouquet, R. Benosman, P. Bergonzo, J.-A. Sahel and S. Picaud, *Biomaterials*, 2015, **67**, 73-83.

324. S. Siddiqui, Z. Dai, C. J. Stavis, H. Zeng, N. Moldovan, R. J. Hamers, J. A. Carlisle and P. U. Arumugam, *Biosens. Bioelectron.*, 2012, **35**, 284-290.

325. C. Comninellis, *Electrochim. Acta*, 1994, **39**, 1857-1862.

326. S. R. Waldvogel and B. Elsler, *Electrochim. Acta*, 2012, **82**, 434-443.

327. C. Heim, M. Ureña de Vivanco, M. Rajab, E. Müller, T. Letzel and B. Helmreich, *Int. J. Environ. Sci. Tech.*, 2015, **12**, 3061-3070.

328. S. Fierro, K. Abe, C. Christos and Y. Einaga, *J. Electrochem. Soc.*, 2011, **158**, F183-F189.

329. S. Fierro, Y. Honda and Y. Einaga, *Bull. Chem. Soc. Jpn.*, 2013, **86**, 749-754.

330. C. Flox, J. A. Garrido, R. M. Rodríguez, F. Centellas, P.-L. Cabot, C. Arias and E. Brillas, *Electrochim. Acta*, 2005, **50**, 3685-3692.

331. M. Panizza, P. A. Michaud, G. Cerisola and C. Comninellis, *J. Electroanal. Chem.*, 2001, **507**, 206-214.

332. G. Zhao, Y. Zhang, Y. Lei, B. Lv, J. Gao, Y. Zhang and D. Li, *Environ. Sci. Technol.*, 2010, **44**, 1754-1759.

333. K. Serrano, P. A. Michaud, C. Comninellis and A. Savall, *Electrochim. Acta*, 2002, **48**, 431-436.

334. J. Davis, J. C. Baygents and J. Farrell, *Electrochim. Acta*, 2014, **150**, 68-74.

335. E. J. Ruiz, R. Ortega-Borges, J. L. Jurado, T. W. Chapman and Y. Meas, *Electrochem. Solid-State Lett.*, 2009, **12**, E1-E4.

336. O. Azizi, D. Hubler, G. Schrader, J. Farrell and B. P. Chaplin, *Environ. Sci. Technol.*, 2011, **45**, 10582-10590.

337. C. D. N. Brito, D. M. de Araújo, C. A. Martínez-Huitle and M. A. Rodrigo, *Electrochem. Commun.*, 2015, **55**, 34-38.

338. D. K. Hubler, J. C. Baygents, B. P. Chaplin and J. Farrel, *J. Electrochem. Soc.*, 2014, **161**, E182-189.

339. C. Sáez, M. A. Rodrigo and P. Cañizares, *AIChE Journal*, 2008, **54**, 1600-1607.

340. Y. Honda, T. A. Ivandini, T. Watanabe, K. Murata and Y. Einaga, *Diam. Relat. Mater.*, 2013, **40**, 7-11.

341. R. Oliveira, F. Bento and D. Geraldo, *J. Electroanal. Chem.*, 2012, **682**, 7-13.

342. A. El-Ghenymy, C. Arias, P. L. Cabot, F. Centellas, J. A. Garrido, R. M. Rodríguez and E. Brillas, *Chemosphere*, 2012, **87**, 1126-1133.

343. J. J. Pignatello, E. Oliveros and A. MacKay, *Environ. Sci. Technol.*, 2007, **36**, 1-84.

344. A. Kraft, M. Stadelmann and M. Blaschke, *J. Hazard. Mater.*, 2003, **103**, 247-261.

345. B. Boye, E. Brillas, B. Marselli, P.-A. Michaud, C. Comninellis, G. Farnia and G. Sandonà, *Electrochim. Acta*, 2006, **51**, 2872-2880.

346. B. Boye, E. Brillas, B. Marselli, P.-A. Michaud, C. Comninellis and M. Dieng, *Bull. Chem. Soc. Ethiop*, 2004, **18**, 205-214.

347. M. Panizza, M. Delucchi and G. Cerisola, *J. Appl. Electrochem.*, 2005, **35**, 357-361.

348. H. Zhao, G. Wei, J. Gao, Z. Liu and G. Zhao, *ChemElectroChem*, 2015, **2**, 366-373.

349. G. Zhao, X. Tong, Z. Hu, X. Xiao and D. Li, *Electrochim. Acta*, 2008, **53**, 4283-4292.

350. G. Zhao, Y. Pang, L. Liu, J. Gao and B. Lv, *J. Hazard. Mater.*, 2010, **179**, 1078-1083.

351. G. Zhao, P. Li, F. Nong, M. Li, J. Gao and D. Li, *J. Phys. Chem. C.*, 2010, **114**, 5906-5913.

352. H. Xiao, B. Lv, G. Zhao, Y. Wang, M. Li and D. Li, *J. Phys. Chem. A*, 2011, **115**, 13836-13841.

353. Z. Wu, G. Zhao, Y.-n. Zhang, H. Tian and D. Li, *J. Phys. Chem. C*, 2012, **116**, 12829-12835.

354. M. Wu, G. Zhao, M. Li, L. Liu and D. Li, *J. Hazard. Mater.*, 2009, **163**, 26-31.

355. X.-L. Tong, G.-H. Zhao, X.-E. Xiao and H.-K. Hu, *Acta Phys-Chim. Sin.*, 2008, **24**, 416-422.

356. X. Tong, G. Zhao, M. Liu, T. Cao, L. Liu and P. Li, *J. Phys. Chem. C.*, 2009, **113**, 13787-13792.

357. X. Tong, M. Liu and G. Zhao, *J. Solid State Electr.*, 2009, **14**, 221.

358. L. Liu, G. Zhao, M. Wu, Y. Lei and R. Geng, *J. Hazard. Mater.*, 2009, **168**, 179-186.

359. L. Liu, G. Zhao, Y. Pang, Y. Lei, J. Gao and M. Liu, *Ind. Eng. Chem. Res.*, 2010, **49**, 5496-5503.

360. J. Gao, G. Zhao, W. Shi and D. Li, *Chemosphere*, 2009, **75**, 519-525.

361. J. Gao, G. Zhao, M. Liu and D. Li, *J. Phys. Chem. A*, 2009, **113**, 10466-10473.

362. J. Fan, H. Shi, H. Xiao and G. Zhao, *Acs Appl. Mater. Inter.*, 2016, **8**, 28306-28315.

363. S. Chai, G. Zhao, Y.-n. Zhang, Y. Wang, F. Nong, M. Li and D. Li, *Environ. Sci. Technol.*, 2012, **46**, 10182-10190.

364. S. Chai, Y. Wang, Y.-n. Zhang, M. Liu, Y. Wang and G. Zhao, *Environ. Sci. Technol.*, 2017, **51**, 8067-8076.

365. H. Zhao, L. Qian, Y. Chen, Q. Wang and G. Zhao, *Chem. Eng. J.*, 2018, **332**, 486-498.

366. H. Zhao, L. Qian, X. Guan, D. Wu and G. Zhao, *Environ. Sci. Technol.*, 2016, **50**, 5225-5233.

367. J. A. Simpson, K. H. Cheeseman, S. E. Smith and R. T. Dean, *Biochem. J.*, 1988, **254**, 519-523.

368. Y. Wang, H. Zhao, J. Gao, G. Zhao, Y. Zhang and Y. Zhang, *J. Phys. Chem. C*, 2012, **116**, 7457-7463.

369. A. Ventura, G. Jacquet, A. Bermond and V. Camel, *Water Res.*, 2001, **36**, 3517-3522.

370. G. Zhao, S. Shen, M. Li, M. Wu, T. Cao and D. Li, *Chemosphere*, 2008, **73**, 1407-1413.

371. U. Griesbach, I. M. Malkowsky and S. R. Waldvogel, *Green Electroorganic Synthesis Using BDD Electrodes* in *Electrochemistry for the Environment*, C. Comninellis and G. Chen (eds.), Springer, New York, 2010, 3-17.

372. E. Weiss, K. Groenen-Serrano and A. Savall, *J. App. Electrochem.*, 2007, **37**, 1337-1344.

373. A. Urtiaga, C. Fernández-González, S. Gómez-Lavín and I. Ortiz, *Chemosphere*, 2015, **129**, 20-26.

374. H. Bai, P. He, J. Pan, J. Chen, Y. Chen, F. Dong and H. Li, *J. Colloid Interface Sci.*, 2017, **497**, 422-428.

375. X. Zhu, J. Ni and P. Lai, *Water Res.*, 2009, **43**, 4347-4355.

376. S. A. Alves, T. C. R. Ferreira, N. S. Sabatini, A. C. A. Trientini, F. L. Migliorini, M. R. Baldan, N. G. Ferreira and M. R. V. Lanza, *Chemosphere*, 2012, **88**, 155-160.

377. L. S. Andrade, T. T. Tasso, D. L. da Silva, R. C. Rocha-Filho, N. Bocchi and S. R. Biaggio, *Electrochim. Acta*, 2009, **54**, 2024-2030.

378. C. Bruguera-Casamada, I. Sirés, E. Brillas and R. M. Araujo, *Sep. Purif. Technol.*, 2017, **178**, 224-231.

379. N. Flores, I. Sirés, R. M. Rodríguez, F. Centellas, P. L. Cabot, J. A. Garrido and E. Brillas, *J. Electroanal. Chem.*, 2017, **793**, 58-65.

380. F. L. Migliorini, J. R. Steter, R. S. Rocha, M. R. V. Lanza, M. R. Baldan and N. G. Ferreira, *Diamond Relat. Mater.*, 2016, **65**, 5-12.

381. F. Souza, S. Quijorna, M. R. V. Lanza, C. Sáez, P. Cañizares and M. A. Rodrigo, *Catal. Today*, 2017, **280**, 192-198.

382. V. M. Vasconcelos, F. L. Migliorini, J. R. Steter, M. R. Baldan, N. G. Ferreira and M. R. de Vasconcelos Lanza, *J. Environ. Chem. Eng.*, 2016, **4**, 3900-3909.

383. V. M. Vasconcelos, F. L. Ribeiro, F. L. Migliorini, S. A. Alves, J. R. Steter, M. R. Baldan, N. G. Ferreira and M. R. V. Lanza, *Electrochim. Acta*, 2015, **178**, 484-493.

384. G. Zhao, J. Gao, S. Shen, M. Liu, D. Li, M. Wu and Y. Lei, *J. Hazard. Mater.*, 2009, **172**, 1076-1081.

385. E. Brillas, J. C. Calpe and J. Casado, *Wat. Res.*, 2000, **34**, 2253-2262.

386. Y. Sun and J. J. Pignatello, *Environ. Sci. Technol.*, 1993, **27**, 304-310.

387. C. Flox, J. A. Garrido, R. M. Rodríguez, P.-L. Cabot, F. Centellas, C. Arias and E. Brillas, *Catal. Today*, 2007, **129**, 29-36.

388. M. A. Oturan and E. Brillas, *Port. Electrochim. Acta*, 2007, **27**, 1-18.

389. O. García, E. Isarain-Chávez, S. Garcia-Segura, E. Brillas and J. M. Peralta-Hernández, *Electrocatalysis*, 2013, **4**, 224-234.

390. D. R. V. Guelfi, F. Gozzi, I. Sirés, E. Brillas, A. Machulek and S. C. de Oliveira, *Environ. Sci. Pollut. Res.*, 2017, **24**, 6083-6095.

391. Y.-C. Chen and P. Smirniotis, *Ind. Eng. Chem. Res.*, 2002, **41**, 5958-5965.

392. D. Amado-Piña, G. Roa-Morales, C. Barrera-Díaz, P. Balderas-Hernandez, R. Romero, E. Martín del Campo and R. Natividad, *Fuel*, 2017, **198**, 82-90.

393. C. Qiu, S. Yuan, X. Li, H. Wang, B. Bakheet, S. Komarneni and Y. Wang, *J. Hazard. Mater.*, 2014, **280**, 644-653.

394. M. Pera-Titus, V. García-Molina, M. A. Baños, J. Giménez and S. Esplugas, *Appl. Catal. B. Environ.*, 2004, **47**, 219-256.

395. P. Alderson, *Int. J. Soc. Res. Methodol.*, 2001, **4**, 139-153.

396. M. A. Ghanem, R. G. Compton, B. A. Coles, E. Psillakis, M. A. Kulandainathan and F. Marken, *Electrochim. Acta*, 2007, **53**, 1092-1099.

397. R. G. Compton, B. A. Coles and F. Marken, *Chem. Commun.*, 1998, 2595-2596.

398. A. El-Ghenymy, F. Centellas, J. A. Garrido, R. M. Rodríguez, I. Sirés, P. L. Cabot and E. Brillas, *Electrochim. Acta*, 2014, **130**, 568-576.

399. F. C. Moreira, R. A. R. Boaventura, E. Brillas and V. J. P. Vilar, *Water Res.*, 2015, **75**, 95-108.

400. N. Oturan, E. D. van Hullebusch, H. Zhang, L. Mazeas, H. Budzinski, K. L. Menach and M. A. Oturan, *Environ. Sci. Technol.*, 2015, **49**, 12187-12196.

401. J. Wang, K. Li, H. Zhang, Q. Wang, Y. Wang, C. Yang, Q. Guo and J. Jia, *Res. Chem. Intermed.*, 2012, **38**, 2285-2294.

402. N. Borràs, R. Oliver, C. Arias and E. Brillas, *J. Phys. Chem. A*, 2010, **114**, 6613-6621.

403. E. Guinea, F. Centellas, E. Brillas, P. Cañizares, C. Sáez and M. A. Rodrigo, *Appl. Catal. B. Environ.*, 2009, **89**, 645-650.

404. E. Brillas, M. Á. Baños, M. Skoumal, P. L. Cabot, J. A. Garrido and R. M. Rodríguez, *Chemosphere*, 2007, **68**, 199-209.

405. M. A. García-Morales, G. Roa-Morales, C. Barrera-Díaz, B. Bilyeu and M. A. Rodrigo, *Electrochem. Commun.*, 2013, **27**, 34-37.

406. J. L. A. de Queiroz, A. R. L. da Silva, D. C. de Moura, D. R. da Silva and C. A. Martínez-Huitle, *J. Electroanal. Chem.*, 2017, **794**, 204-211.

407. D. Clematis, G. Cerisola and M. Panizza, *Electrochem. Commun.*, 2017, **75**, 21-24.

408. W. Li, B. Li, W. Ding, J. Wu, C. Zhang and D. Fu, *Diam. Relat. Material.*, 2014, **50**, 1-8.

409. X. Du, Z. Zhang, C. Zhang and D. Fu, *Chemosphere*, 2017, **171**, 362-369.

410. R. M. Farinos and L. A. M. Ruotolo, *Electrochim. Acta*, 2017, **224**, 32-39.

411. N. H. Abdessamad, H. Akrout, G. Hamdaoui, K. Elghniji, M. Ksibi and L. Bousselmi, *Chemosphere*, 2013, **93**, 1309-1316.

412. X. Li, H. Li, M. Li, C. Li, D. Sun, Y. Lei and B. Yang, *Carbon*, 2018, **129**, 543-551.

413. E. V. dos Santos, C. Sáez, C. A. Martínez-Huitle, P. Cañizares and M. A. Rodrigo, *J. Environ. Manage.*, 2016, **171**, 260-266.

414. E. V. dos Santos, C. Sáez, P. Cañizares, D. R. da Silva, C. A. Martínez-Huitle and M. A. Rodrigo, *Chem. Eng. J.*, 2017, **310**, 581-588.

415. N. Rabaaoui, M. E. K. Saad, Y. Moussaoui, M. S. Allagui, A. Bedoui and E. Elaloui, *J. Hazard. Mater.*, 2013, **250-251**, 447-453.

416. C. N. Brito, M. B. Ferreira, S. M. L. de O. Marcionilio, E. C. M. de Moura Santos, J. J. L. Léon, S. O. Ganiyu and C. A. Martínez-Huitle, *J. Electrochem. Soc.*, 2018, **165**, E250-E255.

417. F. L. Migliorini, M. D. Alegre, S. A. Alves, M. R. V. Lanza, M. R. Baldan and N. G. Ferreira, *ECS Trans.*, 2014, **58**, 27-33.

418. M. Shestakova and M. Sillanpää, *Revi. Environ. Sci. Bio/Technol.*, 2017, **16**, 1-16.

419. A. M. S. Solano, C. A. Martínez-Huitle, S. Garcia-Segura, A. El-Ghenymy and E. Brillas, *Electrochim. Acta*, 2016, **197**, 210-220.

420. E. Brillas, I. Sires and M. A. Oturan, *Chem. Rev.*, 2009, **109**, 6570-6631.

421. I. Sirés, E. Brillas, M. A. Oturan, M. A. Rodrigo and M. Panizza, *Environ. Sci. Pollut. Res.*, 2014, **21**, 8336-8367.

422. Y. Lan, C. Coetsier, C. Causserand and K. G. Serrano, *Chem. Eng. J.*, 2018, **333**, 486-494.

423. N. Contreras, J. Vidal, C. Berríos, L. Villegas and R. Salazar, *Int. J. Electrochem. Sci.*, 2015, **10**, 9269-9285.

424. M. Murugananthan, S. Yoshihara, T. Rakuma and T. Shirakashi, *J. Hazard. Mater.*, 2008, **154**, 213-220.

425. O. Ganzenko, N. Oturan, D. Huguenot, E. D. van Hullebusch, G. Esposito and M. A. Oturan, *Sep. Purif. Technol.*, 2015, **156**, 987-995.

426. C. Zhang, L. Liu, J. Wang, F. Rong and D. Fu, *Sep. Purif. Technol.*, 2013, **107**, 91-101.

427. N. Klidi, D. Clematis, M. Delucchi, A. Gadri, S. Ammar and M. Panizza, *J. Electroanal. Chem.*, 2018, **815**, 16-23.

428. S. Ammar, R. Abelhedi, C. Fox and E. Brillas, *Environ. Chem. Lett.*, 2016, **4**, 229-233.

429. X. Zhu, S. Shi, J. Wei, F. Lv, H. Zhao, J. Kong, Q. He and J. Ni, *Environ. Sci. Technol.*, 2007, **41**, 6541-6546.

430. A. Y. Bagastyo, D. J. Batstone, K. Rabaey and J. Radjenovic, *Water Res.*, 2013, **47**, 242-250.

431. N. Barhoumi, L. Labiadh, M. A. Oturan, N. Oturan, A. Gadri, S. Ammar and E. Brillas, *Chemosphere*, 2015, **141**, 250-257.

432. C. M. Dominguez, N. Oturan, A. Romero, A. Santos and M. A. Oturan, *Water Res.*, 2018, **135**, 220-230.

433. H. T. Madsen, E. G. Søgaard and J. Muff, *Chemosphere*, 2014, **109**, 84-91.

434. J. R. Domínguez, M. J. Muñoz-Peña, T. González, P. Palo and E. M. Cuerda-Correa, *Environ. Sci. Pollut. Res.*, 2016, **23**, 20315-20330.

435. S. Garcia-Segura, J. Keller, E. Brillas and J. Radjenovic, *J. Hazard. Mater.*, 2015, **283**, 551-557.

436. A. Urtiaga, P. Gómez, A. Arruti and I. Ortiz, *J. Chem. Technol. Biotechnol.*, 2014, **89**, 1243-1250.

437. R. Ennouri, M. Kchaw, M. Panizza and S. C. Elaoud, *J. Electrochem. Soc.*, 2017, **164**, E213-E216.

438. S. C. Elaoud, M. Panizza, G. Cerisola and T. Mhiri, *Desalination*, 2011, **272**, 18-153.

439. N. Flores, P. L. Cabot, F. Centellas, J. A. Garrido, R. M. Rodríguez, E. Brillas and I. Sirés, *J. Hazard. Mater.*, 2017, **321**, 566-575.

440. M. Ghazouani, H. Akrout and L. Bousselmi, *Environ. Sci. Pollut. Res. Int.*, 2017, **24**, 9895-9906.

441. E. V. dos Santos, C. Sáez, P. Cañizares, M. A. Rodrigo and C. A. Martínez-Huitle, *J. Electrochem. Soc.*, 2018, **165**, E262-E267.

442. S. Velazquez-Peña, I. Linares-Hernández, V. Martínez-Miranda, C. Barrera-Díaz and B. Bilyeu, *Fuel*, 2013, **110**, 12-16.

443. S. Velazquez-Peña, I. Linares-Hernández, V. Martínez-Miranda, C. Barrera-Díaz, V. Lugo-Lugo and B. Bilyeu, *Sep. Sci. Technol.*, 2013, **48**, 2900-2909.

444. C. E. Schaefer, C. Andaya, A. Urtiaga, E. R. McKenzie and C. P. Higgins, *J. Hazard. Mater.*, 2015, **295**, 170-175.

445. C. R. Costa, F. Montilla, E. Morallón and P. Olivi, *J. Hazard. Mater.*, 2010, **180**, 429-435.

446. H. Jian, Y. Youping, Q. Yan, W. Su and W. Xinchi, *Chin. J. Chem. Eng.*, 2012, **6**, 3679-3683.

447. E. Tsantaki, T. Velegraki, A. Katsaounis and D. Mantzavinos, *J. Hazard. Mater.*, 2012, **207-208**, 91-96.

448. A. Thiam, E. Brillas, F. Centellas, P. L. Cabot and I. Sirés, *Electrochim. Acta*, 2015, **173**, 523-533.

449. A. Farhat, J. Keller, S. Tait and J. Radjenovic, *Environ. Sci. Technol.*, 2015, **49**, 14326-14333.

450. S. Komtchou, A. Dirany, P. Drogui, D. Robert and P. Lafrance, *Water Res.*, 2017, **125**, 91-103.

451. L. Labiadh, A. Barbucci, M. P. Carpanese and M. Panizza, *J. Electroanal. Chem.*, 2016, **766**, 94-99.

452. M. Ghazouani, H. Akrout, S. Jomaa, S. Jellali and L. Bousselmi, *J. Electroanal. Chem.*, 2016, **783**, 28-40.

453. C. Durante, M. Cuscov, A. A. Isse, G. Sandona and A. Gennaro, *Water Res.*, 2011, **45**, 2122-2130.

454. D. Voglar and D. Lestan, *Water Res.*, 2012, **46**, 1999-2008.

455. S. Komtchou, A. Dirany, P. Drogui and A. Bermond, *Environ. Sci. Pollut. Res.*, 2015, **22**, 11513-11525.

456. J. P. d. P. Barreto, K. C. d. F. Araújo, D. M. de Araújo and C. A. Martínez-Huitle, *ECS Electrochem. Lett.*, 2015, **4**, E9-E11.

457. L. C. Espinoza, A. Henríquez, D. Contreras and R. Salazar, *Electrochem. Commun.*, 2018, **90**, 30-33.

458. F. L. Souza, C. Saéz, M. R. V. Lanza, P. Cañizares and M. A. Rodrigo, *Electrochim. Acta*, 2016, **187**, 119-124.

459. R. Bogdanowicz, A. Fabiańska, L. Golunski, M. Sobaszek, M. Gnyba, J. Ryl, K. Darowicki, T. Ossowski, S. D. Janssens, K. Haenen and E. M. Siedlecka, *Diamond Relat. Mater.*, 2013, **39**, 82-88.

460. F. L. Migliorini, N. A. Braga, S. A. Alves, M. R. V. Lanza, M. R. Baldan and N. G. Ferreira, *J. Hazard. Mater.*, 2011, **192**, 1683-1689.

461. C. Salazar, C. Ridruejo, E. Brillas, J. Yáñez, H. D. Mansilla and I. Sirés, *Appl. Catal. B. Environ.*, 2017, **203**, 189-198.

462. Y. He, W. Huang, R. Chen, W. Zhang and H. Lin, *J. Electroanal. Chem.*, 2015, **758**, 170-177.

463. Y. He, W. Huang, R. Chen, W. Zhang and H. Lin, *Sep. Purif. Technol.*, 2015, **149**, 124-131.

464. C.-H. Lee, E.-S. Lee, Y.-K. Lim, K.-H. Park, H.-D. Park and D.-S. Lim, *RSC Adv.*, 2017, **7**, 6229-6235.

465. E. Steckhan, T. Arns, W. R. Heineman, G. Hilt, D. Hoormann, J. Jörissen, L. Kröner, B. Lewall and H. Pütter, *Chemosphere*, 2001, **43**, 63-73.

466. D. Zollinger, U. Griesbach, H. Pütter and C. Comninellis, *Electrochem. Commun.*, 2004, **6**, 605-608.

467. R. Fardel, U. Griesbach, H. Pütter and C. Comninellis, *J. Appl. Electrochem.*, 2006, **36**, 249-253.

468. T. Sumi, T. Saitoh, K. Natsui, T. Yamamoto, M. Atobe, Y. Einaga and S. Nishiyama, *Angew. Chem. Int. Ed.*, 2012, **51**, 5443-5446.

469. K. R. Saravanan, V. Selvamani, K. Kulangiappar, D. Velayutham and V. Suryanarayanan, *Electrochem. Commun.*, 2013, **28**, 31-33.

470. I. M. Malkowsky, U. Griesbach, H. Pütter and S. R. Waldvogel, *Eur. J. Org. Chem.*, 2006, 4569.

471. A. Kirste, M. Nieger, I. M. Malkowsky, F. Stecker, A. Fischer and S. R. Waldvogel, *Chem. Eur. J.*, 2009, **15**, 2273-2277.

472. A. Kirste, G. Schnakenburg, F. Stecker, A. Fischer and R. Waldvogel Siegfried, *Angew. Chem. Int. Ed.*, 2010, **49**, 971-975.

473. A. Kirste, B. Elsler, G. Schnakenburg and S. R. Waldvogel, *J. Am. Chem. Soc.*, 2012, **134**, 3571-3576.

474. B. Elsler, D. Schollmeyer, M. Dyballa Katrin, R. Franke and R. Waldvogel Siegfried, *Angew. Chem. Int. Ed.*, 2014, **53**, 5210-5213.

475. B. Elsler, A. Wiebe, D. Schollmeyer, K. M. Dyballa, R. Franke and S. R. Waldvogel, *Chem. Eur. J.*, 2015, **21**, 12321-12325.

476. A. Wiebe, D. Schollmeyer, M. Dyballa Katrin, R. Franke and R. Waldvogel Siegfried, *Angew. Chem. Int. Ed.*, 2016, **55**, 11801-11805.

477. A. Wiebe, S. Lips, D. Schollmeyer, R. Franke and R. Waldvogel Siegfried, *Angew. Chem. Int. Ed.*, 2017, **56**, 14727-14731.

478. T. Yamamoto, B. Riehl, K. Naba, K. Nakahara, A. Wiebe, T. Saitoh, S. R. Waldvogel and Y. Einaga, *Chem. Commun.*, 2018, **54**, 2771-2773.

479. T. Kojima, R. Obata, T. Saitoh, Y. Einaga and S. Nishiyama, *B. J. Org. Chem.*, 2015, **11**, 200-203.

480. N. Roy, Y. Hirano, H. Kuriyama, P. Sudhagar, N. Suzuki, K.-I. Katsumata, K. Nakata, T. Kondo, M. Yuasa, I. Serizawa, T. Takayama, A. Kudo, A. Fujishima and C. Terashima, *Sci. Rep.*, 2016, **6**, 38010.

481. D. Pletcher, *Electrochem. Commun.*, 2015, **61**, 97-101.

482. K. Nakata, T. Ozaki, C. Terashima, A. Fujishima and Y. Einaga, *Angew. Chem. Int. Ed.*, 2014, **53**, 871-874.

483. Y. Hori, H. Wakebe, T. Tsukamoto and O. Koga, *Electrochim. Acta*, 1994, **39**, 1833-1839.

484. M. Jitaru, D. A. Lowy, M. Toma, B. C. Toma and L. Oniciu, *J. Appl. Electrochem.*, 1997, **27**, 875-889.

485. M. Gattrell, N. Gupta and A. Co, *J. Electroanal. Chem.*, 2006, **594**, 1-19.

486. M. Łukaszewski, H. Siwek and A. Czerwiński, *J. Solid State Electrochem.*, 2009, **13**, 813-827.

487. N. Yang, S. R. Waldvogel and X. Jiang, *ACS Appl. Material Interfaces*, 2016, **8**, 28357-28371.

488. L. Zhang, D. Zhu, M. Nathanson Gilbert and J. Hamers Robert, *Angew. Chem. Int. Ed.*, 2014, **53**, 9746-9750.

489. L. Zhang and R. J. Hamers, *Diam. Relat. Mater.*, 2017, **78**, 24-30.

490. Y. Y. Birdja and M. T. M. Koper, *Journal of the American Chemical Society*, 2017, **139**, 2030-2034.

491. K. Natsui, H. Iwakawa, N. Ikemiya, K. Nakata and Y. Einaga, *Angew. Chem. Int. Ed.*, 2018, **57**, 2639-2643.

492. P. K. Jiwanti, K. Natsui, K. Nakata and Y. Einaga, *RSC Adv.*, 2016, **6**, 102214-102217.

493. P. K. Jiwanti, K. Natsui, K. Nakata and Y. Einaga, *Electrochim. Acta*, 2018, **266**, 414-419.

494. J. Xu, K. Natsui, S. Naoi, K. Nakata and Y. Einaga, *Diam. Relat. Mater.*, 2018, **86**, 167-172.

495. N. Ikemiya, K. Natsui, K. Nakata and Y. Einaga, *ACS Sustainable Chem. Engineer.*, 2018, **6**, 8108-8112.

496. S. A. Yao, R. E. Ruther, L. Zhang, R. A. Franking, R. J. Hamers and J. F. Berry, *J. Am. Chem. Soc.*, 2012, **134**, 15632-15635.

497. Y. Liu, S. Chen, X. Quan and H. Yu, *J. Am. Chem. Soc.*, 2015, **137**, 11631-11636.

498. Y. Wang, J. Zang, L. Dong, H. Pan, Y. Yuan and Y. Wang, *Electrochim. Acta*, 2013, **113**, 583-590.

499. L. La-Torre-Riveros, R. Guzman-Blas, A. E. Méndez-Torres, M. Prelas, D. A. Tryk and C. R. Cabrera, *ACS Appl. Mater. Interfaces*, 2012, **4**, 1134-1147.

500. Y. Wang, Y. Zhao, R. Lu, L. Dong, J. Zang, J. Lu and X. Xu, *J. Electrochem. Soc.*, 2015, **162**, F211-F215.

501. Y. Zhao, Y. Wang, L. Dong, Y. Zhang, J. Huang, J. Zang, J. Lu and X. Xu, *Electrochim. Acta*, 2014, **148**, 8-14.

502. G. R. Salazar-Banda, K. I. B. Eguiluz and L. A. Avaca, *Electrochem. Commun.*, 2007, **9**, 59-64.

503. N. Spătaru, X. Zhang, T. Spătaru, D. A. Tryk and A. Fujishima, *J. Electrochem. Soc.*, 2008, **155**, D73-D77.

504. Y. Wang and Y. Xia, *Adv. Mater.*, 2013, **25**, 5336-5342.

505. L. L. Zhang, R. Zhou and X. S. Zhao, *J. Mater. Chem.*, 2010, **20**, 5983-5992.

506. J. R. Miller and A. F. Burke, *Electrochem. Soc. Interface* 2008, **17**, 53-57.

507. R. Raccichini, A. Varzi, S. Passerini and B. Scrosati, *Nat. Mater.*, 2014, **14**, 271.

508. S. L. Candelaria, Y. Shao, W. Zhou, X. Li, J. Xiao, J.-G. Zhang, Y. Wang, J. Liu, J. Li and G. Cao, *Nano Energy*, 2012, **1**, 195-220.

509. S. Yu, High Performance Diamond Supercapacitors: Concepts and Devices, PhD thesis, University of Siegen, Germany, 2018.

510. M. Yoshimura, K. Honda, R. Uchikado, T. Kondo, T. N. Rao, D. A. Tryk, A. Fujishima, Y. Sakamoto, K. Yasui and H. Masuda, *Diam. Relat. Mater.*, 2001, **10**, 620-626.

511. T. Ohashi, W. Sugimoto and Y. Takasu, *Electrochim. Acta*, 2009, **54**, 5223-5229.

512. F. Gao, M. T. Wolfer and C. E. Nebel, *Carbon*, 2014, **80**, 833-840.

513. F. Gao, G. Lewes-Malandrakis, M. T. Wolfer, W. Müller-Sebert, P. Gentile, D. Aradilla, T. Schubert and C. E. Nebel, *Diam. Relat. Mater.*, 2015, **51**, 1-6.

514. C. Hébert, E. Scorsone, M. Mermoux and P. Bergonzo, *Carbon*, 2015, **90**, 102-109.

515. H. Zanin, P. W. May, D. J. Fermin, D. Plana, S. M. C. Vieira, W. I. Milne and E. J. Corat, *ACS Appl. Mater. Interfaces*, 2014, **6**, 990-995.

516. E. C. Almeida, M. R. Baldan, J. M. Rosolen and N. G. Ferreira, *Diam. Relat. Mater.*, 2008, **17**, 1529-1533.

517. T. Kondo, S. Lee, K. Honda and T. Kawai, *Electrochem. Commun.*, 2009, **11**, 1688-1691.

518. K. Honda, M. Yoshimura, K. Kawakita, A. Fujishima, Y. Sakamoto, K. Yasui, N. Nishio and H. Masuda, *J. Electrochem. Soc.*, 2004, **151**, A532-A541.

519. C. H. Y. Xuan Lim, A. Sorkin, Q. Bao, A. Li, K. Zhang, M. Nesladek and K. P. Loh, *Nat. Commun.*, 2013, **4**, 1556.

520. S. Yu, N. Yang, M. Vogel, S. Mandal, A. Williams Oliver, S. Jiang, H. Schönherr, B. Yang and X. Jiang, *Adv. Energy Mater.*, 2018, **8**, 1702947.

521. Y. Sun, Q. Wu, Y. Xu, H. Bai, C. Li and G. Shi, *J. Mater. Chem.*, 2011, **21**, 7154-7160.

522. E. G. Bushueva, P. S. Galkin, A. V. Okotrub, L. G. Bulusheva, N. N. Gavrilov, V. L. Kuznetsov and S. I. Moiseekov, *Phys. Status Solidi B*, 2008, **245**, 2296-2299.

523. Q. Wang, N. Plylahan, M. V. Shelke, R. R. Devarapalli, M. Li, P. Subramanian, T. Djenizian, R. Boukherroub and S. Szunerits, *Carbon*, 2014, **68**, 175-184.

524. M. Sobaszek, K. Siuzdak, M. Sawczak, J. Ryl and R. Bogdanowicz, *Thin Solid Films*, 2016, **601**, 35-40.

525. K. Siuzdak, R. Bogdanowicz, M. Sawczak and M. Sobaszek, *Nanoscale*, 2015, **7**, 551-558.

526. F. Gao and E. Nebel Christoph, *Phys. Status Solidi A*, 2015, **212**, 2533-2538.

527. I. Kovalenko, G. Bucknall David and G. Yushin, *Adv. Funct. Mater.*, 2010, **20**, 3979-3986.

528. S. Yu, N. Yang, H. Zhuang, S. Mandal, O. A. Williams, B. Yang, N. Huang and X. Jiang, *J. Mater. Chem. A*, 2017, **5**, 1778-1785.

529. E. C. Almeida, V. J. Trava-Airoldi, N. G. Ferreira and J. M. Rosolen, *Diam. Relat. Mater.*, 2005, **14**, 1673-1677.

530. C. Delfaure, M. Pomorski, J. de Sanoit, P. Bergonzo and S. Saada, *Appl. Phys. Lett.*, 2016, **108**, 252105.

531. Y.-W. Cheng, C.-K. Lin, Y.-C. Chu, A. Abouimrane, Z. Chen, Y. Ren, C.-P. Liu, Y. Tzeng and O. Auciello, *Adv. Mater.*, 2014, **26**, 3724-3729.

532. X.-B. Cheng, M.-Q. Zhao, C. Chen, A. Pentecost, K. Maleski, T. Mathis, X.-Q. Zhang, Q. Zhang, J. Jiang and Y. Gogotsi, *Nat. Commun.*, 2017, **8**, 336.

533. Y. Liu, Y.-K. Tzeng, D. Lin, A. Pei, H. Lu, N. A. Melosh, Z.-X. Shen, S. Chu and Y. Cui, *Joule*, 2018, DOI: https://doi.org/10.1016/j.joule.2018.05.007.

534. D. Aurbach, Y. Gofer and J. Langzam, *J. Electrochem. Soc.*, 1989, **136**, 3198-3205.

535. V. Bormashov, S. Troschiev, A. Volkov, S. Tarelkin, E. Korostylev, A. Golovanov, M. Kuznetsov, D. Teteruk, N. Kornilov, S. Terentiev, S. Buga and V. Blank, *Phys. Status Solidi A*, 2015, **212**, 2539-2547.

536. Y. L. Zhong, A. Midya, Z. Ng, Z.-K. Chen, M. Daenen, M. Nesladek and K. P. Loh, *J. Am. Chem. Soc.*, 2008, **130**, 17218-17219.

537. C. Petkov, U. Glebe, E. Petkov, A. Pasquarelli, C. Pietzka, M. Veres, L. Himics, R. Merz, W. Kulisch, U. Siemeling, P. Reithmaier Johann and C. Popov, *Phys. Status Solidi A*, 2013, **210**, 2048-2054.

538. J. Bechter, C. Pietzka, C. Petkov, P. Reintanz, U. Siemeling, C. Popov and A. Pasquarelli, *Phys. Status Solidi A*, 2014, **211**, 2333-2338.

539. H. Krysova, L. Kavan, Z. V. Zivcova, W. S. Yeap, P. Verstappen, W. Maes, K. Haenen, F. Gao and C. E. Nebel, *RSC Adv.*, 2015, **5**, 81069-81077.

540. Irkham, T. Watanabe, A. Fiorani, G. Valenti, F. Paolucci and Y. Einaga, *J. Am. Chem. Soc.*, 2016, **138**, 15636-15641.

541. Y. Yang, J.-W. Oh, Y.-R. Kim, C. Terashima, A. Fujishima, J. S. Kim and H. Kim, *Chem. Commun.*, 2010, **46**, 5793-5795.

542. G. D. O'Neil, M. E. Newton and J. V. Macpherson, *Anal. Chem.*, 2015, **87**, 4933-4940.

543. H. E. M. Hussein, H. Amari and J. V. Macpherson, *ACS Catal.*, 2017, **7**, 7388-7398.

544. D. Neubauer, J. Scharpf, A. Pasquarelli, B. Mizaikoff and C. Kranz, *Analyst*, 2013, **138**, 6746-6752.

545. J. Izquierdo, B. Mizaikoff and C. Kranz, *Phys. Status Solidi A*, 2016, **213**, 2056-2062.

546. L. Meng, J. Ustarroz, M. E. Newton and J. V. Macpherson, *J. Phy. Chem. C*, 2017, **121**, 6835-6843.

547. H. E. M. Hussein, R. J. Maurer, H. Amari, J. J. P. Peters, L. Meng, R. Beanland, M. E. Newton and J. V. Macpherson, *ACS Nano*, 2018.

548. L. Meng, J. G. Iacobini, M. B. Joseph, J. V. Macpherson and M. E. Newton, *Faraday Discuss.*, 2014, **172**, 421-438.

549. L. Meng, J. Ustarroz, M. E. Newton and J. V. Macpherson, *J. Phys. Chem. C*, 2017, **121**, 6835-6843.

550. K. Tsunozaki, Y. Einaga, T. N. Rao and A. Fujishima, *Chem. Lett.*, 2002, **31**, 502-503.

551. J. Hees, R. Hoffmann, A. Kriele, W. Smirnov, H. Obloh, K. Glorer, B. Raynor, R. Driad, N. Yang, O. A. Williams and C. E. Nebel, *ACS Nano*, 2011, **5**, 3339-3346.

552. A. Eifert, P. Langenwalter, J. Higl, M. Lindén, C. E. Nebel, B. Mizaikoff and C. Kranz, *Electrochim. Acta*, 2014, **130**, 418-425.

553. W. Smirnov, A. Kriele, R. Hoffmann, E. Sillero, J. Hees, O. A. Williams, N. Yang, C. Kranz and C. E. Nebel, *Anal. Chem.*, 2011, **83**, 4936-4941.

554. A. E. Hess, D. M. Sabens, H. B. Martin and C. A. Zorman, *J. Microelectromech. Syst.*, 2011, **20**, 867-875.

555. Z. Gao, V. Carabelli, E. Carbone, E. Colombo, M. Dipalo, C. Manfredotti, A. Pasquarelli, A. Feneberg, K. Thonke and E. Vittone, *2009 IEEE 3rd International Conference on Nano/Molecular Medicine and Engineering*, 2011, **6**, 33-37.

556. R. Kiran, L. Rousseau, G. Lissorgues, E. Scorsone, A. Bongrain, B. Yvert, S. Picaud, P. Mailley and P. Bergonzo, *Sensors*, 2012, **12**, 7669-7681.

557. M. Sentic, F. Virgilio, A. Zanut, D. Manojlovic, S. Arbault, M. Tormen, N. Sojic and P. Ugo, *Anal. Bioanal. Chem.*, 2016, **408**, 7085-7094.

558. C. A. Rusinek, M. F. Becker, R. Rechenberg and T. Schuelke, *Electrochem. Commun.*, 2016, **73**, 10-14.

559. C. Dincer, E. Laubender, J. Hees, C. E. Nebel, G. Urban and J. Heinze, *Electrochem. Commun.*, 2012, **24**, 123-127.

560. C. Kranz, *Electroanalysis*, 2016, **28**, 35-45.

561. A. Avdic, A. Lugstein, M. Wu, B. Gollas, I. Pobelov, T. Wandlowski, K. Leonhardt, G. Denuault and E. Bertagnolli, *Nanotechnology*, 2011, **22**, 145306.

562. A. Eifert, W. Smirnov, S. Frittmann, C. Nebel, B. Mizaikoff and C. Kranz, *Electrochem. Commun.*, 2012, **25**, 30-34.

563. K. Reizo and O. Shigemitu, *Jpn. J. Appl. Phys.*, 1990, **29**, 1854-1855.

564. E. P. Visser, J. W. Gerritsen, W. J. P. v. Enckevort and H. v. Kempen, *Appl. Phys. Lett.*, 1992, **60**, 3232-3234.

565. Z. Chang, Z. Ma, J. Shen, X. Chu, C. Zhu, J. Wang, S. Pang and Z. Xue, *Appl. Surf. Sci.*, 1993, **70-71**, 407-412.

566. S. Albin, J. Zheng, J. B. Cooper, W. Fu and A. C. Lavarias, *Appl. Phys. Lett.*, 1997, **71**, 2848-2850.

567. O. Lysenko, N. Novikov, A. Gontar, V. Grushko and A. Shcherbakov, *J. Phys.: Conf. Ser.*, 2007, **61**, 740-744.

568. O. Lysenko, N. Novikov, V. Grushko, A. Shcherbakov, A. Katrusha, S. Ivakhnenko, V. Tkach and A. Gontar, *Diam. Relat. Mater.*, 2008, **17**, 1316-1319.

569. A. P. Chepugov, A. N. Chaika, V. I. Grushko, E. I. Mitskevich and O. G. Lysenko, *J. Superhard Material.*, 2013, **35**, 151-157.

570. V. Grushko, O. Lübben, A. N. Chaika, N. Novikov, E. Mitskevich, A. Chepugov, O. Lysenko, B. E. Murphy, S. A. Krasnikov and I. V. Shvets, *Nanotechnology*, 2014, **25**, 025706.

571. J. R. Webb, A. A. Martin, R. P. Johnson, M. B. Joseph, M. E. Newton, I. Aharonovich, M. Toth and J. V. Macpherson, *Carbon*, 2017, **122**, 319-328.

572. N. Yang and X. Jiang, *Carbon*, 2017, **115**, 293-311.

Appendix I: Abbreviation

Abbreviation	Meaning
CNTs	carbon nanotubes
BDD	boron-doped diamond
CVD	chemical vapour deposition
NDC	non-diamond carbon
HPHT	high-pressure high-temperature
HFCVD	hot-filament
MW	microwave plasma
RF	radio-frequency plasma
UNCD	ultrananocrystalline diamond
MCD	microcrystalline diamond
NCD	nanocrystalline diamond
B/C	the boron-to-carbon
SQUID	superconductive quantum interference device
NDD	nitrogen-doped diamond
HCDCP	hot-cathode-direct-current plasma
PDD	phosphorus-doped diamond
DND	detonation nanodiamond
GC	glassy carbon
UV	ultraviolet
XPS	X-ray photoelectron spectroscopy
APTES	3-aminopropyltriethoxysilane
HER	hydrogen evolution reaction
ORR	oxygen reduction reaction
ET	electron-transfer
SECM	scanning electrochemical microscopy
DOS	density of state
FIA	flow injection analysis
LC	liquid chromatography
NP	nanoparticle
RE	reference electrode
CE	counter electrode
EIS	electrochemical impedance spectroscopy
IFV	influenza virus
FET	field effect transistor
IS	ion-selective
SG	solution-gate
EN	enzyme-modified
ME	microelectrode
UME	ultramicroelectrode
NE	nanoelectrode
CE	capillary electrophoresis
MEA	ME array
UMEA	UME array
NEA	NE array
3D	three-dimensional
DBM	diamond-based multiarray
AOP	advanced oxidation process
EAOP	electrochemical AOP

COD	oxygen demand
BOD	biochemical oxygen demand
TOC	total organic carbon
DOC	dissolved organic carbon
THF	tetrahydrofuran
BPA	bisphenol A
ESR	electron spin resonance
BND	boron and nitrogen co-doped nanodiamond
SC	supercapacitors
EDLC	electrical double layer capacitor
PC	pseudocapacitors
CNF	carbon nanofiber
LED	light-emitting diode
USB	universal serial bus
ECL	electrogenerated chemiluminescence
TEM	transmission electron microscopy
EC-XRF	electrochemical X-ray fluorescence
FIB	Focused ion beam
SEM	scanning electron microscopy
AFM	atomic force microscopy
SPM	scanning probe microscopy
STM	scanning tunneling microscopy
RIE	reactive ion etching

Appendix II: Symbol

Symbol	Meaning
E_{VB}	valence band
E_{CB}	conduction band
E^{o}	standard potential
T_c	transition temperature
ΔE_p	potential difference of anode oxidation wave from cathodic wave
C	capacitance
P	power density
E	energy density

Appendix III: Author biosketches

Dr. Nianjun Yang is a senior scientist and the group leader at the Institute of Materials Engineering, University of Siegen, Germany. H works on the growth and electrochemical applications of advanced carbon materials. He has (co)-authored more than 120 journal papers, is editing 1 book series, edited 4 books, and contributed 9 book chapters, was the main organizer of 7 European Material Research Society symposiums, was the guest-editor of several journals, is the editor board member of the journals of *Scientific Reports* and *Diamond and Related Materials*, and is the program committee member of several diamond related international conferences.

Dr. Julie V. Macpherson is Professor in the Department of Chemistry, University of Warwick and is also a Royal Society Industry Fellow. Her current work is associated with the development of electrochemical sensors based on carbon materials for the monitoring of solution species. She has published over 170 papers and filled 15 patents. She has won the RSC Marlow Medal and the McBain medal. In 2016 she was named as one of the Top 50 Women in Analytical Science. She is currently significantly involved with the CDT Training Centre for PhD scientists in Diamond Science and Technology at Warwick University.

Dr. Yasuaki Einaga is a Professor in the Department of Chemistry at Keio University, Japan. He was also a research director of JST-CREST (2011-2014), and JST-ACCEL (2014 – present). His research interests include functional materials science, photochemistry, electrochemistry, and diamond electrodes. He has published more than 200 papers in peer-reviewed journals, edited 1 book, contributed 4 book chapters, and delivered more than 40 invited talks at international conferences. He has organized international symposiums on diamond electrochemistry in Japan (2004, 2005, 2007, 2014).

Dr. Guohua Zhao is a professor at School of Chemical Science and Engineering, Tongji University, China where he obtained his PhD degree in environment in 1999. After one year visiting fellow at University of Stuttgart, he joined School of Chemical Science and Engineering, Tongji

University. His current research interests include photoelectric catalysis and environmental energy chemistry using diamond and diamond/metal oxide composites, committed to cross field research work of environment and energy, such as CO_2 reduction, hydrogen production, photoelectrocatalytic oxidation and analysis of pollutants. Up to now, he has published 1 academic book and 150 research papers in peer-reviewed journals.

Dr. Greg M. Swain is a Professor in the Department of Chemistry, Michigan State University. His group's current research is at the crossroads of carbon materials science and physical and analytical electrochemistry. Current projects include diamond and diamond-like carbon electrodes for electroanalysis, optically transparent diamond electrodes for spectroelectrochemistry, nanocarbon powders as advanced materials for separations, and diamond microelectrodes for neuroanalytical chemistry and chemical and biochemical sensors. He previously served as Editor and Editor-in-Chief of Diamond and Related Materials (Elsevier) 2011-2015 and he currently serves on the advisory board of Advanced Engineering Materials (Wiley)**.**

Dr. Xin Jiang is a professor and the chair holder of Surface and Materials Technology at University of Siegen (Siegen, Germany) since 2003. He received the award "State Specially Recruited Expert" of China in 2013. He was a Changjiang-Visiting Chair Professor at Dalian University and Science and Technology, China. His current research fields cover the growth and applications of diamond thin films, metal nanomaterials as well as materials characterization. He has published over 320 peer reviewed journal papers, and contributed 8 books and book chapters. He has delivered numerous invited talks/lectures at international conferences.

Graphic Abstract: This review summarizes systematically the growth, properties, and electrochemical applications of conductive diamond.